Adaptive Fuzzy Sliding Mode Control of DFIG Wind Turbines to Capture Optimal Power Output

Elshaday Petros Gilja

A Thesis Submitted to

Department of Electrical Power and Control Engineering

School of Electrical Engineering and Computing

Presented in Partial Fulfillment of the Requirement for the Degree of Master's in Electrical Power and Control Engineering (Control Engineering)

Office of Graduate Studies

Adama Science and Technology University

September, 2024

Adama, Ethiopia

Adaptive Fuzzy Sliding Mode Control of DFIG Wind Turbines to Capture Optimal Power Output

Elshaday Petros Gilja

Advisor: Professor Gang Gyoo Jin

A Thesis Submitted to

Department of Electrical Power and Control Engineering

School of Electrical Engineering and Computing

Presented in Partial Fulfillment of the Requirement for the Degree of Master's in Electrical Power and Control Engineering (Control Engineering)

Office of Graduate Studies

Adama Science and Technology University

September, 2024

Adama, Ethiopia

DECLARATION

I hereby declare that this Master Thesis entitled "**Adaptive Fuzzy Sliding Mode Control of DFIG Wind Turbines to Capture Optimal Power Output**" is my original work. That is, it has not been submitted for the award of any academic degree, diploma, or certificate in any other university. Proper citation has been done for all materials used in this thesis to acknowledge their sources.

Elshaday Petros Gilja		
Name of the student	Signature	Date

RECOMMENDATION

I, the advisor of the thesis, hereby certify that I have read the revised version of the thesis entitled "**Adaptive Fuzzy Sliding Mode Control of DFIG Wind Turbines to Capture Optimal Power Output**" prepared under my guidance by **Elshaday Petros** submitted in partial fulfillment of the requirements for the degree of Master of Science in Control Engineering. Therefore, I recommend the submission of the revised version of the thesis to the department following the applicable procedures.

Prof. Gang Gyoo Jin		
Advisor	Signature	Date

APPROVAL SHEET

I, the advisor of the thesis entitled "**Adaptive Fuzzy Sliding Mode Control of DFIG Wind Turbines to Capture Optimal Power Output**" and developed by **Elshaday Petros**, hereby certify that the recommendation and suggestions made by the board of examiners are appropriately incorporated into the final version of the thesis.

Prof Gang Gyoo Jin	______________	____________
Major Advisor	Signature	Date

We, the undersigned, members of the Board of Examiners of the thesis by **Elshaday Petros** have read and evaluated the thesis entitled "**Adaptive Fuzzy Sliding Mode Control of DFIG Wind Turbines to Capture Optimal Power Output**" and examined the candidate during open defense. This is, therefore, to certify that the thesis is accepted for partial fulfillment of the requirement of the degree of Master of Science in Electrical Power and Control Engineering (Control Engineering).

____________________	______________	______________
Chairperson	Signature	Date
____________________	______________	______________
Internal Examiner	Signature	Date
Dr Beteley Teka		Sept 20, 2024
External Examiner	Signature	Date

Final approval and acceptance of the thesis is contingent upon submission of its final copy to the Office of Postgraduate Studies (OPGS) through the Department Graduate Council (DGC) and School Graduate Committee (SGC).

____________________	______________	______________
Department Head	Signature	Date
____________________	______________	______________
School Dean	Signature	Date
____________________	______________	______________
Office of Postgraduate Studies, Dean	Signature	Date

ACKNOWLEDGEMENTS

Before anything else, I thank God for His continuous guidance, mercy, and favors throughout my time in college. Without His miraculous intervention, this thesis would not have been completed.

Beyond that, I want to sincerely thank my family for their constant devotion, encouragement, and support. their firm belief in what I can achieve has kept me strong and motivated even during the most trying moments of my studies.

Furthermore, I am profoundly thankful to my advisor, Professor Gang Gyoo Jin, for his exceptional guidance, insightful feedback, and unwavering support throughout the course of this thesis. His knowledge and mentorship have been invaluable in determining the main point and caliber of my work. I am truly honored to have had the opportunity to work under his supervision.

Table of Contents

LIST OF TABLES

LIST OF FIGURES

LIST OF ACRONYMS

Abbreviations	Description
AC	Alternating Current
AFSMC	Adaptive Fuzzy Sliding Mode Control
ASTC	Anti-Sway Torque Control
ASTU	Adama Science and Technology University
BFASMC	Backstepping Fuzzy Adaptive Sliding Mode Control
COG	Center of Gravity
DC	Direct Current
DFIG	Doubly Fed Induction Generator
DPC	Direct Power Control
FIS	Fuzzy Inference System
FLC	Fuzzy Logic Controller
FSMC	Fuzzy Sliding Mode Controller
GSC	Grid Side Converter
HAWT	Horizontal Axis Wind Turbine
IBC	Incremental conductance
IPC	Indirect power control
IRC	Ideal relation-centered
MBLC	Model-based loss minimization control
MPPT	Maximum Power Point Tracking
MW	Megawatt

OT	Optimal Torque
PI	Proportional-Integral (controller)
PSF	Power Signal Feedback
PSO	Particle Swarm Optimization
RPS	Revolutions per Second
RSC	Rotor Side Converter
SMC	Sliding Mode Control
STC	Standard Test Conditions
TSR	Tip Speed Ratio
VAWT	Vertical Axis Wind Turbine
VSWT	Variable Speed Wind Turbine
WECS	Wind Energy Conversion System
WT	Wind Turbine
WTGS	Wind Turbine Generator System

NOMENCLUTURE

ρ	Air density
$\alpha_1, \alpha_2, \lambda_1, \lambda_2$	Control parameters
vdr	Direct-axis rotor voltage
idr, iqr	Direct and Quadrature-axis rotor current
ω	Electrical angular frequency
ε	Error
f_s	Frequency of AC voltages induced
f_r	Frequency of current supplied to the rotor of DFIG
J	Inertia of the rotating parts
p	Machine's pole pair
L_m	Magnetizing inductance
T_m	Mechanical Torque
Ωopt	Optimal speed
ΔB , ΔR_r	Parameter uncertainties of the damping and resistance
β	Pitch angle
vqr	Quadrature-axis rotor voltage
Ωref	Reference speed
i_{ar} , i_{br} , i_{cr}	Rotor currents in phases a, b, and c
$\vec{i}_r^r$	Rotor current space vector
ψ_{ar} , ψ_{br} , ψ_{cr}	Rotor flux in phases a,b, and c
$\vec{\psi}_r^r$	Rotor flux space vector

L_r	Rotor inductance
L_{sr}	Rotor leakage inductance
V_{ar} , V_{br} , V_{cr}	Rotor voltages in phases a,b, and c
$\overrightarrow{V_r^r}$	Rotor voltage space vector
Ω	Rotational speed
i_{as} , i_{bs} , i_{cs}	Stator current in levels a,b, and c
ψ_{as} , ψ_{bs} , ψ_{cs}	Stator flux in levels a, b, and c
L_s	Stator inductance
L_{ss}	Stator leakage inductance
V_{as} , V_{bs} , V_{cs}	Stator voltage in level a,b, and c
Rs, Rr	Stator and Rotor winding resistance
λ	Tip speed ratio

ABSTRACT

Maximizing power extraction is crucial for optimizing Wind Energy Conversion Systems (WECS) as wind energy is an important renewable resource. DFIGs are commonly utilized because of their capacity to function at different wind speed. Still, a significant hurdle persists: achieving optimal power generation amidst varying wind patterns. Conventional PI controllers frequently struggle to sustain the ideal rotor speed, leading to decreased efficiency in power generation. This research introduces Adaptive Fuzzy Sliding Mode Controller (AFSMC) aimed at improving rotor speed regulation and maximizing power capture from wind turbines. MATLAB/SIMULINK simulations show that the AFSMC attains a maximum rotor speed of 1,420.55 RPM, exceeding the 1,417.69 RPM achieved by traditional PI controllers. This enhancement results in a 2.7% boost in power extraction efficiency. The AFSMC also greatly cuts down on response times, with a 1.2-second rise time and a 2.768 second settling time, as opposed to the PI controller's 1.8 and 4.952 seconds, respectively. Moreover, the system achieves a higher efficiency of 98.5% in extracting wind energy, compared to the 95.8% efficiency reached by PI controllers. The AFSMC allows the DFIG-based wind turbine to consistently operate at its Maximum Power Point (MPP) by adjusting control parameters in response to changing wind speeds. This guarantees both increased power capture efficiency and enhanced grid stability. The suggested controller focuses on maximizing power extraction, leading to improved system performance and energy efficiency.

Keywords: *DFIG , maximum power extraction, rotor speed, AFSMC, Wind turbine*

CHAPTER ONE

INTRODUCTION

1.1 Background of the study

Supplying energy is essential for the advancement of a country's social and economic development. The global challenge of limited and expensive essential energy resources has arisen due to the growing energy consumption. Despite the fact that there is a lot of coal available, worries continue about the eventual running out of oil and natural gas reserves. Furthermore, the use of conventional carbon-based energy sources will have negative effects on the environment, such as global warming and climate change. Consequently, there has been a strong focus on employing renewable resources such as wind, solar, small hydro, wave, tidal, biomass, and geothermal energy to produce a sustainable energy source (Aimin Pan, 2024).

Globally, wind energy is a rapidly expanding sustainable energy source with a lot of potential. Africa, particularly in the north and south, boasts abundant wind and wave energy resources that remain largely untapped. Sub-Saharan Africa, specifically the highlands of Chad and Ethiopia, as well as coastal regions, possess significant wind potential. Despite this, the area currently represents less than 1% of the total global wind power capacity [L1]. Ethiopia, rich in renewable energy resources, have the capacity to meet its nationwide electrification needs through these resources. However, while it works to provide for nearly 110 million people and is predicted to increase by 2.5% year, the nation is facing load shedding and energy shortages (Kumsa, 2020). It is estimated that Ethiopia could produce 1,350,000 MW of electricity from wind power, however, at present only three wind farms are producing a total of 324 MW of electricity. This consists of the Adama II and Ashegoda wind farms producing 153 MW each. A crucial obstacle in wind energy systems (WECs) is optimizing electricity energy production from the wind turbine even with changing wind speeds and loads. DFIG-based WECS have become widely used in different wind energy systems because of their benefits, as shown in Figure 1.1. This includes operating at a consistent speed with adjustable speeds, producing active and reactive power in all areas, using converters that are set at approximately 30% of the generator’s power, and offering cost savings and less power loss when compared to fixed-speed induction generators and synchronous generators. (Aziz Watil, 2020).

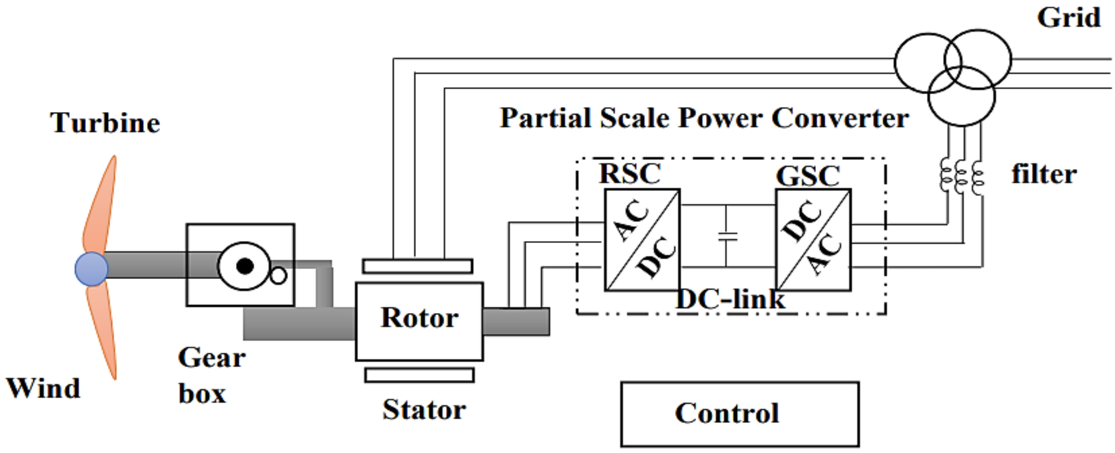

Figure 1.1 General supply configuration of DFIG (Power, 2015)

In spite of the features mentioned earlier, DFIG also has some disadvantages like susceptibility to disruptions in the grid, rotor over currents, parameter uncertainties, and nonlinearities (Mansoor Ahmad Soomro, 2021). Therefore, creating a reliable and effective control approach for a DFIG-based WECS is a crucial and difficult task. Recently, many new control techniques have been created to manage the generation of electrical power. However, due to the intricate control algorithms and the nonlinear nature of the systems they are meant to regulate, the control system's reliability hasn't always been assured.

The primary goal of this dissertation is to provide a control scheme for DFIG-based WECS that can enhance power extraction performance under various wind speeds and load scenarios. PI controllers are commonly used in commercial appliances due to multiple advantages, such as system durability, slight parameter adjustments, uncomplicated design, and various stability levels (Aziz Hadoune1, 2023). The system starts to lose its stability because of PI controllers are sensitive to fluctuations in the system's nonlinearity and variability (Jorge-Humberto, 2021). - (Elmostafa Chetouani, 2023) . AFLC for PI is essential for solving these issues compared to PI controllers. The use of an adaptive fuzzy logic controller increases the volatility of the integrated control system. AFLC utilizes fuzzy logic controllers to optimize the input of PI. AFLCs possess inherent benefits like their ability to manage unpredictability in systems, their straightforward design. AFLC displays improved Performance in power tracking compare to PI and traditional FLC (A. A. Salem, 2021). This investigation explored enhancing the AFLC introduced in (M. M. Gulzar, 2021) – (K. Zeb,

2017) by adding sliding mode to AFLC. AFSMC is the new term for this control method. The outcomes obtained from utilizing AFSMCs show a rapid time response, a quick convergence rate, smaller peak overshoot, reduced undershoot, with negligible steady-state inaccuracy in contrast to outcomes obtained using PI and AFLC. Moreover, the DFIG system uncertainties and nonlinearities can be effectively addressed by utilizing AFSMC.

A coordinated rotor speed control that can achieve MPPT and enhancement of energy efficiency by regulating the reactive and active power outputs of the DFIG. A control method uses AFSMC to adaptively modify the DFIG controller parameters based on changes in wind speed and load (Milton Ernesto, 2020).

1.2 Statement of the problem

The growing demand for eco-friendly energy solutions requires a substantial boost in the utilization of wind power. Despite its possibilities to decrease dependence on limited resources and improve grid stability, increasing the effectiveness of wind turbines remains a difficult challenge. Changes in wind speed, grid interruptions, and unexpected system modifications create difficulties in accurately controlling rotor speed, an important element in power generation and system stability. Traditional methods of controlling Double-Fed Induction Generators (DFIGs), with SMC and FLC, frequently face difficulties in effectively addressing these challenges. Although these conventional approaches provide answers, they often fail to reach the best possible results. This analysis addresses a significant gap in existing DFIG control methods through the implementation of the Adaptive Fuzzy Sliding Mode Control (AFSMC) approach. AFSMC presents a novel approach by combining FLC and SMC to improve rotor speed control, leading to higher power generation and grid resilience. This ability assists AFSMC in maintaining stability of DFIG in difficult situations, minimizing risks from grid outages, changing wind speeds, and unforeseen system disturbances. The study's objective is to increase wind turbine performance by using AFSMC to achieve three key improvements. AFSMC diligently tracks the optimal power point in varying wind conditions to enhance wind energy usage and boost energy conversion effectiveness. Improved Power Quality: Maintaining optimal rotor speed and power output with AFSMC ensures a reliable provision of clean electricity to the grid. This method of regulation reduces power fluctuations and voltage variations, making certain a constant and dependable power supply, ultimately strengthening grid stability and facilitating the seamless integration of wind energy into existing power systems. Enhanced DFIG Stability:

AFSMC focuses on preserving DFIG stability in challenging operating conditions. This guarantees reliable functioning of WT and reduces possible dangers linked to grid disruptions, variations in wind speed, and unexpected system disturbances. The potential for revolutionizing wind turbine control strategies is considerable with the creation and application of AFSMC. It makes a big difference in addressing current obstacles in harnessing wind power, opening up possibilities for wind to fully become a reliable and environmentally friendly energy source moving forward.

1.3 Objective

1.3.1 General objective

The general objective of this thesis is to present an AFSMC approach for DFIG in wind generators to enhance the power extraction capacity while maintaining stable operation under different wind conditions.

1.3.2 Specific Objective

- To develop a mathematical model of the DFIG-based wind turbine system.
- To design and implement an Adaptive Fuzzy Sliding Mode Controller (AFSMC).
- To evaluate the performance of the AFSMC in comparison with traditional PI controllers.
- To analyze the impact of the AFSMC on overall power efficiency.

1.4 Scope of the study

The use and assessment of the control method of AFSMC for DFIG wind turbines is the main focus of this thesis. It includes the application of the AFSMC algorithms to the WT control system's overall mathematical model. To maximize the extraction of power and increase the wind turbine system's efficiency, via MATLAB/SIMULINK, performance is assessed and compared to current control techniques, taking into account variables such as transient response, system stability, and power extraction efficiency. Furthermore, the effects and trade-offs of the suggested control technique on mechanical stresses, rotor currents, power quality, and other elements of system behavior are examined.

1.5 Limitation of the study

Due to its reliance on MATLAB/SIMULINK simulations without physical implementation, this work has limitations because it may not accurately represent real-world situations. Real-time implementation is difficult due to the Adaptive Fuzzy Sliding Mode Controller's (AFSMC) complexity, which also necessitates large computer resources. Adjusting the sophisticated controller architecture for ideal performance in real-world situations could potentially be challenging.

1.6 Motivation of the study

Recently, there has been a lot of focus on renewable energy, specifically wind energy, because it has the potential to meet increasing energy needs and decrease greenhouse gas emissions. DFIG-based wind turbines are now commonly utilized as a cutting-edge method of obtaining wind energy. Nevertheless, maximizing the power output of DFIG WT is crucial to efficiently harness wind resources. Controlling the rotor speed of WT is a crucial factor that directly impacts the power output. Conventional control techniques may not consistently deliver top-notch performance and struggle to adjust to changing wind conditions and load fluctuations. The aim behind this thesis is to improve the electricity production of DFIG wind turbines by effectively controlling the rotor speed. The study seeks to enhance power capture efficiency, decrease mechanical stress on turbine components, and improve stability in different operating conditions through the use of AFSMC.

1.7 Significant of the study

The renewable energy industry gains significant advantages from the suggested research on strategies for controlling wind turbines. The aim of this investigation is to improve the power generation and uphold the general wind turbine's efficiency and stability through focusing on control methods for DFIG. The importance of this dissertation is its impact on enhancing wind turbine efficiency, a crucial factor in increasing power generation from sustainable sources. An innovative method is introduced to enhance control abilities and flexibility in response to varying environmental conditions by integrating an AFSMC mechanism. The AFSMC control technique is evaluated through testing on MATLAB/Simulink. This thesis enhances our knowledge of wind turbine control while also showing potential for boosting power extraction, improving efficiency, ensuring stability, and encouraging the broader to use sustainable energy sources.

1.8 Thesis Organization

The thesis consists of six chapters, with each one examining key factors of the study.
Chapter 1 introduces the background and significance of renewable energy, particularly wind power, and outlines the challenges faced in optimizing DFIG systems. It establishes the objectives of the study, including the development of an effective control method to improve power extraction and maintain stability under varying wind conditions.

Chapter 2 provides a literature review, discussing existing control techniques for DFIG systems and highlighting the limitations of traditional methods. This chapter provides the context of the proposed AFSMC approach by identifying gaps in current research.

Chapter 3 details the methodology employed in the study, including the mathematical modeling of the DFIG system and the simulation tools used for evaluation. It outlines the steps taken to develop the AFSMC and the rationale behind its design.

Chapter 4 focuses on the controller design, explaining the principles of SMC and the integration of fuzzy logic. This chapter emphasizes the advantages of the AFSMC in addressing nonlinearities and uncertainties in DFIG systems.

Chapter 5 shows the results of the AFSMC's performance evaluation and simulation and comparing it with traditional control methods. It highlights the significant improvements achieved in key performance metrics, demonstrating the efficacy of the proposed control method.

Finally, Chapter 6 concludes the thesis by summarizing the findings and offering suggestions for further studies. This chapter underscores the potential of AFSMC to improve the effectiveness and dependability of DFIG wind turbines, contributing to the advancement of renewable energy technologies.

CHAPTER TWO

LITERATURE REVIEW

2.1 Chapter Overview

This chapter contains three main sections. The starting section provides a review of wind energy, specifically focusing on VSWTs and Doubly-fed Induction Generator (DFIG) technology. In addition to explaining the benefits of DFIG, it discusses their control mechanisms, exploring two levels: turbine control to maximize power extraction and converter control to maximize reliability. The second section is a review of existing control techniques of DFIG.

2.2 Theoretical background

A wind turbine is a device that transforms wind power into electricity. Based on how their speed is regulated, wind turbines can be classified into two different groups: fixed-speed and variable-speed. Constant-speed WT operate at a steady state, where as variable-speed wind turbines can change their speed according to wind conditions for better power generation and efficiency (Iliev, 2019). Comparing VSWT versus fixed-speed wind turbines provides several benefits., including decreased mechanical stress, boosted power production, and enhanced energy generation. The variable-speed DFIG based WT is a popular choice for various wind turbine models. A DFIG has two sets of three-phase windings, one on the stator and one on the rotor. The stator winding is connected to the grid, while the rotor winding is connected to the grid through a back-to-back converter that comprises a rotor-side converter (RSC) and a grid-side converter (GSC) (Jesús Castro Martínez, 2023). The rotor has the ability to function at varying speeds and allows separate management of the DFIG's reactive and active power through the converter. Running a WT with a DFIG system involves overseeing both the turbine itself and the generator separately. The primary task of turbine level control is to enhance wind power generation by modifying angle of blade pitch and rotor speed. Various techniques such as PI control, direct power control, FLC, NNC, SMC, adaptive control, and others are available for governing the converter. However, potential disadvantages include complex designs, susceptibility to parameter adjustments, insufficient stability, and similar issues. It is essential to use advanced and intelligent control techniques to increase the effectivenes of DFIG-based wind turbines and address these challenges.

The rotor's location determines the structure of wind turbines into two groups. Horizontal Axis Wind Turbine (HAWT) and Vertical Axis Wind Turbine (VAWT)

1. **Horizontal axis wind turbine (HAWT):** are the most typically seen form of wind turbine. Their design has propeller-like blades that revolve horizontally.

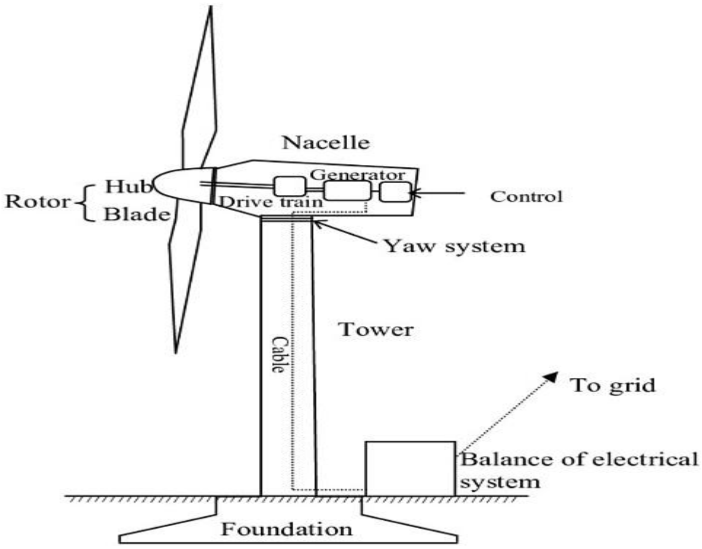

Figure 2.1 Horizontal axis wind turbine (HAWT) (Albadi, 2010).

2. **Vertical axis wind turbine (VAWT):** Feature blades that spin around a vertical axis. While not as common as HAWTs, VAWTs have their own benefits, like being able to operate in turbulent winds and being closer to the ground when installed.

Figure 2.2 Vertical axis wind turbine (VAWT) (ChristianT, 2010)

2.3 Parts of a Wind Power Transformation System

A wind energy system produces electricity by harnessing wind energy. Its various components all function harmoniously as a whole. These include:

Blades used in wind turbines are designed in the wind to harness wind energy and use it to deive rotation. The gearbox has a crucial function in maximizing energy conversion. The torque is increased while the shaft rotates slowly rising from the blade to a level sufficient for effective power. The generator is positioned at the core of the system, converting mechanical energy from the shaft of the gearbox into electricity. This conversion process is consistent with the fundamentals of Electromagnetic Induction (Belachew Desalegn, 2022). As wind speed changes, wind turbines generate power at different intensities and frequencies. A power converter with AC/DC/AC conversion stages converts the generator's AC output to DC, before converting it back to AC at the specified voltage and frequency to ensure grid connection. Step-up transformers provide low voltage power. The step-up transformer increases the voltage to reduce transmission losses at a distance before entering the power system. The diagram illustrating a standard WECS is shown in Figure 2.3.

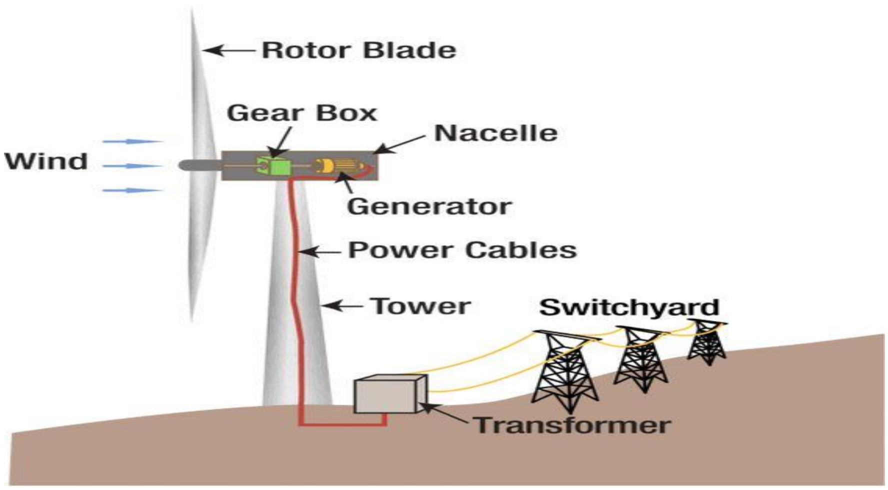

Figure 2.3 Parts of a wind turbine-generator energy conversion system [L2].

2.3.1 Topologies of Wind turbines

Wind turbine systems can be broadly categorized into two main sectors: mechanical and electrical. The key elements of the technology industry are the wind turbine and gearbox. This field’s characteristics are defined by the turbine’s basic equation of motion and the control of the pitch angle actuator; however, the main focus of this topic is on the electrical aspects of the system. The study focuses specifically on double-fed induction generators

(DFIG) and associated electronic power converters (Mahmoud Elgendi, 2023). Wind turbines are divided into two categories according to their operating speed: fixed-speed wind turbines and variable-speed wind turbines (Shobole, 2015).

Wind turbines are only efficient at narrow wind speeds, and because wind is a variable and nonlinear medium, Grid power characteristics are negatively impacted by power fluctuationns, induction generators with squirrel cage are commonly utilized in wind turbines with fixed speeds.. Wind energy generation generally utilize fixed or variable speed wind turbines, which are divided into four main types: Types 1,2,3, and 4. A sophisticated wind turbine of Type 3, operating at variable speeds where you can control the maximum power output (Group, p. 2019).

2.3.2 Operating Area of a System for Generating Wind Turbine Energy.

Wind turbine performance fluctuates with varying wind speeds. Figure 2.4 illustrates the key points on the wind turbine power curve and wind speed curve, including the cut-in, rated, and cut-off speeds. Cut-in speed given by point A wind speed at which the blades start rotating, and power generation sequences begin. As the wind speed increases, the maximum limit is reached in the power output, the rated speed, which is indicated by point C. At this point the turbine reaches the maximum power, known as the rated power laid down. The range of speeds between the fixed speed and the cut-in speed, which is Zone 2 in study and legal specifications known as the (MPPT region), that is where maximum power point tracking (MPPT) algorithms operate (Ahmed G, 2019). wind turbine systems use the maximum power point tracking (MPPT) control method to ensure optimum energy over all variable wind speeds. This is usually done by controlling the turbine enters safety shutdown mode to avoid any mechanical damage when the wind is strong. The cutout speed indicates the wind speed at which this throw occurs (Zone 3). As mentioned in (Abate, 2019), cutoff protection is essential to preserve the mechanical efficiency of the turbine in high wind conditions. Figure 2.4 shows the locations of the WT generator system.

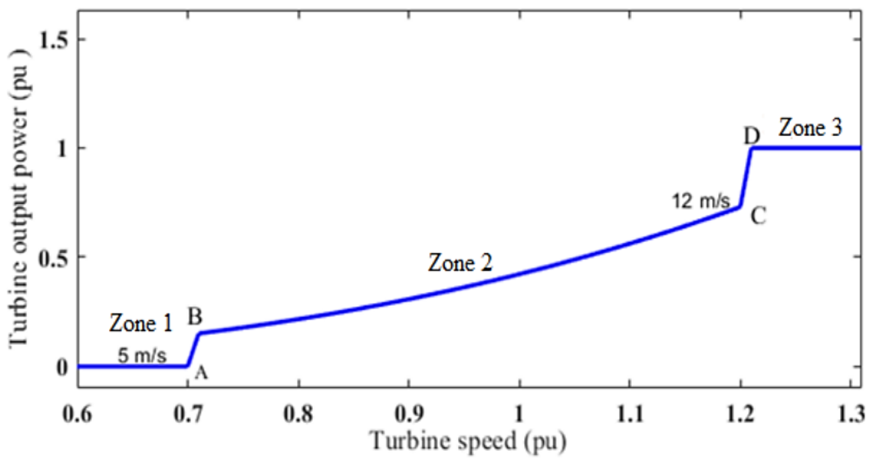

Figure 2.4 Power output of turbines versus wind speed curve (Tadesse, 2016).

2.4 Principle Of Variable Pitch Control

When wind speed exceeds the rated speed, pitch angle control provides a simple means of controlling the aerodynamic pressures on the wind turbine's rotor blades (Senjyu, et al., 2006). It permits servo operations, which maximize wind power extraction by adjusting the blade's pitch in accordance with wind velocity. Various pitch angle controller solutions for DFIG-based wind turbines have been presented in (Gnanamalar, 2017).

Using AFSMC controllers, pitch angle control is accomplished by feeding the actuator with the reference pitch signal, which activates the servo motor and modifies the pitch angle to the desired value (Miller, Sanchez-Gasca, Price, & Delmerico, 2023). An open-loop pitch angle control model with a rate-limited actuator is depicted in Figure 2.5.

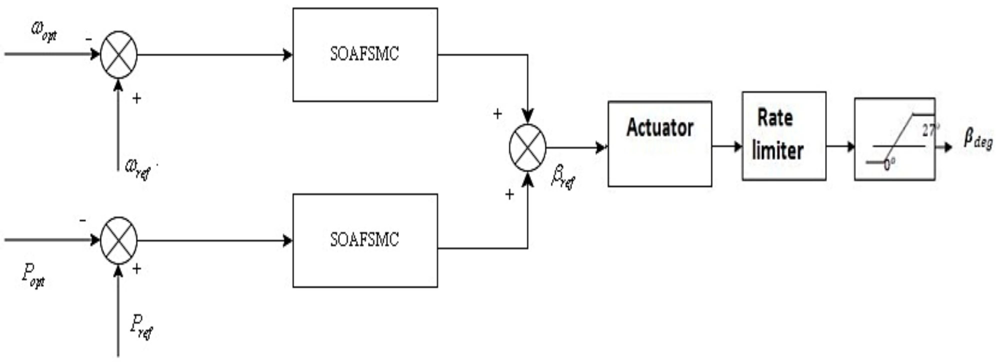

Figure 2.5 Model for controlling pitch angle in DFIG-based WTS

2.5 Review of Related Works

An overview of the literature on DFIG optimization control techniques and various strategies used to maximize wind turbine power production is presented in this section. It describes the DFIG control mechanism and earlier studies on a double-fed induction generator.

Numerous studies have investigated various control methods to boost the effectiveness of DFIGs in WECS. Among them, Particle swarm optimization (PSO) proposes a control approach to improve the effectiveness of fixed-pitch wind turbines with doubly-fed induction generators by using PSO to correct inaccuracies in calculating the generator circuit parameters. The suggested control method generates a speed reference to maximize mechanical power collected from the wind and optimizes the d-axis rotor current by regulating stator reactive power, to reduce electrical losses in the doubly-fed generator. A PSO algorithm finds the optimal d-axis rotor current, while MPPT soft-stalling control over rated wind speed and control below rated wind speed establish the best speed target. The authors show through numerical simulations that the suggested control system can produce additional energy compared to a traditional model-based loss minimization approach, particularly when there is uncertainty in the DFIG parameters. The effectiveness of PSO-based optimization is demonstrated in addressing the challenges of model-based loss minimization control in the presence of parameter uncertainty. Accurate understanding of the DFIG parameters, especially the mutual inductance L_m is essential for the suggested control strategy effectively reduces the electrical losses of the generator. The writers point out that in real-world scenarios, these factors are only approximately understood and some, such as the rotor resistance, are greatly impacted by temperature, resulting in imprecise identification of the best operational settings. The paper suggests that parameter uncertainty hinders the effectiveness of model-based loss minimization control (MBLC) approaches. In order to address this constraint, the authors suggest employing a PSO algorithm to find the best d-axis rotor current reference without needing exact information about the DFIG parameters. Nevertheless, the search results do not offer insights into the performance of PSO-based optimization in comparison to the MBLC approach across different levels of parameter uncertainty. The PSO technique's ability to address parameter errors has not been fully measured or evaluated (Cherngchai Sompracha, 2019).

This Article (Bouchaib Rached, "Fuzzy Logic Control for Wind Energy Conversion System based on DFIG", 2019), presents a fuzzy logic control (FLC) technique for a wind energy conversion system (WECS) equipped with a double-fed induction generator (DFIG). The suggested method uses four different FLCs to control the grid-side converter (GSC) maximum power point tracking (MPPT), DC-link voltage, and rotor-side converter (RSC). The primary objectives include managing active power extraction, maintaining zero stator reactive power, and achieving maximum energy generation with a power factor of one. The conversation involves simulation of components in the WECS, like wind turbines, DFIG, and power converters. Information is given regarding the membership function for input/output and rule bases that are used in the FLC design of each subsystem. The GSC FLC regulates the grid-side currents and DC-link voltage, while the RSC FLC controls the rotor currents to balance active and reactive power. The MPPT FLC adjusts the power setpoint to maximize energy capture based on the optimal TSR. The simulation findings indicate that the recommended FLC strategy excels in stability, accuracy, and resilience when facing varying wind speeds. The advantages of FLC were demonstrated when compared to a typical PI controller, including reduced oscillations during transitions, enhanced disturbance rejection, and greater stability against parameter variations. The researchers propose that the FLC technique effectively achieves the desired objectives of efficient power extraction, unity power factor, and separate control of reactive and active power. The paper focuses on the control aspects of the DFIG system, neglecting crucial factors such as mechanical stress, fatigue loads, and wind turbine structural dynamics.

The Article (Ayman Safwat1*, 2020)**,** compares traditional PI controllers with an adaptive fuzzy self-tuning PI controller for regulating the rotor-side converter (RSC) of a doubly-fed induction generator (DFIG) in a wind energy conversion system (WECS). The vector control technique is employed in developing the DFIG model, allowing for separate control of reactive and active power. Aerodynamic equations are used to model the WT, and a MPPT algorithm indirectly maximizes power extraction. The adaptive fuzzy self-tuning controller is a combination of a conventional PI controller and a FLC, adjusting the PI gains (Kp and Ki) based on error and rate of error changes. The fuzzy controller utilizes Mamdani-style fuzzy reasoning with pre-established rule bases and membership functions for variables of input (error, change of error) and output variables (Kp1, Ki1). Results from simulations with varying wind speeds show that the adaptive fuzzy self-tuning PI controller is more effective than the traditional PI controller, achieving quicker settling time, minimized fluctuations, and improved accuracy in tracking the MPPT torque reference and grid active power output. The enhanced efficiency of the fuzzy controller is due to its capability to adjust to system nonlinearities and changes in operating conditions. The research focuses on a fluctuating wind speed pattern, but it does not specifically discuss other possible disruptions or uncertainties, like turbulence, grid faults, or parameter changes, that may impact the controller's effectiveness.

The Article (Ayyarao, 2019), suggests a revised vector control strategy for a doubly-fed induction generator (DFIG) wind power system utilizing a barrier function adaptive sliding mode control (BFASMC) technique. The traditional vector control method for DFIG systems, using PI controllers, is not able to handle grid disturbances and changes in parameters effectively. To tackle this issue, the authors substitute the internal current control loop with a BFASMC scheme. This results in quicker convergence, lack of chattering, and enhanced robustness when compared to first-order sliding mode control. The grid-side converter (GSC) and rotor-side converter (RSC) loops are controlled by the BFASMC. The objective is to control the rotor d-q currents and grid-side d-axis current to their reference values in a set period of time. The suggested composite control strategy is evaluated on a typical multi-machine power system model, including BFASMC for the inner current loops with PI control for the outer loop. Results from simulations show that the method is efficient in mitigating different types of disturbances like three-phase faults, changes in parameters, and varying wind speeds. In contrast to traditional PI control and first-order sliding mode control, the new BFASMC method demonstrates improved transient response speed, reduced overshoots, and enhanced steady-state performance. However, it solely focuses on regulating the DFIG system without considering the wind turbine system's complete dynamics and connections with the grid. The assessment does not evaluate how effectively the approach deals with broader disturbances and uncertainties at the system level.

The Article (Mostefa Amara, 2022), introduces an improved control approach for a wind turbine (WT) system equipped with a grid-connected Doubly Fed Induction Generator (DFIG). The suggested plan relies on Super Twisting Control (STC) in a modified form using adaptive gains, suitable for incorporation into the cascaded system setup involving speed and power control loops. The main contributions of the paper include: Formulating an ASTC plan for the grid-connected DFIG-WT system. An analysis comparing STC and ASTC control for the DFIG-WT system using simulated data. The ASTC method is efficient in decreasing and evening out the control exertion through creating a straightforward expression of sliding gain despite disturbances related to changes in parameters and the unpredictable aspect of wind velocity. In comparison to traditional STC, ASTC guarantees rapid and accurate system response, while also significantly reducing chattering to achieve smoother control input. The wind energy system model is introduced in the paper, which includes the wind turbine, DFIG, and control schemes. It goes on to describe the wind turbine and DFIG modeling and control, which includes the Maximum Power Point Tracking (MPPT) control. Next, the text details the STC and ASTC techniques of Second-Order Sliding Mode Control (SOSMC). The ASTC uses adjustable gains regarding the sign function in order to attain more rapid convergence and reduce chattering when compared to the STC with fixed gains. Nevertheless, it does not address how the ASTC approach is affected by factors like parameter changes, modeling uncertainties, or alterations in operating conditions outside of the simulated scenarios. The resilience of the ASTC under real-life disruptions is not completely understood.

The Article (Mohamed Horch, 2023)**,** suggests a new method for adjusting the gain in a Sliding-mode controller (SMC) to control a doubly-fed induction generator's (DFIG) reactive and active power in a wind energy conversion system (WECS). The traditional SMC is resilient regarding modifications in the parameters and external disruptions, yet it is prone to the chattering effect, which can hinder system performance and lead to harm. In order to address this problem, the SMC's switching gains are adjusted adaptively with the help of a supervisory fuzzy logic system, which helps decrease chattering while maintaining the controller's robustness. The control plan includes two primary elements: using an SMC-based MPPT algorithm to optimize the rotor speed of the wind turbine for extracting the optimal power. A sliding surface is established, and a Lyapunov stability analysis is conducted in order to determine the corresponding control law and switching control law for the SMC. A flexible fuzzy logic system modifies the switching gains of the SMC based on fuzzy rules, successfully decreasing the chattering issue linked to high gain values in traditional SMC. The suggested control method is applied in combination with vector control of the DFIG to attain accurate regulation of reactive and active power in the WECS. The effectiveness of the adaptive fuzzy-SMC method is evaluated using numerical simulations in different wind conditions and uncertainties of parameters. The findings show resilience to changes in machine parameters and outside disturbances, accurate reference tracking and response qualities, and less chattering phenomenon when compared to traditional SMC. The suggested method cleverly merges the durability of SMC with the flexibility of fuzzy logic systems, resulting in enhanced control performance for WECS utilizing DFIGs. Even though the suggested method shows resilience to changes in parameters and disruptions in the simulated environment, its effectiveness during severe or very unstable wind conditions has not been specifically assessed. In recent days, adaptive fuzzy sliding mode control (AFSMC) has emerged as a promising control technique for DFIGs. AFSMC combining SMC's resilience with the adaptability of FLC, making it a promising approach for addressing the challenges of DFIG control. However, existing AFSMC techniques for DFIGs may not adequately consider the specific uncertainties or variations in the wind conditions that may affect the performance of the controller.

Generally, Conventional PI controllers often struggle with managing the nonlinearities and parameter changes in DFIG systems, leading to stability issues in varying wind conditions. While fuzzy logic controllers and sliding mode controllers have been used independently, there is a lack of methods that successfully combine their advantages. Many current methods fail to achieve optimal power generation across all wind speeds and load conditions. Additionally, existing techniques often have difficulty effectively handling uncertainties and disturbances in DFIG wind turbines. To address these challenges, this research suggests a new method called Adaptive Fuzzy Sliding Mode Control (AFSMC). The AFSMC approach merges the flexibility of fuzzy logic with the stability of sliding mode control to handle nonlinearities and parameter changes effectively. This method aims to provide faster reaction times, quicker convergence, and reduced steady-state errors compared to PI and traditional FLC. It aims to improve MPPT across various wind speeds, enhancing system stability and power quality by controlling rotor speed and power output more efficiently. Additionally, the AFSMC technique enhances the DFIG's ability to maintain performance during grid disruptions and unforeseen system changes.

CHAPTER THREE

METHODOLOGY AND SYSTEM MODELING

3.1 Chapter Overview

This chapter describes the supplies and techniques utilized to complete this research work. Additionally, it focusses on acquiring the double-feed induction generator and WECS through mathematical modeling.

3.2 Materials

The simulation tool MATLAB/SIMULINK was utilized to test and analyze the system model in this thesis. This software is the general-purpose computing software which consist a broad range of many toolboxes. It has a high-level mathematical package design for doing numerical solutions and graphical user interfacing. Edraw-Max used to design block diagrams, electrical circuits and flow charts. Also, MS-Office (Word 2021) used to write the whole documentation rather than equations and MATHTYPE to write the equations or formulas.

3.3 Methods

The flowchart in Figure 3.1 outlines the steps involved in developing a novel control technique named AFSMC. The first step is to identify the issue and examine relevant literature. Next, design stages are illustrated: designing the AFSM controller and developing the Fuzzy Rule Base. MATLAB/Simulink simulation is carried out. According to the simulation findings, the process diverges into two potential outcomes. When the solution meets the criteria, the results are shared. If necessary, modifications to the design will be implemented, and the process will return to simulation. This process continues until a solution is discovered that fulfills the criteria.

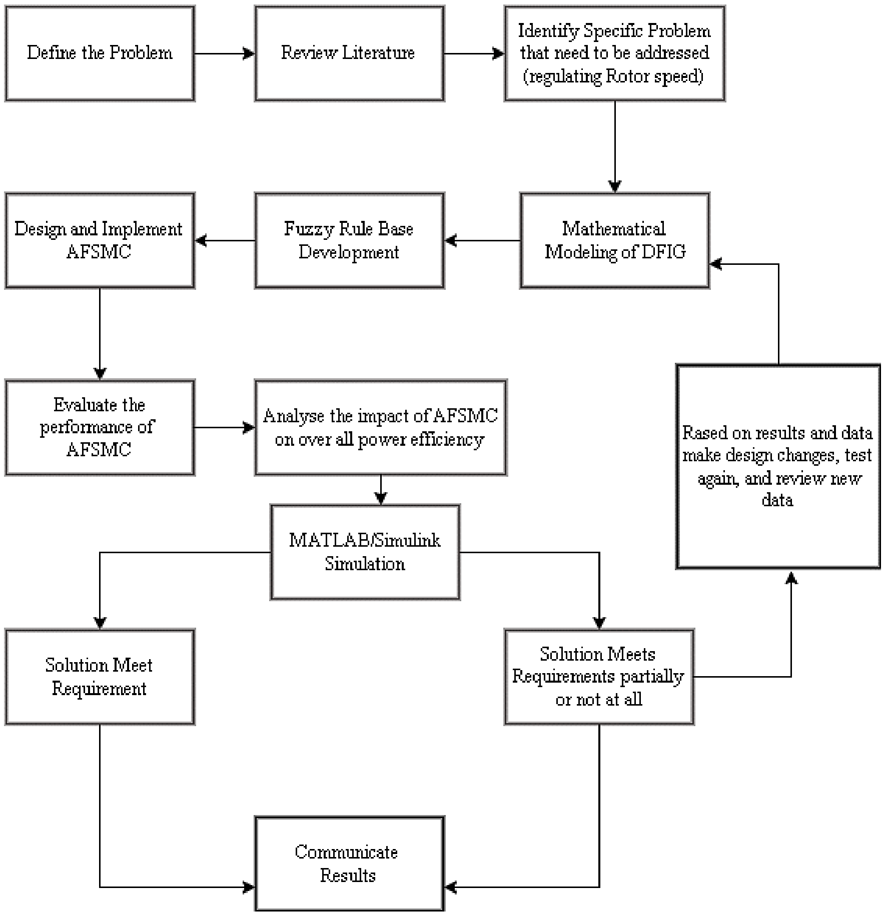

Figure 3.1 Flow chart of the methodology used in the study

3.4 Block Schematic of the Suggested Control Mechanism.

A control system is depicted in Figure 3.2 for modifying the shaft rotational speed (ω) of a wind turbine. The wind turbine rotates the shaft in the first stage by harnessing the kinetic energy of the wind. The generator receives an increase in shaft speed from the transmission, which transforms it into electrical power (Vabc). The dq transformer turns the three-phase system into a two-phase rotating reference frame, simplifying analysis, while the 2-to-3 transformer modifies voltage levels. The reference speed (ω_{ref}) is a crucial component. This figure represents the desired rotational velocity for maximizing power generation or achieving other operational objectives. The rotor speed control block continuously compares ω_{ref} with the current speed (ω) and generates an error signal (ω_{ref} - ω_{opt}). This error is the primary input for the control system. The error signal is used by the PI controller to manage the generator's Id current. The goal of the PI controller's Id adjustments is to reduce the error between actual speed (ω) and a desired speed (ω_{ref}). Essentially, the control system functions to regularly adjust the generator's current to maintain the desired rotational speed for optimal performance. The Enhanced AFSM controller likely collaborates with the PI controller, potentially providing additional control in managing generator currents to enhance rotor speed regulation. Overall, the diagram illustrates that the control system employs a combination of reference speed, error correction, and current control to ensure the wind turbine shaft rotates at the intended speed, in order to optimize efficiency or achieve other operational objectives.

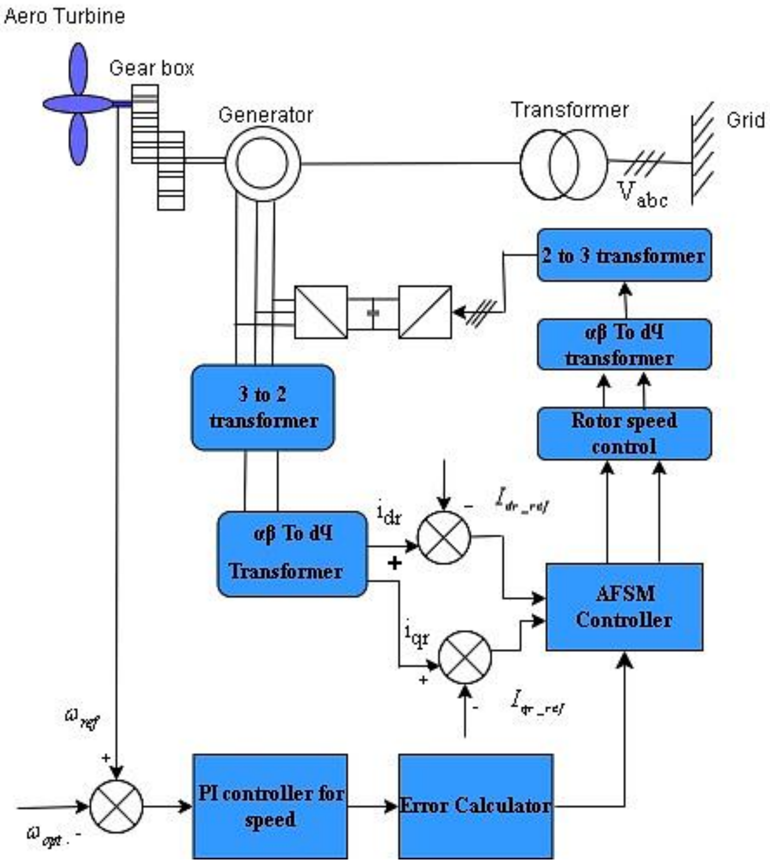

Figure 3.2 Schematic diagram of the suggested control mechanism

3.5 Wind Turbine Generator System Modeling

Wind turbine generator systems (WTGS) use doubly-fed induction generators (DFIGs) to transform wind energy from kinetic to electrical form, which is subsequently connected to the grid. It is essential to constract a suitable model of the grid- connected variable speed wind turbine generator systems (WTGS) in order to obtain a greater understanding of power quality and issues related to variable speed DFIG systems, including their impact on the grid and different control methods. WT are remarkable engineering examples that transform wind's inherent power into usable electricity. This conversion occurs in two distinct stages. Initially, the wind turbine operates as an aerodynamic extractor, utilizing lift and drag forces to capture wind's kinetic energy. This causes the rotor to turn. The spinning represents the captured mechanical power generated by the wind. Subsequently, the mechanical energy that has been captured is transformed into electric power. The generator in the nacelle receives energy from the rotating rotor shaft and acts as an electro-mechanical transducer, converting mechanical energy to electrical energy.

$$E = \frac{1}{2} m v^2 \tag{3.1}$$

Where E represents the air particle's kinetic energy, m denotes its mass, and v denotes the wind's speed. The mass of all air particle m with in a certain time interval t is represented by the equation below.

$$m = \rho A v t = \rho \pi r^2 v t \tag{3.2}$$

Where A is the area the wind turbine's blades sweep, r is the blades' radius, and ρ is the air density. Equation (3.1) can be used to find the kinetic energy of the air particles by substituting into Equation (3.2) as follows.

$$E = \frac{1}{2} \rho \pi r^2 v^3 t \tag{3.3}$$

The correlation between the mechanical input power and the wind speed traversing a turbine rotor plane can be articulated as follows (Iulian Munteanu, 2018).

The power of the wind given as

$$P_{wind} = \frac{E}{t} \tag{3.4}$$

Equation (3.3) can be substituted into Equation (3.4) to obtain

$$P_{wind} = \frac{(1/2)}{t} \rho \pi r^2 v^3 t \tag{3.5 a}$$

$$= \frac{1}{2} \rho \pi r^2 v^3 \tag{3.5 b}$$

Equation (3.6 c) indicates the power generated by a WT is directly related to the cube of the wind speed and also grows in proportional to the turbine blade's size. The total wind energy output is represented by Equation (3.6 c). Still, wind can harness some of this energy. A spinning machine converts the motion energy of a liquid into physical energy. In 1933, Albert Betz introduced a fundamental principle in the theory of wind turbines. He mentioned that the wind blade results in a decrease in wind speed upon impact. This suggests that there is still residual kinetic energy in the wind once it has passed the rotor blades. As a result, the power coefficient (Cp) concept inherently restricts the potential wind power generation. This demonstrates the wind turbine's ability to produce power compared to the maximum power the wind can provide (Betz, 2015).

$$C_p(\lambda,\beta) = \frac{P_{turbine}}{P_{Wind}} \tag{3.6 a}$$

$$P_{turbine} = \mathrm{P}_{Wind} C_p(\lambda,\beta) \tag{3.6 b}$$

$$= \frac{1}{2}\rho\pi \mathrm{r}^2 v^3 Cp(\lambda,\beta) \tag{3.6 c}$$

Where the air density ρ , rotor blade radius *r*, and wind speed *v*, define the wind turrbine’s captured power. The power coefficient of the turbine can be ascertained by calculating the pitch angle β and tip speed ratio λ . The efficiency with which a wind turbine transforms the kinetic energy of the wind into mechanical power is measured by this unitless factor. Additionally, achieving a power coefficient (Cp) of one is unattainable, illustrating the impossibility of achieving full efficiency in wind energy conversion. The Betz limit principle sets a boundary for Cp, capping it at around 0.593. In other words, the Betz limit declares that a typical wind turbine can utilize a maximum of 59.3% of the wind's kinetic energy. If a wind turbine were to achieve 100% efficiency, it would essentially halt the movement of the wind. The complete stoppage of wind would prevent any further movement of wind to the turbine blades, resulting in a complete halt of energy extraction. Therefore, the Betz limit serves as a crucial principle in the design and evaluation of wind turbines, as it represents the maximum power coefficient achievable. Wind turbines that are effective usually function within the range of 35% to 45%.

The wind turbine’s power coefficient can be defined as

$$C_p = \mathrm{e}_1(e_2\frac{1}{\lambda_i} - e_3\beta - e_4)\exp^{-e_5\frac{1}{\lambda_i}} + e_6\lambda \tag{3.7}$$

Where, e_1=0.5167, e_2=116, e_3=0.4, e_4=5, e_5= 21, and e_6= 0.0068

The values of coefficients e_1 to e_6 change depending on the design and type of wind turbine utilized. The coefficients needed for accurately modeling the power performance of each wind turbine are usually given by the manufacturer.

$$\frac{1}{\lambda_i} = \frac{1}{\lambda + 0.08\beta} - \frac{0.035}{1+\beta^3} \tag{3.8}$$

The symbol β in this formula represents the blade's pitch angle. The angle of the blade is determined by the pitch angle in relation to the wind speed approaching. When the blade has a pitch angle of zero, it is positioned to capture the maximum amount of wind, enabling the wind turbine to utilize the wind's power to its fullest extent. Moreover, the symbol λ is used to indicate the relationship between the rotor speed and the wind speed, also known as the tip speed ratio. (Petras, 2018) gives the mathematical equation for tip speed.

$$\lambda = \omega_m \frac{R}{V} \tag{3.9}$$

Figure 3.3 shows that the power coefficient reaches its maximum at a pitch angle of 0° and a velocity ratio λ_{nom} = 8.1. The power coefficient at λ_{nom} is $C_{P\max}$ = 0.48.

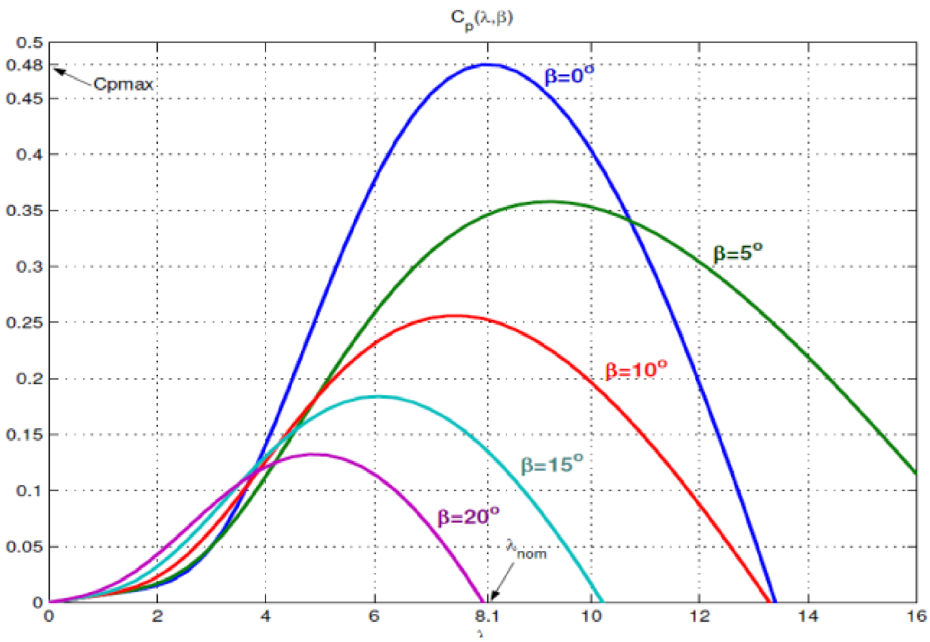

Figure 3.3 Feature of the power coefficient (Mostefa Amara1, 2021).

In this formula, ω_m stands for the angular speed of the wind turbine generator, while R denotes the radius of the rotor. The primary goal of a wind turbine is to convert the wind's kinetic energy into rotational mechanical energy. The wind passing through the turbine blades causes them to rotate, resulting in the exertion of a turning force. The turning motion is transmitted to a spindle located within the nacelle, which is connected to the gearbox.

The gearbox's role is to increase the rotational speed to a suitable level for the generator. Smaller wind turbines have a gear ratio of 1:1, causing the rotor and generator to spin at identical speeds. The term T_m represents the mechanical torque according to (Ross Guttromson, 2018).

$$T_m = \frac{P_m}{\omega_m} = \frac{1}{2\omega_m}\rho\pi r^2 v^3 Cp(\lambda, \beta) \tag{3.10}$$

3.6 Optimal strategy for controlling Maximum Power Point Tracking (MPPT).

MPPT algorithms are essential for wind energy conversion systems to maximize power output. The goal is to operate the turbine at its Maximum Power Point (MPP), which varies with wind speed. MPPT methods can be categorized based on their use of speed sensors:

1. **Direct Power Control (DPC):** Algorithms like Perturb & Observe (P&O), Incremental Conductance (IBC), and Ideal Relation-Centered (IRC) directly control the turbine to track the MPP.
2. **Indirect Power Control (IPC):** Methods like Power Signal Feedback (PSF) and Optimal Torque (OT) indirectly control the turbine by pre-determining the optimal power output based on wind speed characteristics.

Systems of management like Fuzzy Logic Controllers (FLCs) can be used to optimize system performance. Tip Speed Ratio (TSR) is a common parameter considered in MPPT algorithms.

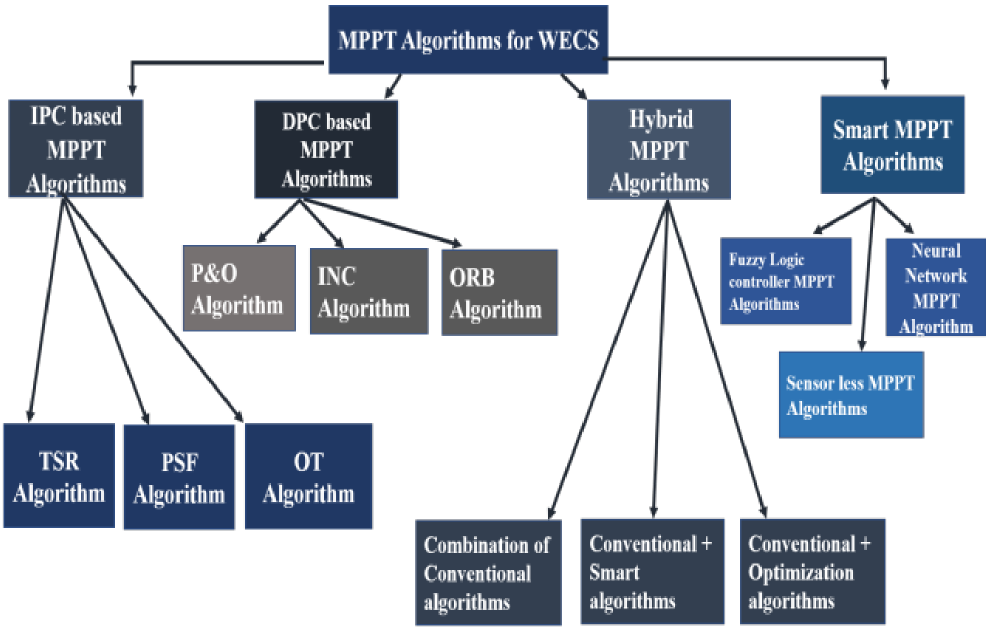

Figure 3.4 Classifications of MPPT Algorithms for Wind Energy Conversion Systems (Jayshree Pande, 2021).

Controlling tip speed ratio is a method to enhance power output by determining rotor and wind speeds, resulting in the generation of an optimal rotor speed reference ω_{ref} . The TSR MPPT algorithm is utilized for controlling the optimal rotor speed in varying environmental conditions.

$$\omega_{opt} = \frac{\lambda_{opt} * v}{R} \tag{3.11}$$

Where,

ω_{opt} , Maximum Rotational Speed.

λ_{opt}, The optimum tip speed ratio.

v, Wind speed.

R , Rotor Radius.

The power output of a wind turbine is directly linked to its tip speed ratio (TSR), which is the ratio of blade tip speed to wind speed. Turbines generate maximum power at specific rotational speeds when the blade pitch angle is fixed (O. Apata, 2020). To maximize energy extraction, especially in lower wind speeds, it's crucial to maintain an optimal TSR. The optimal torque control technique is another strategy employed to achieve this maximum power point.

$$\lambda = \frac{\omega_r R}{v} \tag{3.12}$$

$$v = \frac{\omega_r R}{\lambda} \tag{3.13}$$

The formula for mechanical power can be expressed as:

$$P_m = \frac{1}{2}\rho\pi R^2 (\frac{\omega_r R}{\lambda})^3 C_p(\lambda, \beta) \tag{3.14}$$

Analysis of wind turbine performance shows that there is a particular tip speed ratio, labeled as λ_{opt}, at which the highest power coefficient, Cp-max, is reached. This λ_{opt} value allows for the best extraction of power, P_{m_opt}. Given in Equation (3.15) written as:

$$P_{m\_opt} = \frac{1}{2}\rho\pi R^2 (\frac{\omega_r R}{\lambda_{opt}})^3 C_{p\_\max}(\lambda, \beta) \tag{3.15}$$

$$P_{m\_opt} = \frac{1}{2}\rho\pi R^5 \frac{\omega_r^{\ 3}}{\lambda_{opt^3}} C_{p\_\max}(\lambda, \beta) \tag{3.16 a}$$

$$= \frac{\frac{1}{2}\rho\pi R^5 C_{p\_\max}(\lambda, \beta)}{\lambda_{opt^3}} \cdot \omega_r^{\ 3} \tag{3.16 b}$$

Equation (3.16) can be reformulated in relation to K_{opt} resulting in Equation (3.17).

$$P_{m\_opt} = \mathrm{K}_{opt} \cdot \omega_r^{\ 3} \tag{3.17}$$

Equation (3.10) defines the connection between mechanical power and torque.

$$T_{m\_opt} = \frac{P_{m\_opt}}{\omega_r} \tag{3.18 a}$$

$$= \mathrm{K}_{opt} \cdot \omega_r^{\ 2} \tag{3.18 b}$$

3.7 Drive Train Model

The rotor and the stator make up the two-mass drive train of a Doubly Fed Induction Generator (DFIG), which is used in wind turbines. The wind turbine's working mechanism is represented by the rotor, and effective energy conversion and variable speed operation are made possible by the stator's connection to the grid. Reliability and performance are increased by this arrangement, which reduces mechanical stress and improves the system's reaction to wind gusts and fluctuations. The DFIG is appropriate for integrating renewable energy sources into the power grid since it also allows for real-time control of reactive power compensation and power output.

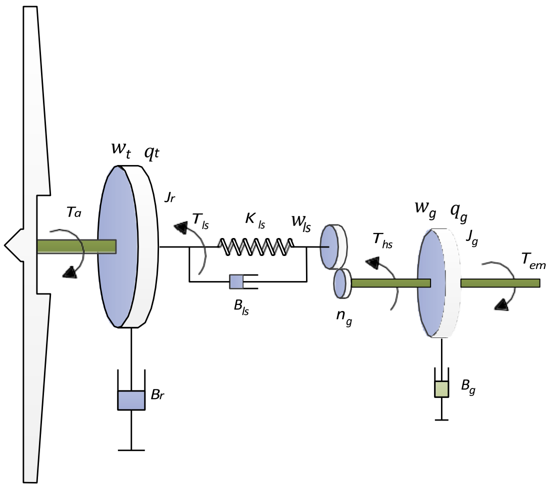

Figure 3.5 Dual-mass drive train model

Spring that stands for K_{Is} of shaft stiffness. The high-speed shaft and generator are represented by a viscous damper with a damping constant B_g and a rotational moment of inertia J_g. A gearbox ratio ng, which is intended to be absolutely rigid, is used to model the gearbox.

The following differential equations describe the mathematical model shown in Figure 3.5:

$$\begin{aligned} J_r\dot{\omega}_t &= T_a - T_{Is} - B_r\omega_t \\ J_g\dot{\omega}_g &= T_{hs} - B_g\omega_g - T_{em} \\ T_{Is} &= K_{Is}(\upsilon_t - \upsilon_{Is}) + B_{Is}(\omega_t - \omega_{Is}) \end{aligned} \tag{3.19}$$

The gearbox ratio is described as

$$n = \frac{T_{ls}}{T_{hs}} = \frac{\omega_g}{\omega_{ls}} = \frac{\upsilon_g}{\upsilon_{ls}} \tag{3.20}$$

3.8 Working Principle of Double-Fed Induction Generator (DFIG)

A wound rotor induction machine with three phases can also be set up as a doubly fed induction generator (DFIG). In this setup, the prime mover transfers mechanical energy to the shaft, which is then transformed into electrical power by the stator and rotor windings and sent to the AC power grid. The DFIG shows traits that are similar to those of a synchronous generator. However, unlike a synchronous generator that has a fixed synchronous speed, the DFIG allows for the adjustment of its synchronous speed. Controlling is accomplished by adjusting the frequency of the alternating currents supplied to the rotor windings. Consequently, the DFIG can transform the mechanical power from the shaft into electrical power at the stator terminals and can operate at varying speeds. It is crucial to compare this to traditional (singly-fed) induction generators, in which a specific equation dictates the connection between the stator output voltage frequency and the rotor speed.

$$f_s = \frac{\omega_r * P}{120} \tag{3.21}$$

Where f_s is the frequency of AC voltages induced across the stator windings, ω_r is the speed of rotor in RPS and P is the number of pole in the DFIM per phase

Expanding on the known connection between rotor speed and stator output frequency, it is clear that when a traditional induction generator runs at synchronous speed (rotor speed matches synchronous speed), the stator voltage frequency matches the power grid frequency. This principle holds true in a doubly-fed induction generator (DFIG). The main difference is found in the type of magnetic field produced by the rotor. In contrast to the unchanging magnetic field produced by DC current in a traditional generator, the rotor field in a DFIG is constantly changing. This dynamic movement is a result of the three-phase AC currents being supplied to the rotor windings, which in turn causes the magnetic field to rotate at a rate directly linked to the frequency of the AC current. As a result, the stator windings are exposed to a combined rotating magnetic field generated by both the rotor's physical rotation and the rotational impact of AC currents in the rotor. The speed of the rotating magnetic field in the stator of a DFIG is determined by the interaction of these two factors, which ultimately sets the frequency of the generated alternating voltage.

By utilizing the well-known concepts of doubly-fed induction generators (DFIGs), we are able to assess the influence of rotor magnetic field positioning. When the rotor's magnetic field lines up with the rotor rotation direction, the speeds of the two components add up. The speed at which they move together affects how often the voltages are produced in the stator windings. The specific connection between these elements can be mathematically described using the subsequent equation.

$$f_s = \frac{\omega_r * P}{120} + f_r \tag{3.22}$$

where f_r, Frequency of current supplied to the rotor of DFIG

On the other hand, a situation occurs when the magnetic field of the rotor spins in the opposite direction of the generator rotor. In this scenario, the velocities of these two parts become oppositional. This opposing impact directly impacts the frequency of the voltages generated in the stator coils. The same equation can still be used to mathematically express the relationship between these opposing speeds and the stator voltage frequency.

$$f_s = \frac{\omega_r * P}{120} - f_r \tag{3.23}$$

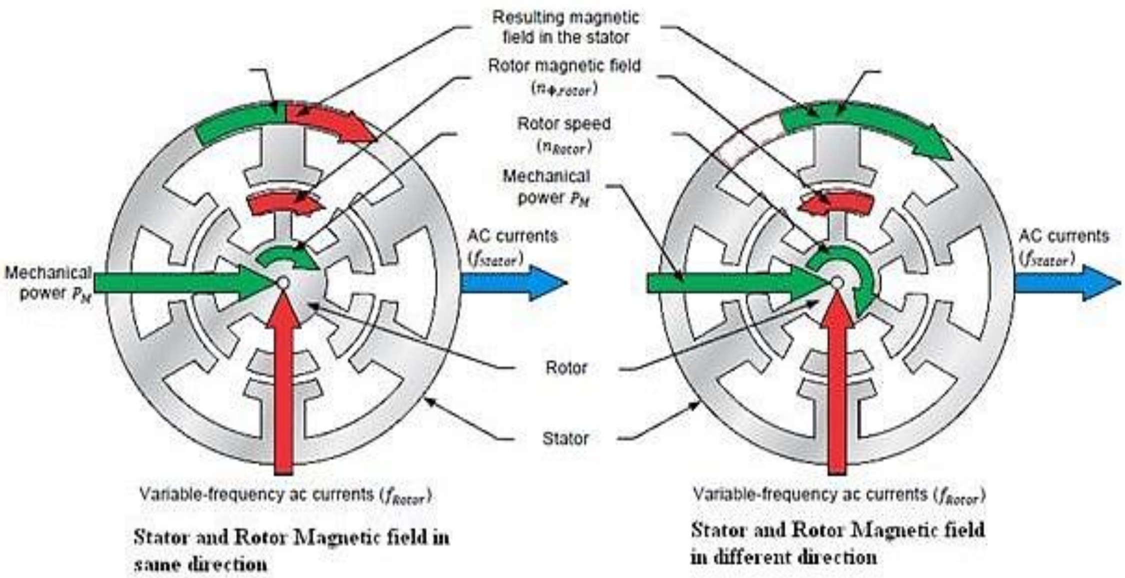

Figure 3.6 Double-Fed Induction Machine (DFIM) (Han, 2014)

3.9 Dynamic Model of a Double-Fed Induction Generator (DFIG)

Building at the work of many academics who have built fashions of AC generators, a simplified and idealized DFIG version may be defined as having three windings in each the stator and the rotor. This layout, as proven in Figure 3.6, is an ideal representation of real generator. It makes it easier to derive an equivalent electric circuit, as proven in Figure 3.7. in this idealized version, the immediate stator voltages, currents, and fluxes can be defined with the aid of the subsequent electric powered equations, which reflect the important relationships that force the generator's behavior.

$$V_{as} = \mathrm{R}_s i_{as} + \frac{d\psi_{as}}{dt} \tag{3.24}$$

$$V_{bs} = \mathrm{R}_s i_{bs} + \frac{d\psi_{bs}}{dt} \tag{3.25}$$

$$V_{cs} = \mathrm{R}_s i_{cs} + \frac{d\psi_{cs}}{dt} \tag{3.26}$$

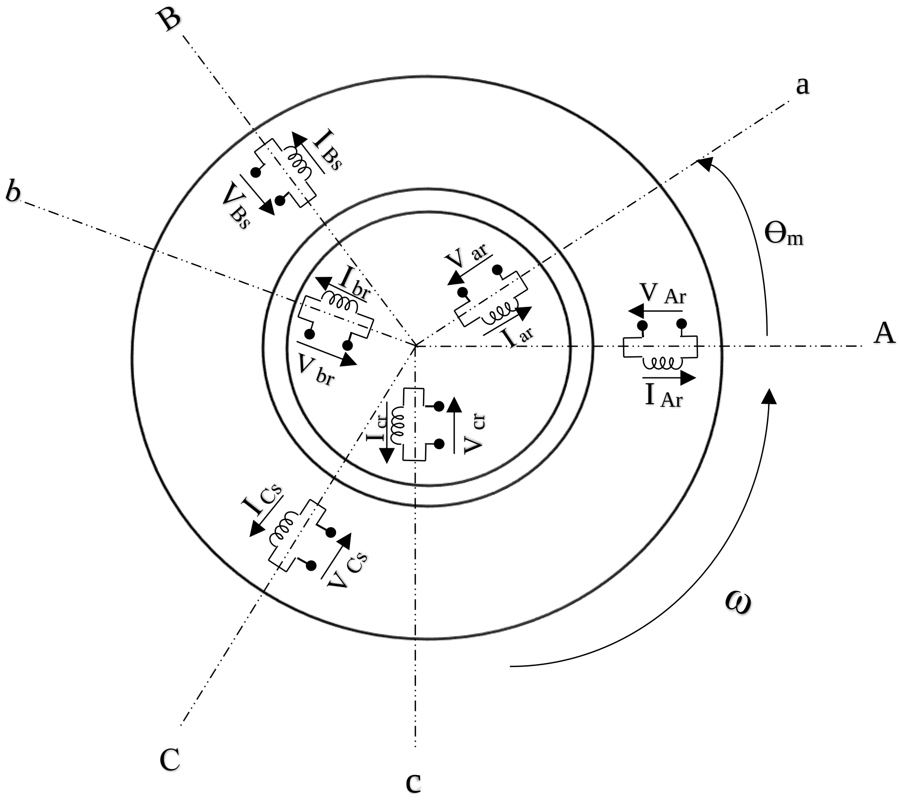

Figure 3.7 A DFIG ideal three-phase windings (stator and rotor) (Gonzalo Abad, 2018).

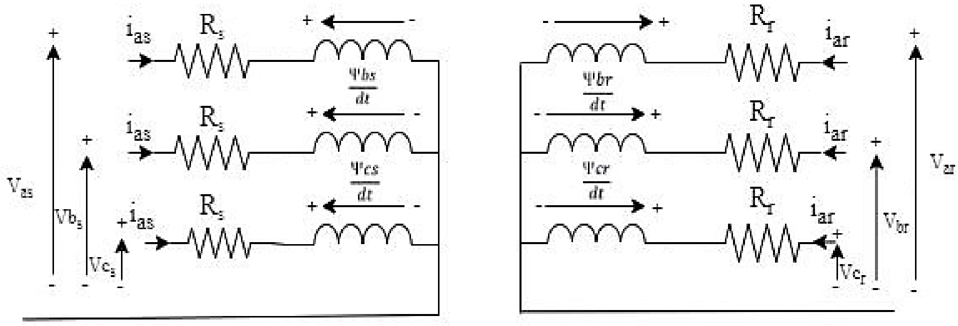

Figure 3.8 DFIG electric equivalent circuit

In the equations R_s denotes the stator resistance. The terms i_{as}, i_{bs}, and i_{cs} talk over with the stator's immediately currents in stages a, b, and c, respectively. Similarly, V_{as}, V_{bs}, and V_{cs} are the voltages carried out to the stator phases a, b, and c. Finally, ψ_{as}, ψ_{bs}, and ψ_{cs} constitute the stator fluxes in levels a, b, and c, respectively. In the steady state, the electrical magnitude at the stator side has a constant sinusoidal angular frequency ω_s, generated by the grid.

Similarly, rotor magnitudes are described as:

$$V_{ar} = \mathrm{R}_r i_{ar} + \frac{d\psi_{ar}}{dt} \tag{3.27}$$

$$V_{br} = \mathrm{R}_r i_{br} + \frac{d\psi_{br}}{dt} \tag{3.28}$$

$$V_{cr} = \mathrm{R}_r i_{cr} + \frac{d\psi_{cr}}{dt} \tag{3.29}$$

The above electrical equations use special symbols to represent the device shape. R_r refers to the rotor resistance, but, for simplicity, it is called the stator part. Similarly, i_{ar}, i_{br}, and i_{cr} refer to the rotor currents in phases a, b, and c, but are discussed in terms of stator size. Similarly, V_{ar}, V_{br}, and V_{cr} refer to the rotor voltages applied to the stator, while ψ_{ar}, ψ_{br}, and ψ_{cr} refers rotor flux respectively. Respectively it is important to note that the steady-state energy. Under operating conditions, the electrical quantity in the rotor section has a constant square frequency. The frequency ω_r can be different from the stator frequency ω_s depending on the operation of the device. Assume a typical DFIG configured with different turns in the stator and rotor, all parameters and dimensions of the rotor are specified for the stator. Relationship between stator angular frequency and the rotor angular frequency is:

$$\omega_r + \omega_m = \omega_s \tag{3.30}$$

Where ω_m represents the electrical angular frequency of the device. The Ω_m represents mechanical angular frequency and is connected to the electrical frequency through two poles.

$$\omega_m = \mathrm{p}\Omega_m \tag{3.31}$$

Due to the rotation of the machine rotor, the associated electrical values such as voltages, current and fluxes exhibit fractional behavior but it is important that throughout the rest of the discussion reference is made to magnitude and parameter attached to the rotor is always understood in terms of uniform stator values.

3.9.1 $\alpha\beta$ Model

This section uses space vector notation in the stator reference framework to generate differential equations representing the Doubly Fed Induction Generator (DFIG) model. The voltage equations of the DFIG are expressed as a space vector after the following steps are completed: Equations (3.22) and (3.25) multiplied by $\frac{2}{3}$, Equations (3.23) and (3.26) multiplied by $\frac{2}{3}a$, and Equations (3.24) and (3.27) by $\frac{2}{3}a^2$.

$$\overrightarrow{V_s^s} = \mathrm{R}_r \overrightarrow{i_s^s} + \frac{d\overrightarrow{\psi_s^s}}{dt} \tag{3.32}$$

$$\overrightarrow{V_r^r} = \mathrm{R}_r \overrightarrow{i_r^r} + \frac{d\overrightarrow{\psi_r^r}}{dt} \tag{3.33}$$

The stator voltage space vector is represented by transitions $\overrightarrow{V_s^s}$, stator current space vector is $\overrightarrow{i_s^s}$, and stator flux vector is $\overrightarrow{\psi_s^s}$. For Equation (3.30), the stator coordinates $\alpha\beta$ are expressed in the frame of reference. The same is true for the rotor voltage space vector $\overrightarrow{V_r^r}$, the rotor current space vector $\overrightarrow{i_r^r}$, and the rotor flux space vector $\overrightarrow{\psi_r^r}$. Equation (3.31) is defined in terms of rotor coordinates, that is, in the (DQ) reference frame.

Space vectors are labeled with ‘s’ and ‘r’. Those letters show the frame used; ‘s’ means stator frame. ‘r’ means rotor frame. The relationship between flux links and currents uses space vector form. It is expressed as the following.

$$\overrightarrow{\psi_s^s} = L_s \overrightarrow{i_s^s} + L_m \overrightarrow{i_r^s} \tag{3.34}$$

$$\overrightarrow{\psi_r^r} = L_r \overrightarrow{i_s^r} + L_m \overrightarrow{i_r^r} \tag{3.35}$$

L_{ss} is related to stator leakage inductance, L_{sr} connects to rotor leakage inductance, L_s represents stator inductance, L_r signifies rotor inductance and L_m is the magnetizing inductance. The equation links these values together.

$$L_s = L_{\sigma s} + L_m \tag{3.36}$$

$$L_r = L_{\sigma r} + L_m \tag{3.37}$$

Equation (3.32) is written from the stator’s view, Equation (3.33) is from the rotor’s viewpoint. When you transform between frames, these formulas apply. The stator equation shows the situation as seen by an outside observer. But the rotor equation describes the motion from the spinning part’s perspective. Changing between these two viewpoints requires certain mathematical rules.

$$\overrightarrow{\psi_s^s} = L_s \overrightarrow{i_s^s} + L_m \overrightarrow{i_r^s} = L_s \overrightarrow{i_s^s} + L_m e^{j\theta_m} \overrightarrow{i_r^r} \tag{3.38}$$

$$\overrightarrow{\psi_r^r} = L_m \overrightarrow{i_s^r} + L_r \overrightarrow{i_r^r} = L_m e^{-j\theta_m} \overrightarrow{i_s^s} + L_r \overrightarrow{i_r^r} \tag{3.39}$$

Multiplying Equation (3.31) by $e^{j\theta_m}$ yields the $\alpha\beta$ model of the DFIG in stator coordinates. Relate the space vectors to the stator frame to achieve this. The stator equations are:

$$\overrightarrow{V_s^s} = R_s \overrightarrow{i_s^s} + \frac{d\overrightarrow{\psi_s^s}}{dt} \tag{3.40}$$

$$\overrightarrow{V_s^s} = R_s \overrightarrow{i_s^s} + \frac{d\overrightarrow{\psi_s^s}}{dt} \tag{3.41}$$

$$\overrightarrow{\psi_s^s} = L_s \overrightarrow{i_s^s} + L_m \overrightarrow{i_r^s} \tag{3.42}$$

$$\overrightarrow{\psi_r^s} = \mathrm{L}_s \overrightarrow{i_s^s} + L_m \overrightarrow{i_r^s} \tag{3.43}$$

Note that to transform into Equation (3.39), it is necessary to include.

$$\frac{d\overrightarrow{\psi_r^r}}{dt} e^{j\theta_m} = \frac{d\overrightarrow{\psi_r^s}}{dt} - j\omega_m \overrightarrow{\psi_r^s} \tag{3.44 a}$$

Where,

$$\overrightarrow{\psi_r^r} e^{j\theta_m} = \overrightarrow{\psi_r^s} \tag{3.42 b}$$

Figure 3.8 depicts the $\alpha\beta$ electrical model of the DFIG in stator coordinates

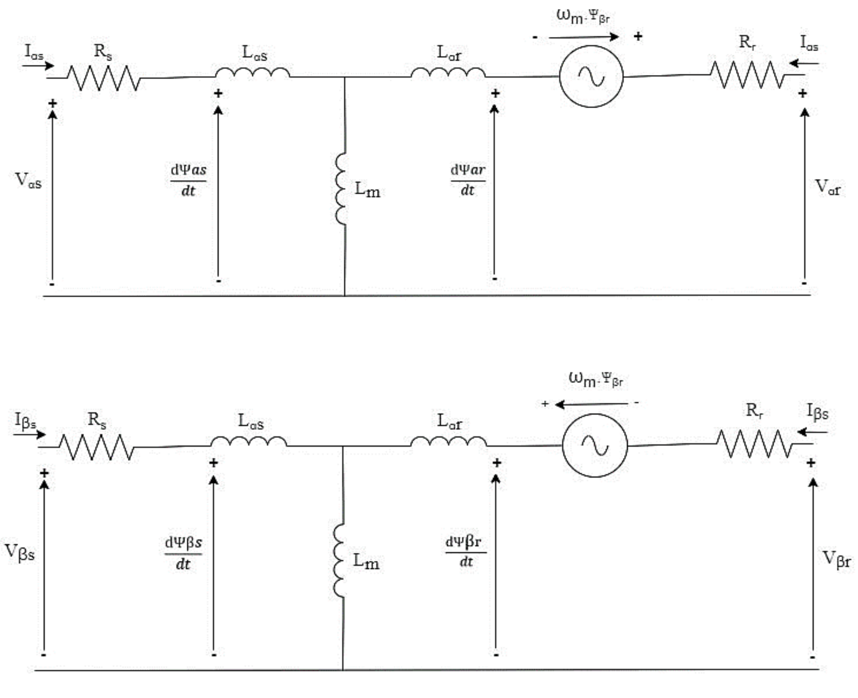

Figure 3.9 Model of the DFIG in stator coordinates.

The calculations determine the electrical energy on the stator and rotor sides. Continuing the mode's process, this is how they are found:

$$P_s = \frac{3}{2}\mathrm{Re}\left\{\overrightarrow{V_s} \cdot \overrightarrow{i_s^*}\right\} = \frac{3}{2}(V_{\alpha s} i_{\alpha s} + V_{\beta s} i_{\beta s}) \tag{3.45}$$

$$P_r = \frac{3}{2}\mathrm{Re}\left\{\overrightarrow{V_r} \cdot \overrightarrow{i_r^*}\right\} = \frac{3}{2}(V_{\alpha r} i_{\alpha r} + V_{\beta r} i_{\beta r}) \tag{3.46}$$

$$Q_s = \frac{3}{2}\mathrm{Im}\left\{\overrightarrow{V_s} \cdot \overrightarrow{i_s^*}\right\} = \frac{3}{2}(V_{\beta s} i_{\alpha s} - V_{\alpha s} i_{\beta s}) \tag{3.47}$$

$$Q_r = \frac{3}{2}\mathrm{Im}\left\{\overrightarrow{V_r}\cdot\overrightarrow{i_r^*}\right\} = \frac{3}{2}(V_{\beta r}i_{\alpha r} - V_{\alpha r}i_{\beta r}) \tag{3.48}$$

The superscript $*$ means the complex conjugate of a space vector, as used in phasors. Finally, the electromagnetic torque can be obtained as:

$$T_{em} = \frac{3}{2}p\,\mathrm{Im}\left\{\overrightarrow{\psi_r}\cdot\overrightarrow{i_r^*}\right\} = \frac{3}{2}p(\psi_{\beta r}i_{\alpha r} - \psi_{\alpha r}i_{\beta r}) \tag{3.49}$$

Equation (3.38) and (3.39) can be substituted into Equationn (3.47) to determine electromagnetic torque, yielding the corresponding expressions:

$$T_{em} = \frac{3}{2}p\frac{L_m}{L_s}\mathrm{Im}\left\{\overrightarrow{\psi_s}\cdot\overrightarrow{i_r^*}\right\} = \frac{3}{2}p\,\mathrm{Im}\left\{\overrightarrow{\psi_s^*}\cdot\overrightarrow{i_s}\right\} = \frac{3}{2}\frac{L_m}{L_r}p\,\mathrm{Im}\left\{\overrightarrow{\psi_r^*}\cdot\overrightarrow{i_s}\right\} \tag{3.50 a}$$

$$= \frac{3}{2}\frac{L_m}{\sigma L_r L_s}p\,\mathrm{Im}\left\{\overrightarrow{\psi_r^*}\cdot\overrightarrow{i_s}\right\} = \frac{3}{2}L_m p\,\mathrm{Im}\left\{\overrightarrow{i_s}\cdot\overrightarrow{i_r^*}\right\} \tag{3.51 b}$$

The leakage coefficient is represented as $\sigma = 1\text{-}\frac{\mathrm{L}_m^2}{L_s L_r}$, while p represents the machine's pole pair. To simplify notation, the superscript s has been removed from the space vector in power and torque expressions.

3.9.2 dq model

in this section, the diffrential equations for the DFIG model are derived using space vector notation in the synchronous reference frame, which is different from the previous section. Multiplying voltage Equations (3.30) and (3.31) by $e^{-j\theta_s}$ and $e^{-j\theta_r}$ results in the stator and rotor voltage equations.

$$\overrightarrow{V_s^a} = \mathrm{R}_s\overrightarrow{i_s^a} + \frac{d\overrightarrow{\psi_s^a}}{dt} + j\omega_s\overrightarrow{\psi_s^a} \tag{3.52 }$$

$$\overrightarrow{V_r^a} = \mathrm{R}_r\overrightarrow{i_r^a} + \frac{d\overrightarrow{\psi_r^a}}{dt} + j\omega_r\overrightarrow{\psi_r^a} \tag{3.53 a}$$

Where

$$\omega_r = \omega_s - \omega_m \tag{3.51 b}$$

In this situation, the superscript a refers to space vectors in a rotating frame. Equations (3.32) and (3.33) use identical flux formulas, resulting in:

$$\overrightarrow{\psi_s^a} = \mathrm{L}_s\overrightarrow{i_s^a} + L_m\overrightarrow{i_r^a} \tag{3.54}$$

$$\overrightarrow{\psi_r^a} = L_m \overrightarrow{i_s^a} + L_r \overrightarrow{i_r^a} \tag{3.55}$$

In steady state, the dq components of voltages, currents, and fluxes remain constant. while the $\alpha\beta$ components are sinusoidal magnitudes. Figure 3.9 shows the DFIG's dq equivalent circuit model in synchronous coordinates.

$$P_s = \frac{3}{2}\mathrm{Re}\left\{\overrightarrow{V_s} \cdot \overrightarrow{i_s^*}\right\} = \frac{3}{2}(V_{ds}i_{ds} + V_{qs}i_{qs}) \tag{3.56}$$

$$P_r = \frac{3}{2}\mathrm{Re}\left\{\overrightarrow{V_r} \cdot \overrightarrow{i_r^*}\right\} = \frac{3}{2}(V_{dr}i_{dr} + V_{qr}i_{qr}) \tag{3.57}$$

$$Q_s = \frac{3}{2}\mathrm{Im}\left\{\overrightarrow{V_s} \cdot \overrightarrow{i_s^*}\right\} = \frac{3}{2}(V_{qs}i_{ds} - V_{ds}i_{qs}) \tag{3.58}$$

$$Q_r = \frac{3}{2}\mathrm{Im}\left\{\overrightarrow{V_r} \cdot \overrightarrow{i_r^*}\right\} = \frac{3}{2}(V_{qr}i_{dr} - V_{dr}i_{qr}) \tag{3.59}$$

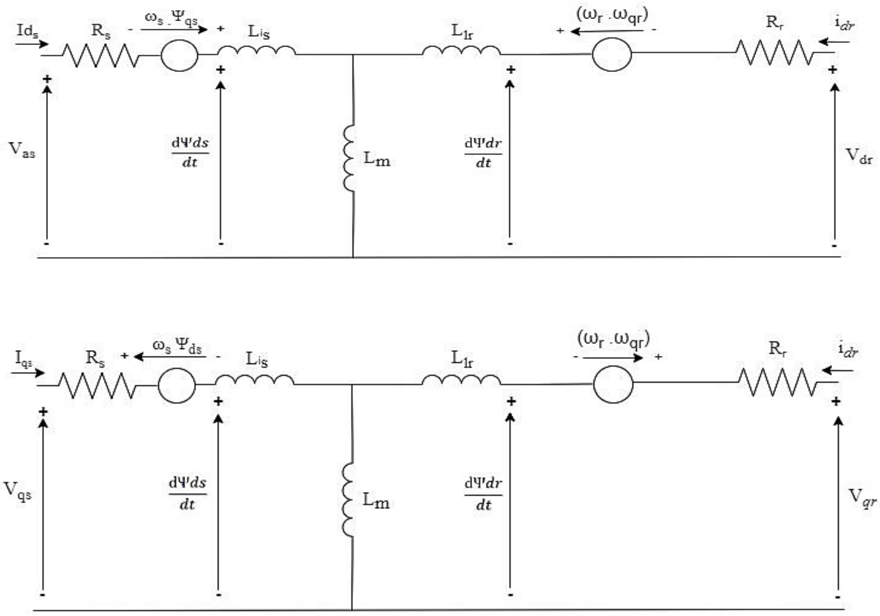

Figure 3.10 dq Synchronous Coordinate Model of the DFIG.

Consequently, the torque expression produces:

$$T_{em} = \frac{3}{2}p\frac{L_m}{L_s}\mathrm{Im}\left\{\overrightarrow{\psi_s} \cdot \overrightarrow{i_r^*}\right\} = \frac{3}{2}p\frac{L_m}{L_s}(\psi_{qs}i_{dr} - \psi_{ds}i_{qr}) \tag{3.60}$$

Similarly, all of the comparable torque formulas in Equation (3.47) remain unchanged. To simplify the power and torque formulas, superscripts for space vectors have been removed.

3.9.3 State-space Representation of the $\alpha\beta$ Model

A state-space equation representation of model $\alpha\beta$ is essential for computer simulation. The DFIG model can be expressed as follows by rearranging Equations (3.38)-(3.41) and defining fluxes as state-space variables:

$$\frac{d}{dt}\begin{bmatrix}\overrightarrow{\psi_s^s}\\ \overrightarrow{\psi_r^s}\end{bmatrix}=\begin{bmatrix}-\dfrac{R_s}{\sigma L_s} & \dfrac{R_s L_m}{\sigma L_s L_r}\\ \dfrac{R_s L_m}{\sigma L_s L_r} & -\dfrac{R_s}{\sigma L_r}+j\omega_m\end{bmatrix}\cdot\begin{bmatrix}\overrightarrow{\psi_s^s}\\ \overrightarrow{\psi_r^s}\end{bmatrix}+\begin{bmatrix}\overrightarrow{V_s^s}\\ \overrightarrow{V_r^s}\end{bmatrix} \tag{3.61}$$

Expanding this last expression in the $\alpha\beta$ components, we get

$$\frac{d}{dt}\begin{bmatrix}\psi_{\alpha s}\\ \psi_{\beta s}\\ \psi_{\alpha r}\\ \psi_{\beta r}\end{bmatrix}=\begin{bmatrix}\dfrac{R_s}{\sigma L_s} & 0 & \dfrac{R_s L_m}{\sigma L_s L_r} & 0\\ 0 & -\dfrac{R_s}{\sigma L_s} & 0 & \dfrac{R_s L_m}{\sigma L_s L_r}\\ \dfrac{R_r L_m}{\sigma L_s L_r} & 0 & -\dfrac{R_r}{\sigma L_r} & -\omega_m\\ 0 & \dfrac{R_r L_m}{\sigma L_s L_r} & \omega_m & -\dfrac{R_r}{\sigma L_r}\end{bmatrix}\cdot\begin{bmatrix}\psi_{\alpha s}\\ \psi_{\beta s}\\ \psi_{\alpha r}\\ \psi_{\beta r}\end{bmatrix}+\begin{bmatrix}V_{\alpha s}\\ V_{\beta s}\\ V_{\alpha r}\\ V_{\beta r}\end{bmatrix} \tag{3.62}$$

Using currents as state-space magnitudes instead of fluxes yields the following DFIG comparable model:

$$\frac{d}{dt}\begin{bmatrix}\overrightarrow{i_s^s}\\ \overrightarrow{i_r^s}\end{bmatrix}=\left(\frac{1}{\sigma L_s L_r}\right)\begin{bmatrix}-R_s L_r - j\omega_m L_m^2 & R_r L_m - j\omega_m L_m L_r\\ R_s L_m + j\omega_m L_m L_s & -R_r L_s + j\omega_m L_r L_s\end{bmatrix}\cdot\begin{bmatrix}\overrightarrow{i_s^s}\\ \overrightarrow{i_r^s}\end{bmatrix}$$

$$+\left(\frac{1}{\sigma L_s L_r}\right)\begin{bmatrix}L_r & -L_m\\ -L_m & L_r\end{bmatrix}\cdot\begin{bmatrix}\overrightarrow{V_s^s}\\ \overrightarrow{V_r^s}\end{bmatrix} \tag{3.63 }$$

Expanding on the $\alpha\beta$ components, we have

$$\frac{d}{dt}\begin{bmatrix}i_{\alpha s}\\ i_{\beta s}\\ i_{\alpha r}\\ i_{\beta r}\end{bmatrix}=\begin{bmatrix}-R_s L_r & \omega_m L_m^2 & R_r L_m & \omega_m L_m L_r\\ -\omega_m L_m^2 & -R_s L_r & -\omega_m L_m L_r & R_r L_m\\ R_s L_m & -\omega_m L_s L_m & -R_r L_s & -\omega_m L_r L_s\\ \omega_m L_s L_m & R_s L_m & \omega_m L_r L_s & -R_r L_s\end{bmatrix}\cdot\begin{bmatrix}i_{\alpha s}\\ i_{\beta s}\\ i_{\alpha r}\\ i_{\beta r}\end{bmatrix}$$

$$+\left(\frac{1}{\sigma L_s L_r}\right)\begin{bmatrix} L_r & 0 & -L_m & 0 \\ 0 & L_r & 0 & -L_m \\ -L_m & 0 & L_s & 0 \\ 0 & -L_m & 0 & L_s \end{bmatrix}\cdot\begin{bmatrix} V_{\alpha s} \\ V_{\beta s} \\ V_{\alpha r} \\ V_{\beta r} \end{bmatrix} \tag{3.64}$$

3.9.4 State-space Representation of the dq Model

Continuing the analysis of the dynamic model, it is also feasible to derive state-space equations for the dq model representation. reorganizing Equations (3.50) – (3.53) and considering the fluxes as state-space variables, the DFIG model can be described as:

$$\frac{d}{dt}\begin{bmatrix} \overrightarrow{\psi_s^a} \\ \overrightarrow{\psi_r^a} \end{bmatrix} = \begin{bmatrix} -\frac{R_s}{\sigma L_s} - j\omega_s & \frac{R_s L_m}{\sigma L_s L_r} \\ \frac{R_r L_m}{\sigma L_s L_r} & -\frac{R_r}{\sigma L_r} - j\omega_r \end{bmatrix}\cdot\begin{bmatrix} \overrightarrow{\psi_s^a} \\ \overrightarrow{\psi_r^a} \end{bmatrix} + \begin{bmatrix} \overrightarrow{V_s^a} \\ \overrightarrow{V_r^a} \end{bmatrix} \tag{3.65}$$

Expanding this final expression by breaking it down into dq components gives us

$$\frac{d}{dt}\begin{bmatrix} \psi_{ds} \\ \psi_{qs} \\ \psi_{dr} \\ \psi_{qr} \end{bmatrix} = \begin{bmatrix} -\frac{R_s}{\sigma L_s} & \omega_s & \frac{R_s L_m}{\sigma L_s L_r} & 0 \\ -\omega_s & -\frac{R_s}{\sigma L_s} & 0 & \frac{R_s L_m}{\sigma L_s L_r} \\ \frac{R_r L_m}{\sigma L_s L_r} & 0 & -\frac{R_r}{\sigma L_r} & \omega_r \\ 0 & \frac{R_r L_m}{\sigma L_s L_r} & -\omega_r & -\frac{R_r}{\sigma L_r} \end{bmatrix}\cdot\begin{bmatrix} \psi_{ds} \\ \psi_{qs} \\ \psi_{dr} \\ \psi_{qr} \end{bmatrix} + \begin{bmatrix} V_{ds} \\ V_{qs} \\ V_{dr} \\ V_{qr} \end{bmatrix} \tag{3.66}$$

If the currents are selected as the state-space instead of the fluxes, once more. The DFIG's equivalent model is expressed as shown for different magnitudes synchronized coordinate system.

$$\frac{d}{dt}\begin{bmatrix} \overrightarrow{i_s^a} \\ \overrightarrow{i_r^a} \end{bmatrix} = \left(\frac{1}{\sigma L_s L_r}\right)\begin{bmatrix} -R_s L_r - j\omega_m L_m^2 - j\omega_s \sigma L_s L_r & R_r L_m - j\omega_m L_m L_r \\ R_s L_m + j\omega_m L_m L_s & -R_r L_s + j\omega_m L_r L_s - j\omega_s \sigma L_s L_r \end{bmatrix}\cdot\begin{bmatrix} \overrightarrow{i_s^a} \\ \overrightarrow{i_r^a} \end{bmatrix}$$

$$+\left(\frac{1}{\sigma L_s L_r}\right)\begin{bmatrix} L_r & -L_m \\ -L_m & L_s \end{bmatrix}\cdot\begin{bmatrix} \overrightarrow{V_s^a} \\ \overrightarrow{V_r^a} \end{bmatrix} \tag{3.67}$$

When we expand in dq components, we discover

$$\frac{d}{dt}\begin{bmatrix} i_{ds} \\ i_{qs} \\ i_{dr} \\ i_{qr} \end{bmatrix} = \left(\frac{1}{\sigma L_s L_r}\right)\begin{bmatrix} -R_s L_r & \omega_m L_m^2 + \omega_s \sigma L_s L_r & R_r L_m & \omega_m L_m L_r \\ \omega_m L_m^2 - \omega_s \sigma L_s L_r & -R_s L_r & -\omega_m L_m L_r & R_r L_m \\ -R_s L_m & -\omega_m L_s L_m & -R_r L_s & -\omega_m L_r L_s + \omega_s \sigma L_s L_r \\ \omega_m L_s L_m & R_s L_m & \omega_m L_r L_s - \omega_s \sigma L_s L_r & -R_r L_s \end{bmatrix} \cdot \begin{bmatrix} i_{ds} \\ i_{qs} \\ i_{dr} \\ i_{qr} \end{bmatrix}$$

$$+\left(\frac{1}{\sigma L_s L_r}\right)\cdot\begin{bmatrix} L_r & 0 & -L_m & 0 \\ 0 & L_r & 0 & -L_m \\ -L_m & 0 & L_s & 0 \\ 0 & -L_m & 0 & L_s \end{bmatrix}\cdot\begin{bmatrix} V_{ds} \\ V_{qs} \\ V_{dr} \\ V_{qr} \end{bmatrix} \tag{3.68}$$

State-space models of the DFIG in the dq reference frame exists. Particularly valuable in achieving a constant state for specified stator and rotor input levels of electrical potential.

3.10 Rotor Side Converter Control

Wind turbine systems using Doubly Fed Induction Generators (DFIG) typically use two types of converters: the rotor side converter (RSC) and the grid side converter (GSC). This thesis is on the rotor side converter (RSC), which regulates rotor currents to maximize power output and improve grid stability.

The Rotor Side Converter uses a vector control method in which the stator flux space vector and the reference frame's d-axis are aligned (Mwana Wa Kalaga Mbukani, 2017). Due to these decisions, the formulas for electromagnetic torque and reactive power can be expressed as:

$$T_{em} = -\frac{3}{2} p \frac{L_m}{L_s} |\vec{\psi}_s| i_{qr} \tag{3.69}$$

$$Q_s = -\frac{3}{2} \omega_s \frac{L_m}{L_s} |\vec{\psi}_s| (i_{dr} - \frac{|\vec{\psi}_s|}{L_m}) \tag{3.70}$$

This indicates that the machine's speed is controlled by the torque applied to the q rotor current component. The stator reactive power is managed by the d-component rotor current. Using stator flux and rotor currents, the voltage equation written as

$$V_{dr} = \mathrm{R}_r i_{dr} + \sigma L_r \frac{d}{dt} i_{dr} - \omega_r \sigma L_r i_{qr} \tag{3.71}$$

$$V_{qr} = \mathrm{R}_r i_{qr} + \sigma L_r \frac{d}{dt} i_{qr} - \omega_r \sigma L_r i_{dr} + \omega_r \frac{L_m}{L_s} |\vec{\psi}_s| \tag{3.72}$$

Where, $\sigma = 1 - \frac{L^2_m}{L_s L_r}$

3.11 Modelling of VSWT System

The primary components of the VSWT system consists of a turbine, a gearbox, and a double-fed induction generator working together to transform wind power into electricity. The WT captures wind power and converts it into energy from machines. The purpose of the gearbox is to boost speed and reduce the amount of torque. The generator changes mechanical energy into another form, which is transformed into electrical power. It is clear that the control challenge is greater in region 2 due to the intricate nature of the dynamics in this area. This study, therefore, focuses on modeling and controlling in this partial region. The mathematical model within this area is composed of equations describing the dynamics of the DFIG and the mechanical components. the dynamics include uncertainties in damping and resistance resulting from extended use and surrounding temperature conditions modifications (Boumerid-Benshila Amine, 2020). The DFIG based VSWT system is represented based on the orientation of the stator flux.

$$\begin{cases} \dot{\omega}_r = \frac{T_a}{J} - \frac{B+\Delta B}{J}\omega_r + \frac{3L_m\psi_s n_p N}{2L_s J} I_{rq} \\ \dot{I}_{rd} = \frac{L_s(R_r+\Delta R_r)}{L_m^2 - L_r L_s} I_{rd} + \omega_l I_{rq} - n_p N \omega_r I_{rq} + \frac{L_s}{L_r L_s - L_m^2} V_{rd} \\ \dot{I}_{rq} = \frac{L_m \psi_s n_p N}{L_r L_s - L_m^2}\omega_r - \omega_l I_{rd} + \frac{L_s(R_r+\Delta R_{r)}}{L_m^2 - L_r L_s} I_{rq} + n_p N \omega_r I_{rd} + \frac{L_s}{L_r L_s - L_m^2} V_{rq} - \frac{L_m \psi_s \omega_l}{L_r L_s - L_m^2} \end{cases} \tag{3.73}$$

Where ω_r is the WT rotor speed, I_{rd} is the d-component of rotor current, I_{rq} is the q-component of current, V_{rd} is the d-component of rotor voltage, V_{rq} is the q-component of rotor voltage. The aerodynamic torque T_a, damping and resistance parameter uncertainties (ΔB and ΔR_r), and constraints ($\Delta B \le 0.5B$ and $\Delta R_r \le 0.5R_r$) are satisfied. Equation (3.73) uses the following positive constraints: J represents the combined rotating parts' inertia, B represents the turbine's total external damping, N represents the gearbox ratio, ψ_s represents stator flux, and L_m represents mutual inductance. The stator leakage inductance is denoted as L_s , the rotor leakage inductance as L_r , and the rotor resistance as R_r. by defining:

$$M1 = 1/J, \quad \mathrm{M2} = B/J, \quad \Delta\mathrm{M2} = \Delta B/J, \quad \mathrm{M3} = 3L_m\psi_s n_p N / 2L_s J,$$
$$M4 = L_s R_r / L_m^2 - L_r L_s, \quad \Delta M4 = \Delta R_r L_s / L_m^2 - L_r L_s, \quad \mathrm{M5} = \omega_l,$$
$$M6 = n_p N, \quad \mathrm{M7} = L_s / L_r L_s - L_m^2, \quad \mathrm{M8} = L_m\psi_s n_p N / L_r L_s - L_m^2, \quad \mathrm{M9} = L_m\psi_s\omega_l / L_r L_s - L_m^2 \tag{3.74}$$

The VSWT model of Equation (3.73) becomes

$$\begin{cases} \dot{\omega}_r = \mathrm{M1T}_a - (M2 + \Delta M2)\omega_r + M3I_{rq} \\ \dot{I}_{rd} = (\mathrm{M4}+\Delta\mathrm{M4})\mathrm{I}_{rd} + M5I_{rq} - M6\omega_r I_{rq} + M7V_{rd} \\ \dot{I}_{rq} = (\mathrm{M4}+\Delta\mathrm{M4})\mathrm{I}_{rq} - M5I_{rd} - M6\omega_r I_{rd} + M7V_{rq} + M8\omega_r - M9 \end{cases} \tag{3.75}$$

CHAPTER FOUR

CONTROLLER DESIGN

4.1 Chapter Overview

This section presents a control approach for a variable-speed wind turbine system utilizing a double-fed induction generator, incorporating sliding mode. The primary goals involve maximizing power extraction by optimizing rotor speed and to comply with grid standards, stator reactive power is adjusted. The representation of the VSWT system model includes equations for non-linear aerodynamic torque and power coefficients. Sliding variables are used in the SMC control method to monitor the optimal rotor speed and regulate rotor current. The adaptive controller is implemented to reduce chattering effects with the super-twisting algorithm. Lyapunov stability analysis aims to find appropriate values of SMC control parameters for sliding variables to reach zero in a defined time frame. Utilizing fuzzy logic for control parameter adjustment enables the system to improve performance based on changing conditions and requirements. It enhances the system’s capacity to react to changes and oscillations in the wind environment. Combining adaptive fuzzy logic control with sliding mode control provides a control strategy that is more versatile and adaptable. This combined approach may lead to higher power extraction effectiveness, enhanced tracking of optimal operating points, and improved regulation of reactive power to satisfy grid requirements. Moreover, the adaptability of fuzzy logic control can enhance wind turbines' reliability and effectiveness by enabling them to withstand disruptions and uncertainties.

4.2 Design of Controller Using Sliding Mode

The variable is the foundation for developing the sliding mode technique, a control framework to tackle the limitations of non-linear control systems. The sliding mode is a technique for system control. Adjust feedback by setting a surface in advance. The system stays unaltered. What is controlled will be forced to the surface next, and the system’s behavior moves towards the desired equilibrium point. The primary characteristic of this command is that we simply have to guide the mistake towards a switching surface operation; it functions smoothly and efficiently. In the system behavior of sliding mode, there is no impact from any outside influences, simulating uncertainties and/or disturbances. The

VSWT system Equation (3.73) exhibits nonlinear dynamics, with the parameters $\omega_r I_{rq}$, $\omega_r I_{rd}$, and T_a being intrinsically a non-linear SMC approach for controlling partial loads.

The specified parameters for the generic sliding mode control (SMC) of the variable-speed wind turbine (VSWT) system consist of the following:

1. **Tracking error:** It is the diffrence between the desired and actual rotor speed,. Identified as ω_{opt} and ω_r respectively.
2. **Error of the d-axis component:** It shows the difference between the rotor current's actual d-axis component and the desired one. amounts are important factors to think about when designing a complete SMC plan for the VSWT system.

$$\begin{cases} e1 = \omega_{ref} - \omega_{opt} \\ e2 = \mathrm{I}_{rd\_ref} - I^{*}_{rd\_ref} \end{cases} \tag{4.1}$$

Next, the sliding variables are described in the following manner:

$$\sigma_1 = \mathrm{ce}_1 + \frac{d}{dt}e1 \quad (4.2\ a)$$

$$= c(\omega_{ref} - \omega_{opt}) + \frac{d}{dt}(\omega_{ref} - \omega_{opt}) \quad (4.2\ b)$$

$$= \dot{\omega}_{ref} + c\omega_{ref} - c\omega_{opt} - \dot{\omega}_{opt} \quad (4.2\ c)$$

Where $c > 0$

$$\sigma_2 = \mathrm{e}_2 = I_{rd\_ref} - I^{*}_{rd\_ref} \tag{4.3}$$

The first derivations of sliding variables, based on the VSWT system model, are

$$\dot{\sigma}_1 = \ddot{\mathrm{e}}_1 + \mathrm{c}\dot{\mathrm{e}}_1 \quad (4.4\ a)$$

$$= M_1\dot{T}_a + (c - M_2 - \Delta M_2)\dot{\omega}_r + M_3 M_7 V_{rq} - \ddot{\omega}_{opt} - c\dot{\omega}_{opt} \quad (4.4\ b)$$

$$+ M_3(M_4 + \Delta M_4)I_{rq} - M_5 I_{rd} + M_6\omega_r I_{rd} + M_8\omega_r - M_9$$

$$= Z_1 + M_3 M_7 V_{rq} \tag{4.4 c}$$

$$\dot{\sigma}_2 = \dot{e}_2 + \dot{I}_{rd\_ref} - I^*_{rd\_ref} \tag{4.5 a}$$

$$=(M_4 + \Delta M_4) I_{rd\_ref} - I^*_{rd\_ref} - M_5 I_{rq} - M_6 \omega_r I_{rq} + M_7 V_{rd} \tag{4.5 b}$$

$$=Z_2 + M_7 V_{rd} \tag{4.5 c}$$

where Z_1 and Z_2 contains the parameter perturbations

$$Z_1 = M_1 \dot{T}_a + (c - M_2 - \Delta M_2)\dot{\omega}_r - \ddot{\omega}_{opt} - c\dot{\omega}_{opt}$$

$$+M_3((M_4 + \Delta M_4) I_{rq} - M_5 I_{rd} + M_6 \omega_r I_{rd} + M_8 \omega_r - M_9) \tag{4.6}$$

$$Z_2 = (M_4 - \Delta M_4) I_{rd} - \dot{I}^*_{rd} + M_5 I_{rq} - M_6 \omega_r I_{rq} \tag{4.7}$$

In Equation (4.2) and (4.4), since $d\sigma_1 / dV_{rq} = 0$ and $d\dot{\sigma}_1 / dV_{rq} \neq 0$, the relative degree with respect to σ_1 equals to 1. Similarly, from Equation (4.3) and (4.5), the relative degree with respect to σ_2 is 1 as well. The selected method for implementing the standard SMC with the approaching law technique is the exponential approach law.

$$\dot{\sigma} = -\varepsilon \cdot \mathrm{sgn}(\sigma) - \delta \cdot \sigma \tag{4.8}$$

By incorporating Equation (4.8) with Equations (4.4) and (4.5), the derived rotor voltage component on the dq-axis can be formulated, with σ denoting the sliding variable, ε and δ as the specified parameters.

$$V_{rq} = \frac{1}{M_3 M_7}(-\varepsilon_1 \cdot \mathrm{sgn}(\sigma_1) - \delta_1 \cdot \sigma_1 - Z_1) \tag{4.9}$$

$$V_{rd} = \frac{1}{M_7}(-\varepsilon_2 \cdot \mathrm{sgn}(\sigma_2) - \delta_2 \cdot \sigma_2 - Z_2) \tag{4.10}$$

In the context mentioned, the values of ε_1, δ_1, ε_2, and δ_2 for control parameters are not specified or determined.

The controller is directly impacted by the presence of the switching term $\varepsilon \cdot \mathrm{sgn}(\sigma)$, leading to discontinuities in the control inputs V_{rd} and V_{rq}. As a result, this causes a noticeable chattering effect with fast and erratic fluctuations in the control signals.

Using the super-twisting algorithm, we can reconstruct the control inputs V_{rd} and V_{rd} with the following expression.

$$\begin{cases} \mathrm{V}_{rq} = \mathrm{u}_1 + u_2 \\ u_1 = -\lambda_1 |\sigma_1|^{1/2} \operatorname{sgn}(\sigma_1) \\ \dot{u}_2 = -\alpha_1 \operatorname{sgn}(\sigma_1) \end{cases} \tag{4.11}$$

$$\begin{cases} \mathrm{V}_{rd} = \mathrm{u}_3 + u_4 \\ u_3 = -\lambda_2 |\sigma_2|^{1/2} \operatorname{sgn}(\sigma_2) \\ \dot{u}_4 = -\alpha_2 \operatorname{sgn}(\sigma_2) \end{cases} \tag{4.12}$$

Unspecified control parameters include λ_1, α_1, λ_2, and α_2 values.

The important point to highlight is that the Sliding mode (SMC) control, which is supper-twisting, displays a discontinuity only in its derivative component. Therefore, the control inputs V_{rd} and V_{rq} in system Equation (4.11) and (4.12) stay continuous. In simpler terms, the SMC control effectively reduces the chattering effect while keeping all the advantages of traditional sliding mode control (SMC).

It is essential to maintain the stable functioning of a WT (Wind Turbine) system when implementing the SMC (Sliding Mode Control) scheme. Choosing the right control parameters is essential in reaching this goal. In this respect, employing the Lyapunov method is advantageous as it helps establish an appropriate range of control parameters. Using this method ensures that the wind turbine system operates smoothly and reliably. It is necessary to introduce the correct rotor voltage for the Doubly Fed Induction Generator (DFIG) in order to accurately track the rotor speed and reactive power of the Wind Turbine (WT) and match them with their set values. Achieving an accurate monitoring of the ideal rotor speed and guaranteeing that σ_1 and $\dot{\sigma}_1$ both reach zero in a limited timeframe requires focusing on the scopes of λ_1 & α_1. To begin with, a change in state is implemented to simplify this procedure.

$$y = \mathrm{Z}_1 - M_3 M_7 \alpha_1 \int_0^t \operatorname{sgn}(\sigma_1) d\tau \tag{4.13}$$

By taking Equation (4.13) into account and including it in the analysis, we can obtain

Equation (4.4) as an outcome.

$$\begin{cases} \dot{\sigma}_1 = -\mathrm{M}_3 M_7 \lambda_1 |\sigma_1|^{1/2} \operatorname{sgn}(\sigma_1) + y \\ \dot{y} = -\mathrm{M}_3 M_7 \lambda_1 |\sigma_1|^{1/2} \operatorname{sgn}(\sigma_1) + \dot{Z}_1 \end{cases} \tag{4.14}$$

As shown in Equation (4.6), the disturbance Z1 is differentiable, with its first-order derivative constrained to a uniform bound. As a result, it meets the condition stated.

$$\left|\dot{Z}_1\right| \le \Phi_1 \quad \forall \mathrm{t} > 0 \tag{4.15}$$

Where Φ_1 is a positive constant

At this point, we should choose the quadratic Lyapunov function.

$$\mathrm{V}(\sigma,\mathrm{y}) = \zeta^T P \zeta \tag{4.16}$$

The quadratic Lyapunov function can be defined as $\zeta = \begin{bmatrix} \zeta_1 & \zeta_2 \end{bmatrix}^T = \begin{bmatrix} |\sigma_1|^{1/2} \operatorname{sgn}(\sigma_1) & y \end{bmatrix}^T$,

and P is symmetric positive definite matrix chosen appropriately.

$$P = \begin{bmatrix} 2M_3M_7\alpha_1 + \frac{1}{2}M_3M_7\lambda_1 & -\frac{1}{2}M_3M_7\lambda_1 \\ -\frac{1}{2}M_3M_7\lambda_1 & 1 \end{bmatrix} \tag{4.17}$$

From $\frac{dx}{dt} = \dot{\mathrm{x}}\mathrm{sgn(x)}$ and Equation (4.15), ζ is deduced as

$$\dot{\zeta} = \frac{1}{|\zeta_1|}(A\zeta + B\hat{\dot{Z}}_1) \tag{4.18}$$

Where the matrix

$$A = \begin{bmatrix} -\frac{1}{2}M_3M_7\lambda_1 & \frac{1}{2} \\ -M_3M_7\alpha_1 & 0 \end{bmatrix}, \ \mathrm{B} = \begin{bmatrix} 0 & 1 \end{bmatrix}^T, \ \hat{\dot{Z}}_1 = |\zeta_1|\dot{Z}_1 \text{ and } C = \begin{bmatrix} 1 & 0 \end{bmatrix}$$

Through the calculation of the derivative of the Lyapunov function along the perturbed system's trajectories Equation (4.16), we can derive the subsequent expression.

$$\dot{\mathrm{V}}(\sigma,\mathrm{y}) = 2\zeta^T P \zeta \tag{4.19 a}$$

$$= \frac{1}{|\zeta_1|}(2\zeta^T A^T + 2\hat{\dot{Z}}_1 B^T)P\zeta \tag{4.19 b}$$

$$\leq \frac{1}{|\zeta_1|}(2\zeta^T A^T P\zeta + 2\hat{\dot{Z}}_1 B^T P\zeta + \Phi_1^2 - \hat{\dot{Z}}_1^2) \tag{4.19 c}$$

$$\Rightarrow \begin{cases} \lambda_2 > \dfrac{2(L_r L_s - L_m^2)}{L_s} \\ \alpha_2 > \dfrac{L_s\lambda_2^2}{4L_s\lambda_2 - 8(L_r L_s - L_m^2)} + \dfrac{\Phi_2^2(L_r L_s - L_m^2)}{L_s\lambda_2} \end{cases} \tag{4.20}$$

Choose $Q = -(A^T P + PA + \Phi_1^2 C^T C + PBB^T P)$, Then

$$\dot{V} \leq -\frac{1}{|\zeta_1|}\zeta^T Q\zeta \tag{4.21}$$

If the symmetric and positive definite matrix Q has a solution $\dot{V} \leq -\frac{1}{|\zeta_1|}\zeta^T Q\zeta < 0$, it meets the requirement outlined in the Lyapunov theorem. Consequently, the control system will reach the origin in a finite amount of time.

The matrix *Q* given as:

$$Q = -(A^T P + PA + \Phi_1^2 C^T C + PBB^T P) \tag{4.22 a}$$

$$= \begin{bmatrix} M_3^2 M_7^2(\frac{1}{2}M_3^2 M_7^2\lambda_1^3 + \lambda_1\alpha_1 - \frac{1}{4}\lambda_1^2) - \Phi_1^2 & \frac{1}{2}M_3 M_7(\lambda_1 - M_3 M_7\lambda_1^2 \\ \frac{1}{2}M_3 M_7(\lambda_1 - M_3 M_7\lambda_1^2 & \frac{1}{2}M_3 M_7\lambda_1 - 1 \end{bmatrix} \tag{4.22 b}$$

In order to obtain finite-time convergence properties, we choose *Q* to be a matrix that is positive definite. To fulfill the requirements of λ_1 and α_1, the following criteria must be satisfied.

$$\begin{cases} \lambda_1 > \dfrac{2}{M_3 M_7} \\ \alpha_1 > \dfrac{M_3 M_7\lambda_1^2}{4(M_3 M_7\lambda_1 - 2)} + \dfrac{\Phi_1^2}{M_3 M_7\lambda_1} \end{cases} \tag{4.23 a}$$

$$\Rightarrow \begin{cases} \lambda_1 > \dfrac{4J(L_rL_s - L_m^2)}{3Nn_pL_m\varphi_s} \\ \alpha_1 > \dfrac{3L_m\varphi_s n_p N\lambda_1^2}{12L_m\varphi_s n_p N\lambda_1 - 16J(L_rL_s - L_m^2)} + \dfrac{2J\Phi_1^2(L_rL_s - L_m^2)}{3L_m\varphi_s n_p N\lambda_1} \end{cases} \tag{4.23 b}$$

Similarly, perturbation *Z2* demonstrates differentiability, as shown in Equation (4.7), with its initial derivative remaining consistently bounded to ensure completion.

$$\left|\dot{Z}_2\right| \leq \Phi_2 \qquad \forall t > 0 \tag{4.24}$$

The ranges for λ_2 and α_2 that ensure σ_2 and $\dot{\sigma}_2$ converge to '0' in a finite time are determined as shown below:

$$\begin{cases} \lambda_2 > \dfrac{2}{M_7} \\ \alpha_2 > \dfrac{M_7\lambda_1^2}{4(M_7\lambda_1 - 2)} + \dfrac{\Phi_1^2}{M_7\lambda_1} \end{cases} \tag{4.25 a}$$

$$\Rightarrow \begin{cases} \lambda_2 > \dfrac{2(L_rL_s - L_m^2)}{L_s} \\ \alpha_2 > \dfrac{L_s\lambda_2^2}{4L_s\lambda_2 - 8(L_rL_s - L_m^2)} + \dfrac{\Phi_2^2(L_rL_s - L_m^2)}{L_s\lambda_2} \end{cases} \tag{4.25 b}$$

If the values of λ_1, α_1, λ_2 and α_2 are within the bounds set by Equations (4.25 a) and (4.25 b), the DFIG-based WT system can function stably.

4.3 Control strategy by Adaptive fuzzy sliding mode

Control systems are essential in multiple industries, such as manufacturing and aerospace. The AFSM control method is now a leading contender among the many advanced control techniques. This method integrates Sliding mode control, Fuzzy logic, and adaptive mechanisms to offer robust and efficient control for nonlinear complex systems, consequently minimizing chattering.

The adaptive fuzzy sliding mode control method achieves the goals mentioned in the introduction by showing resilience to modeling uncertainties related to both the generator and the wind turbine. Therefore, it improves dependability, increases energy effectiveness, and lessens mechanical strain on the wind turbine transmission system overall through vibration prevention. The control law of adaptive fuzzy sliding mode control resembles that of traditional sliding mode control, with the exception of different parameters. The Adaptive Fuzzy sliding mode control adjusts components by employing fuzzy inference.

The control approach being suggested has a control law layout that mirrors that of Sliding Mode Control (SMC), except for the λ (lambda) and α (alpha) parameters. In this method, the component typically controlled by these parameters is adjusted in real-time by a fuzzy inference system. In the suggested control method for a variable-speed wind turbine system based on DFIG, the values λ_1 and α_1, linked to rotor speed modification, are modified in real-time using a fuzzy inference system (FIS) with inputs of tracking error (e_1) and rate of error change (de_1). The FIS utilizes five membership functions for every input to depict the operational range of these variables. Similarly, a separate FIS adjusts λ_2 (lambda2) and α_2 (alpha2) for regulating stator reactive power based on two inputs: reactive power error (e_2) and rate of change of error (de_2). This FIS also uses five membership functions for every input. The control signals "lambda_adjusted" and "alpha_adjusted" are calculated using a third FIS that has 25 membership functions. In order to track rotor speed control, this ultimate FIS uses five fuzzy rules to merge the input and output membership functions. Similarly, stator reactive power control involves the implementation of five fuzzy rules in the ultimate FIS. Overall, the control strategy requires creating 30 fuzzy rules to cover all potential combinations of input and output membership functions for both control goals. Therefore, the control gain become:

- For the first control gain pair:

$$\lambda_1\_adjusted = \lambda_1\_initial + \Delta\lambda_1 \qquad (4.26\ \text{a})$$

$$\alpha_1\_adjusted = \alpha_1\_initial + \Delta\alpha_1;\ \ \Delta\alpha_1 = FLC\ (e1, de1) \qquad (4.26\ \text{b})$$

- For the second control gain pair:

$$\lambda_2\_adjusted = \lambda_2\_initial + \Delta\lambda_2 \qquad (4.27\ \text{a})$$

$$\alpha_2\_adjusted = \alpha_2\_initial + \Delta\alpha_2;\ \ \Delta\alpha_2 = FLC\ (e2, de2) \qquad (4.27\ \text{b})$$

Under stable conditions, "lambda_adjusted" and "alpha_adjusted" approach a value of one in magnitude.

4.3.1 Fuzzy Logic controller Design

The concept of fuzzy logic resembles the way individuals preceive and decide on things. It sets itself apart from conventional control strategies, which employ a point-to-point method, by making use of range-to-range control. The result of a fuzzy controller is determined by converting its inputs and outputs using the correct membership functions. Different members of the membership function are linked to a clear inputs based on its value. Therefore, the output of the controllerimpacted by its MF in different membership functions, displaying a range of inputs. Fuzzy ideas and fuzzy logic are frequently used in our everyday tasks without much recognition. When taking surveys, individuals often provide responses such as ‘not very satisfied’ or ‘quit satisfied’, which may lack clarity or specificity. In these cases, the exact level of satisfaction or dissatisfaction with a certain service or product is unknown. These responses can only be generated and understood by humans, not machines. A computer cannot answer survey questions like a human does. Computers are limited to understanding binary choices like '0' or '1', or distinctions such as 'HIGH' or 'LOW'. This category of information is referred to as crisp or traditional data, and it can be used by various machines for processing. The Fuzzy Inference System (FIS) involves three primary steps: fuzzification, Inference engine, and defuzzification using knowledge as in Figure 4.1.

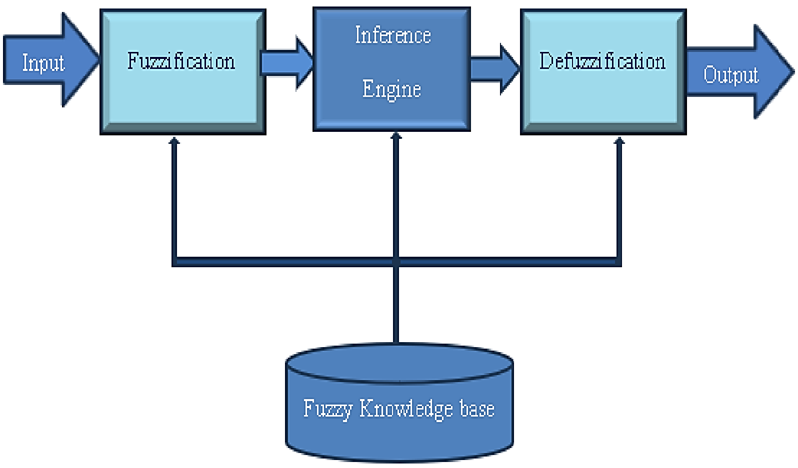

Figure 4.1 Structure of a Fuzzy Inference System

- **Fuzzification:** The process of creating a membership function (MF) and transforming precise inputs into fuzzy values through a conversion process. Different types of membership functions, including Gaussian, triangular, trapezoidal, and others, are utilized in this process.

- **Inference engine :** utilized to establish a link between fuzzy input and output by creating IF-THEN rules. The main distiniction between Mamdani and Sugeno inference systems is their defuzification techiques, making them the two primary type of FIS. The Mamdani FIS utilizes the Center of Gravity (COG) technique to de-fuzzify the fuzzy result and generate an accurate output. This involves determining the weighted average of the fuzzy output's membership function to obtain a single crisp value. On the contraary, the Sugeno-style FIS determines the accurate output using a weighted average method. The Sugeno-type FIS does not defuzzify the output into a single value, but calculates the crisp output by considering the input values and combining the weighted averages of the output fuzzy set.
- **Defuzzification** is a crucial step in fuzzy logic systems since it converts the vague and ambiguous fuzzy output into a specific and understandable output. Its essential function is to enhance the clarity and understandability of fuzzy logic results for further assessment and decision-making. Defuzzification employs various mathematical techniques and algorithms to obtain a singular representative value or a set of values from the fuzzy outcome, ultimately reducing the intricacy and ambiguity present in fuzzy computations. This process enables transforming vague outcomes into concrete actions or meaningful insights in real-life situations.

The FLC modifies control gains of the SOSMC to improve system performance through fuzzy logic rules. The FLC determines necessary adjustments to control gains by using both the error (e) and the derivative of error (de) as inputs. The Fuzzy Logic Controller (FLC) provides a practical choice for systems that do not need a mathematical model. This thesis involves the use of four inputs (e1, de1, e2, and de2) and four outputs (lambda1_adjusted, alpha1_adjusted, lambda2_adjusted, and alpha2_adjusted) by the FLC. The FLC uses these inputs to modify the control parameters of the Second-Order Sliding Mode (SOSM) controller. The main goals of the DFIG-based variable speed wind turbine system are to optimize wind energy extraction and control stator reactive power. In order to achieve these goals, the FLC utilizes five triangular membership functions for inputs and outputs, following the Mamdani FIS model. The membership functions have the following members: ZE (zero), PM (positive medium), NM (negative medium), and PB (positive big), and NB (negative big). In defuzzification, the centroid approach is applied. Tables 4.1 and 4.2

display the recommendations for the correct correlation between error e(t) and change in error de(t), where error values are presented in rows and change in error values are presented in columns.

Table 4-1 Fuzzy Rule for Rotor Speed Adjustment Fuzzy Rule for Rotor Speed Adjustment

e1 \ de1	**NB**	**NM**	**ZE**	**PM**	**PB**
NB	PB	PB	PB	PM	NB
NM	PM	PS	ZE	NS	NM
ZE	PS	ZE	ZE	NS	NB
PM	NS	NM	NM	NB	NB
PB	NB	NB	NB	NB	NB

1. If e1 is Negative Big (NB) and de1 is Negative Big (NB), Then, Increase λ_1 and α_1 by a Positive Big (PB) amount.
2. If e1 is Negative Small (NS) and de1 is Zero (ZE), Then, Increase λ_1 and α_1 by a Positive Small (PS) amount.
3. If e1 is Zero (ZE) and de1 is Zero (ZE), Then, No adjustment (ZE) for λ_1 and α_1.
4. If e1 is Positive Big (PB) and de1 is Positive Big (PB), Then, Decrease λ_1 and α_1 by a Negative Big (NB) amount.

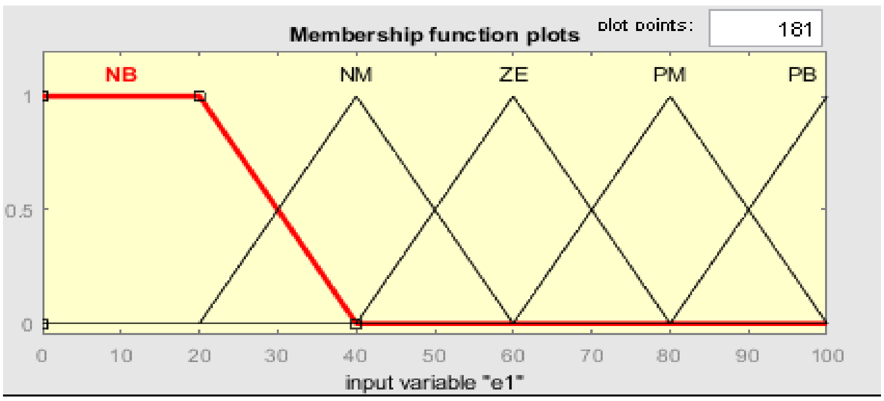

Figure 4.2 Fuzzy partition of input variable "e1"

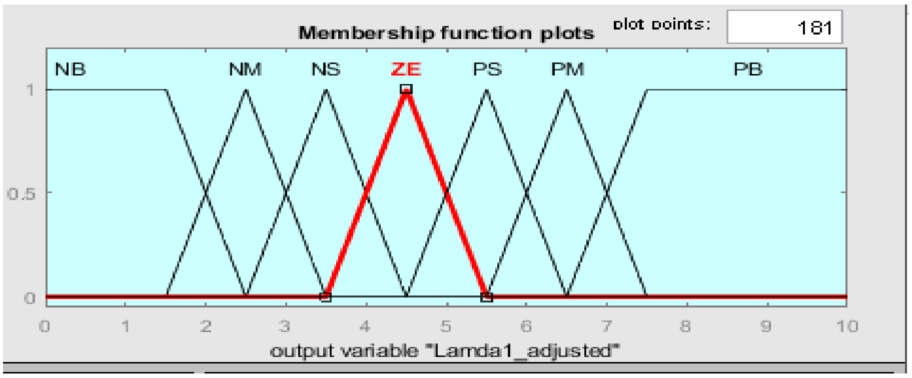

Figure 4.3 Fuzzy partition of output variable lambda1_adjusted

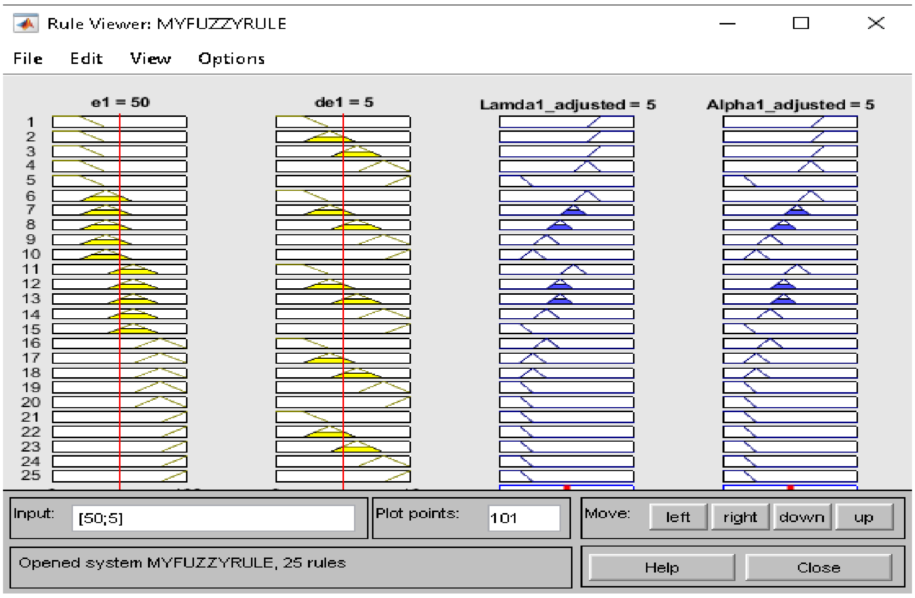

Figure 4.4 Fuzzy rule viewer

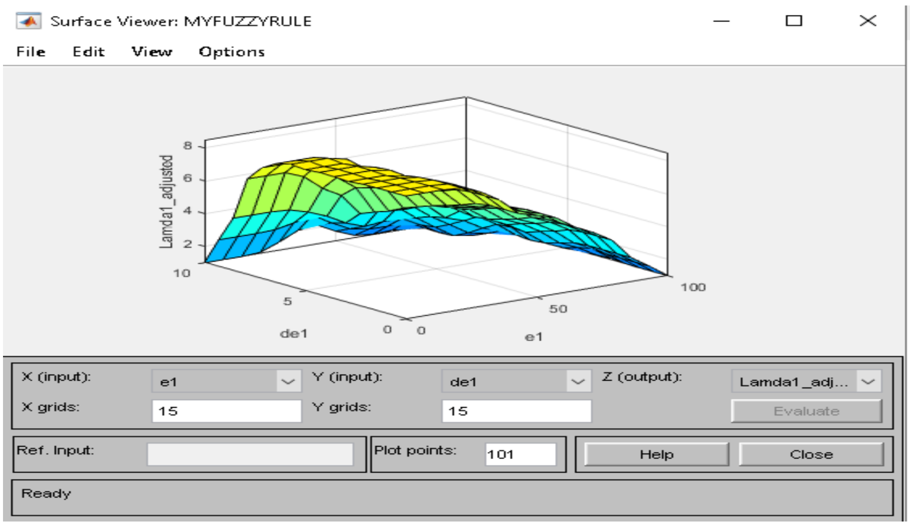

Figure 4.5 3D view of I/O relationship

Table 4-2 Fuzzy Rule for Stator Reactive Power Regulation

e2 \ de2	NB	NM	ZE	PM	PB
NB	PB	PM	ZE	NM	NB
NM	PM	PS	ZE	NS	NB
ZE	PS	ZE	ZE	NS	NB
PM	NS	NM	NM	NB	NB
PB	NB	NB	NB	NB	NB

1. If e2 is Negative Big (NB) and de2 is Negative Big (NB), Then, Increase λ_2 and α_2 by a Positive Big (PB) amount.
2. If e2 is Negative Small (NS) and de2 is Zero (ZE), Then, Increase λ_2 and α_2 by a Positive Small (PS) amount.
3. If e2 is Zero (ZE) and de2 is Zero (ZE), Then, No adjustment (ZE) for λ_2 and α_2.
4. If e2 is Positive Small (PS) and de2 is Positive Small (PS), Then, Decrease λ_2 and α_2 by a Negative Small (NS) amount.
5. If e2 is Positive Big (PB) and de2 is Positive Big (PB), Then, Decrease λ_2 and α_2 by a Negative Big (NB) amount.

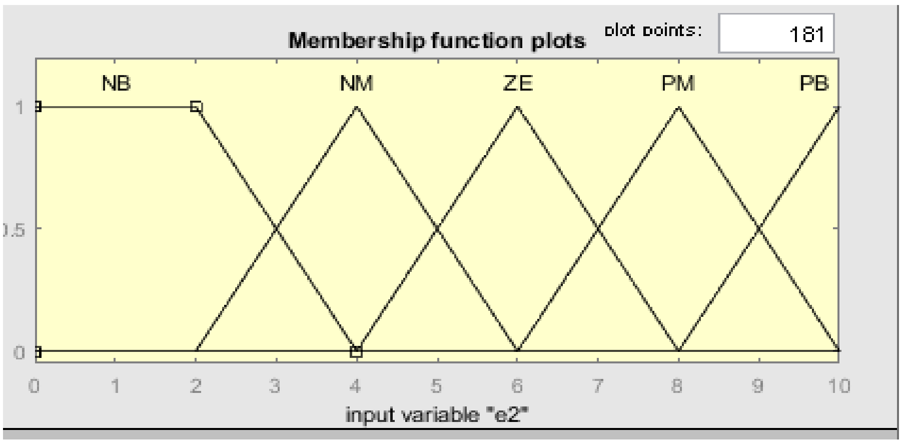

Figure 4.6 Fuzzy partition of input variable "e2"

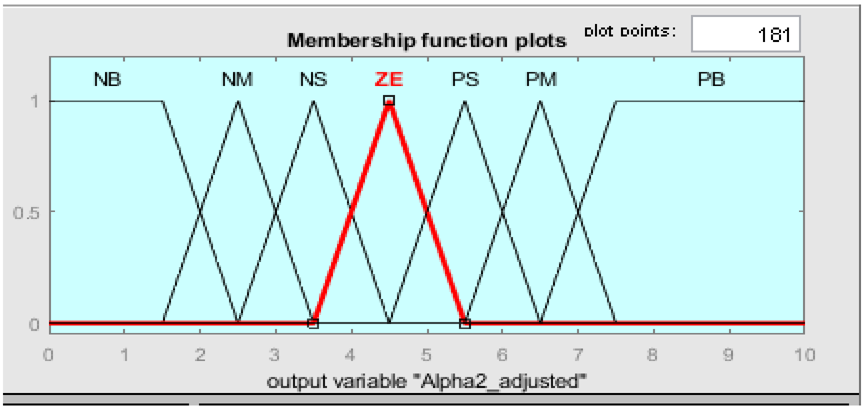

Figure 4.7 Fuzzy partition of output variable Alpha2_adjusted

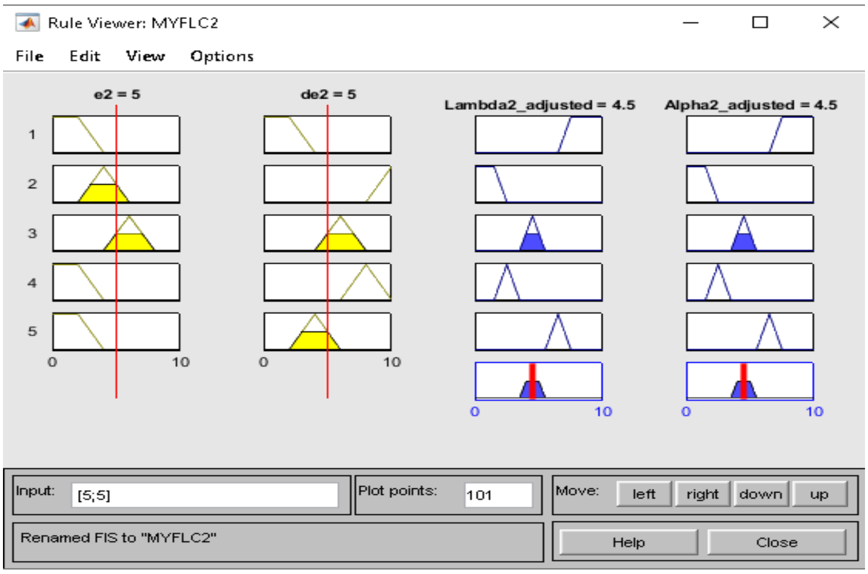

Figure 4.8 Rule viewer

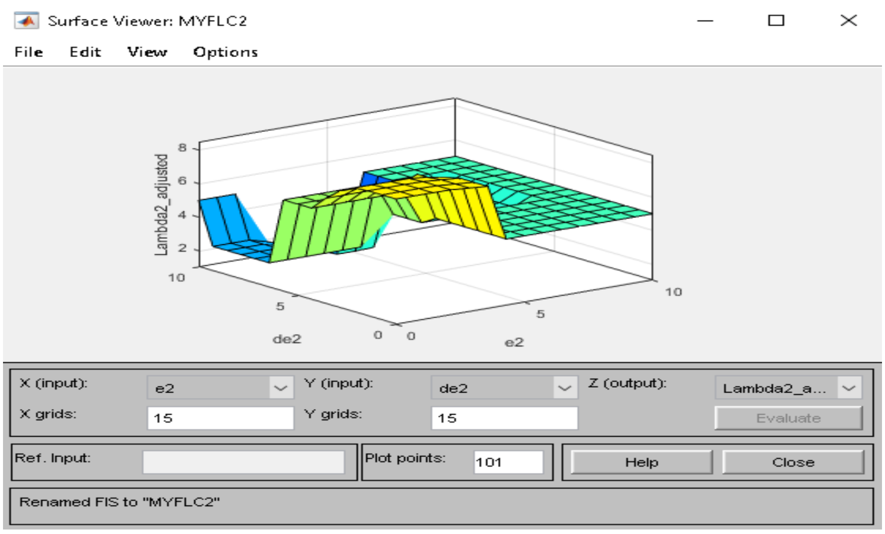

Figure 4.9 3D view of I/O relationship

CHAPTER FIVE

SIMULATION AND RESULT DISCUSSIONS

5.1 Chapter Overview

This chapter includes on the important step of simulating and evaluating results by using the design control technique in the previous chapter for wind turbine systems. This chapter aims to conduct an in-depth evaluation of Adaptive Fuzzy Sliding Mode Control (AFSMC) approaches through simulations carried out in the MATLAB/SIMULINK platform. The effectiveness and efficiency of the wind turbine control system are thoroughly verified during the simulation process.

5.2 Simulation Parameters

The parameters used for simulating the proposed system are based on data gathered from the ADAMA-II wind turbine, which include values such as rated power, voltage, current, frequency, speed, and various electrical and mechanical characteristics (Table 5-1). This ensures that the simulation closely mirrors real-world conditions.

Table 5-1 Parameters of the ADAMA-II WT generator and turbine.

Parameters	Value	Unit
Rated Power	1.5	MW
Number of Pole pair	2	---
Rated Stator Line-to-Line Voltage	690	V
Rated Voltage of Open Circuit	1650	V
Rated Stator Current	1110	A
Frequency	50	Hz
Rated Speed	1800	rpm

Speed Range	1000-2000	rpm
Cut-in Speed	3.5	m/s
Rated Speed	12	m/s
Cut-out Speed	25	m/s
Cp Max	0.4865	---
Lambda Opt	8.1	---
Rated Slip	0.2	---
Transformation Ratio, u	0.42	---
Rated Mechanical Torque	8.5922	K N-m
Stator Winding Resistance, Rs	0.006243	Ω
Rotor Winding Resistance, Rr	0.011074	Ω
Stator Leakage Inductance, Lls	0.198822	mH
Rotor Leakage Inductance, Llr	0.198822	mH
Magnetizing Inductance, Lm	3.976	mH
Inertia	67	---
Gearbox ratio, N	94.7	---
Blad Length	37	m
Rotor diameter	77	m
Dc-link Voltage	1150	V

Table 5-2 Controller parameters and values

Parameters	Values
c	45
λ_1	1×10^5
λ_2	1000
α_1	0.03
α_2	0.03

5.3 Wind Speed Simulation result

Figure5.1 depicts wind speed variations over a 10-unit time period, fluctuating between approximately 7.99 m/s and 8.025 m/s. These variations directly impact the rotor speed of the Doubly-Fed Induction Generator (DFIG) in wind turbines, which in turn affects power output. The adaptive fuzzy sliding mode control (AFSMC) strategy is effective in this context. By combining the robustness of sliding mode control with the adaptability of fuzzy logic, AFSMC dynamically adjusts rotor speed in response to fluctuating wind speeds, ensuring the turbine operates efficiently. This control method handles the inherent variability in wind speed, maintaining system stability and reducing chattering effects. Consequently, AFSMC helps keep the rotor speed within an optimal range, enhancing the efficiency of power capture and improving the overall performance of the WT system.

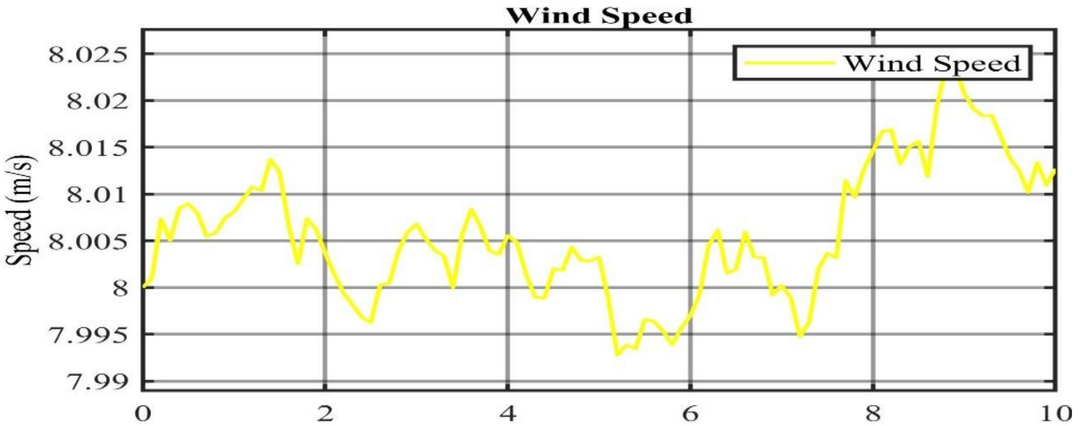

Figure 5.1 Wind speed over time

5.4 Rotor Speed Performance of a DFIG under Different Wind Conditions

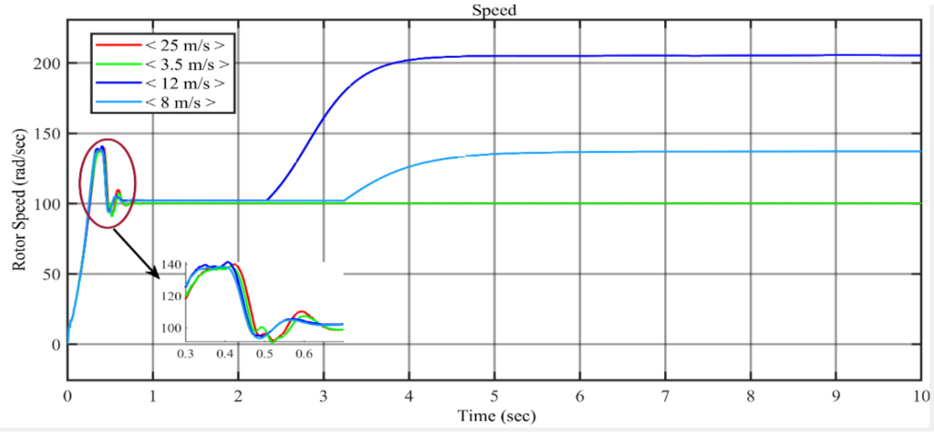

Figure 5.2 Rotor Speed Response to Wind Speed Variations

The above figure shows the rotor speed responses at different wind speeds: typically, 3.5 m/s, 8 m/s, 12 m/s, and 25 m/s.

At the lowest wind speed (3.5 m/s), the rotor speed reaches a peak of approximately 140 rad/sec at around 0.3 seconds, showing significant overshoot. This is followed by an undershoot to about 80 rad/sec before settling at around 100 rad/sec after 1 second. The rise time to reach the initial peak is less than 0.2 seconds.

For wind speeds of 8 m/s, the rotor speed increases more steadily, reaching a peak at around 1 second with less overshoot compared to the 3.5 m/s case. The undershoot is also less pronounced, and the speed stabilizes around 100 rad/sec by 1 seconds.

At wind speeds of 12 m/s, the rotor speed shows minimal overshoot and undershoot, reaching the desired speed of 142 rad/sec in about 6 seconds. The system stabilizes quickly within 1 second, demonstrating a stable and efficient response.

For the highest wind speed of 25 m/s, the rotor speed response exceeds the desired value, indicating an overshoot that can impact power output. The rotor speed reaches and slightly exceeds the desired speed of 142 rad/sec, stabilizing quickly but not without an initial overshoot. This behavior, although quickly stabilized, can affect the power output due to the brief period where the rotor speed exceeds the optimal value.

Overall, the rotor speed response at 12 m/s shows the most balanced performance with rapid rise time, minimal overshoot, and quick settling, ensuring efficient and stable operation. The response at 25 m/s, despite rapid rise time and quick settling, indicates an initial overshoot that could affect power output, suggesting a need for careful management at higher wind speeds to maintain optimal performance.

5.5 Simulation results without external disturbances

In order to test the designed controller's performance, simulations were carried out in controlled settings without taking into account external factors like grid changes, strong winds, or sensor inaccuracies. These findings provide a standard for assessing the controller's performance in a regulated setting.

The following section presents the simulation results for various parameters of a rotor under conditions without external disturbances. The results include the rotor speed, torque, and rotor currents in the d and q reference frames, as well as the rotor voltages in the d and q reference frames. Additionally, the stator voltage and both stator and rotor currents are analyzed in the a, b, and c reference frames. These simulations provide a comprehensive understanding of the rotor's behavior in a controlled environment, free from any external interference.

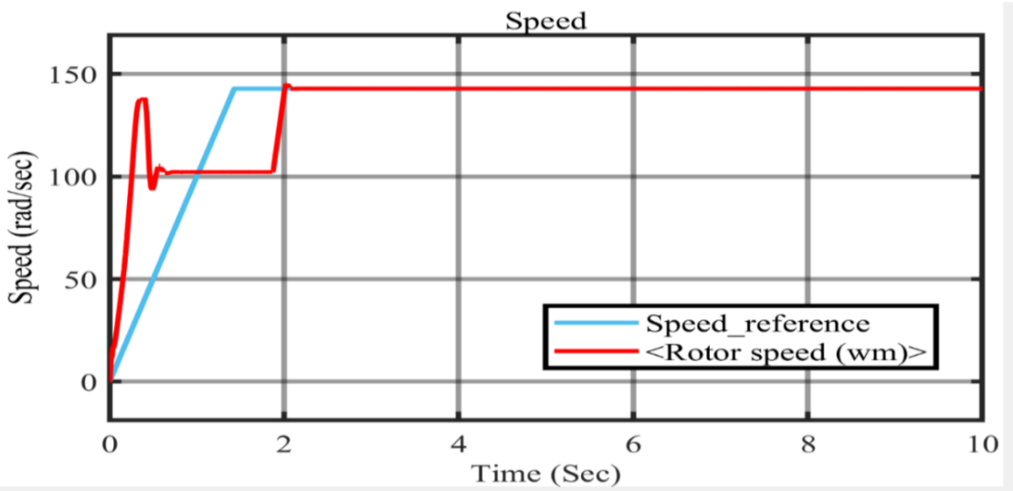

Figure 5.3 Rotor speed tracking response of a DFIG

Figure 5.3 illustrates the speed response of a rotor (red line) compared to a speed reference (blue line) over time. The rotor speed reaches its first peak at approximately 0.3328 seconds, with a speed of 136.8 rad/sec, indicating the peak time. After this initial peak, the rotor speed drops to its lowest point of 94.29 rad/sec at 0.4786 seconds, marking the undershoot. The rise time, which is the duration needed for the speed to increase from 10% to 90% of the final value, occurs before the peak time. The settling time, the time it takes for the rotor speed to stabilize within a certain percentage of the final value, is observed to be around 2.209 seconds, where the rotor speed stabilizes at 142.8 rad/sec.

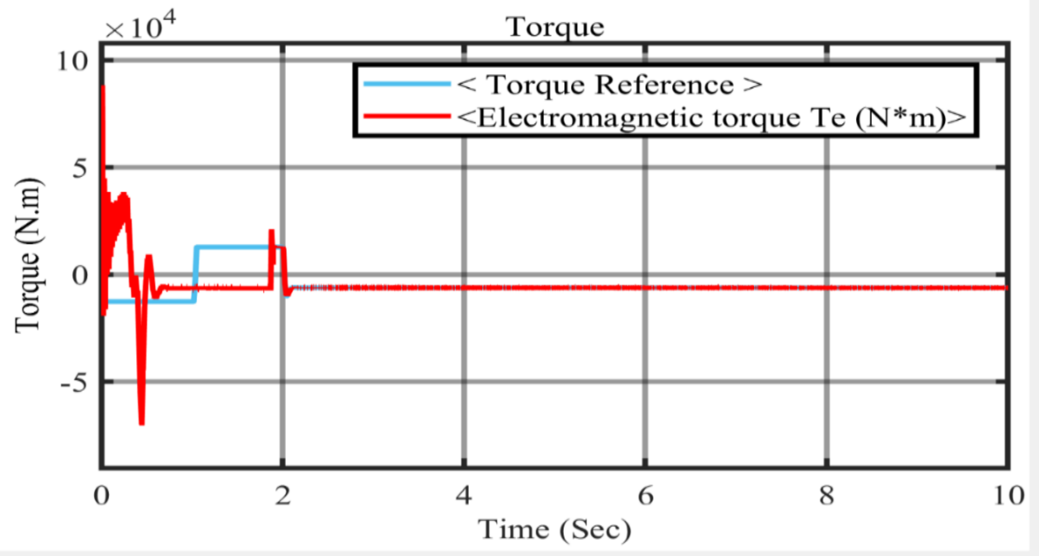

Figure 5.4 Torque tracking response of a DFIG

Figure 5.4 illustrates the electromagnetic torque response (in red) in comparison to the torque reference (in blue) over time. The torque signal reaches its first peak at approximately 0.01161 seconds, with a value of 8.805×10^{4} N·m, indicating a significant overshoot. Following this peak, the torque experiences a notable undershoot at 0.4467 seconds, dropping to -7.036×10^{4} N·m. The rise time, described as the amount of time needed to raise the final value from 10% to 90%., occurs very quickly before the peak time within the first 0.01161 seconds. The torque signal then stabilizes and settles around 3.354 seconds, maintaining a relatively constant value of approximately -6397 N·m. This analysis demonstrates the torque's rapid initial response, significant oscillations, and eventual stabilization.

The figure 5.5 shows the rotor current reaction Iqr in relation to the rotor reference current throughout time. The peak of the current reaction occurs at around 0.44525 seconds, reaching 1.2496×10^{4} A, showing a notable overshoot. At 0.53169 seconds, the current goes below zero, reaching -1.4717×10^{4} A. The time it takes for the signal to increase from 10% to 90% of its peak value, known as rise time, happens rapidly within the initial 0.44525 seconds before the peak. The signal settles at 1.2041×10^3 A after 2.2322 seconds, indicating the end of the settling period.

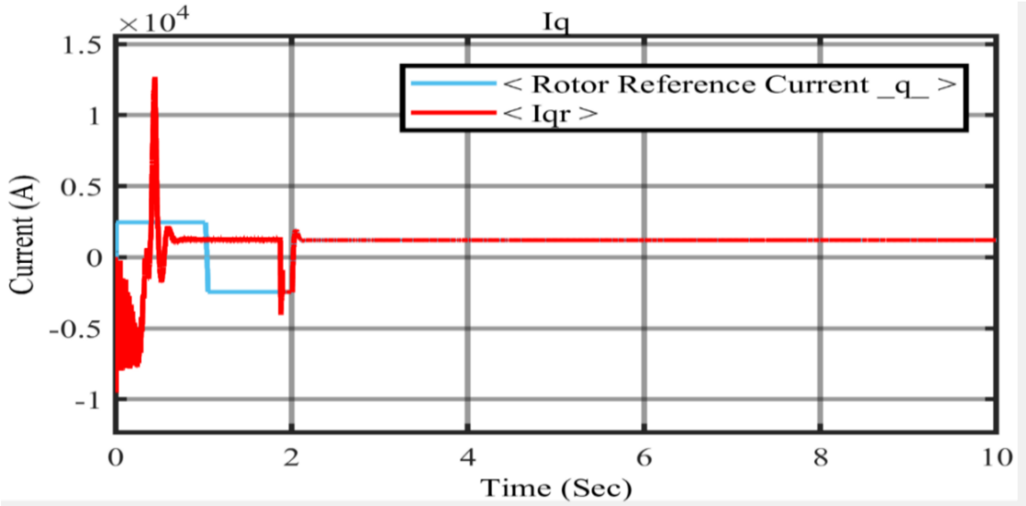

Figure 5.5 Response of rotor current (Iq) in a DFIG

Figure 5.6 displays the characteristics of a current response over a 10-second time span. The signal shows a significant initial peak at approximately 0.36694 seconds, reaching an overshoot of 19594.9287 A, followed by an undershoot around 0.44075 seconds, dipping to -6458.2134 A. The rise time, the duration for the signal to transition from its initial state to the peak, is roughly 0.13 seconds. The signal eventually settles close to 0 A, achieving a settling time of about 0.49694 seconds, stabilizing with minor oscillations around the reference line. By around 6 seconds, the current is almost constant, indicating a steady-state behavior, with a value near 0.3764 A, observed at 5.983 seconds.

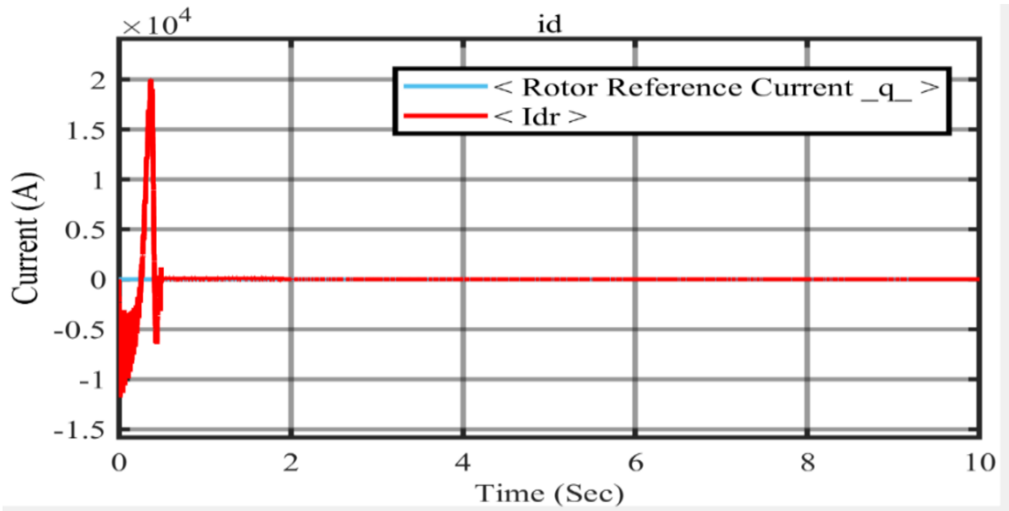

Figure 5.6 Response of rotor current (Iq) in a DFIG under ideal conditions

The provided voltage signal displays three phases: Vs (a), Vs (b), and Vs (c) over a time span of 10 seconds. All three phases show a similar waveform pattern. The voltage oscillates symmetrically around the Zero voltage level, with peak values of approximately 1.5×10^{-3} V and troughs of approximately -1.5×10^{-3} V. This indicates a peak-to-peak voltage swing of 3×10^{-3} V.

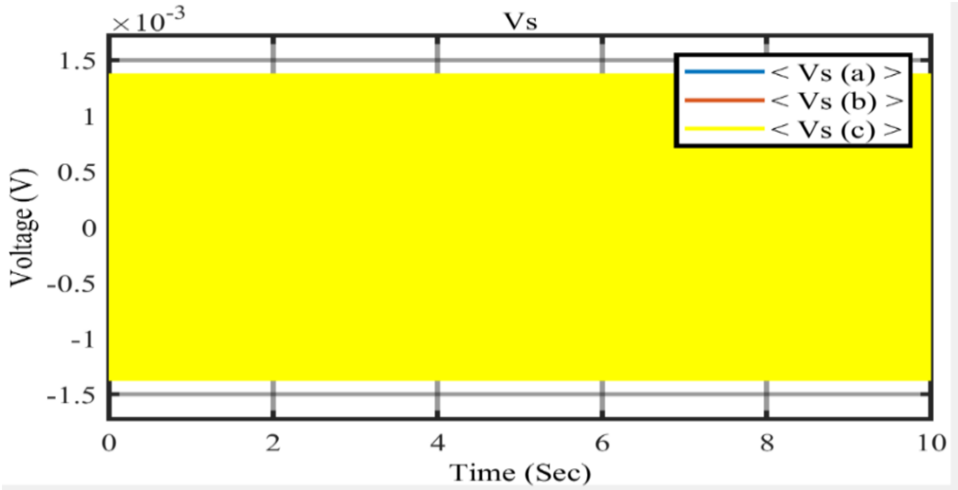

Figure 5.7 Response of stator voltage

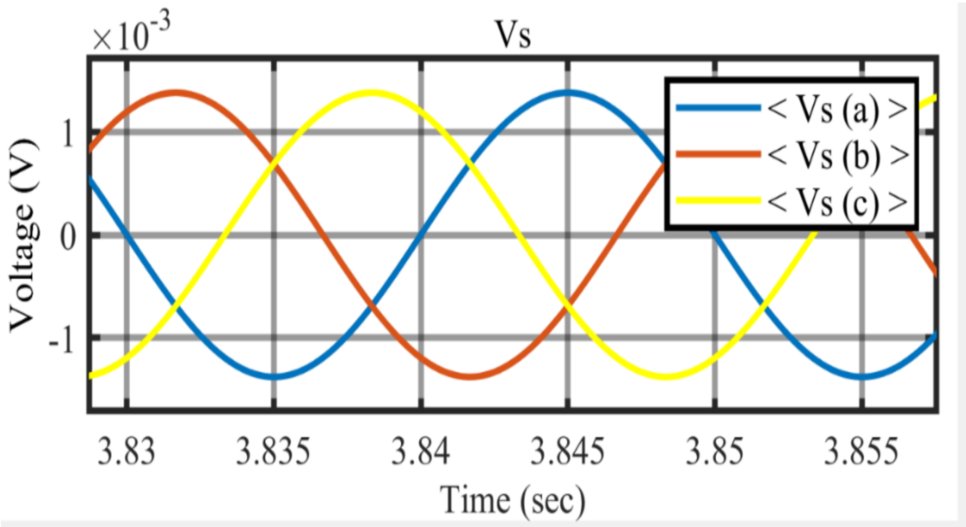

Figure 5.8 Zoom in stator voltage

The figures 5.9 and 5.10 display current signals Is and Ir for three phases over a 10-second interval, both showcasing initial large transient oscillations that dampen over time. The primary difference lies in their steady-state behaviors: Ir maintains small oscillations around zero, while Is stabilizes more distinctly to a near-zero current. This similarity in transient response and stabilization suggests they are measuring related aspects of a system, with Ir reflecting ongoing periodic activity and Is indicating a rapid stabilization to a less active state.

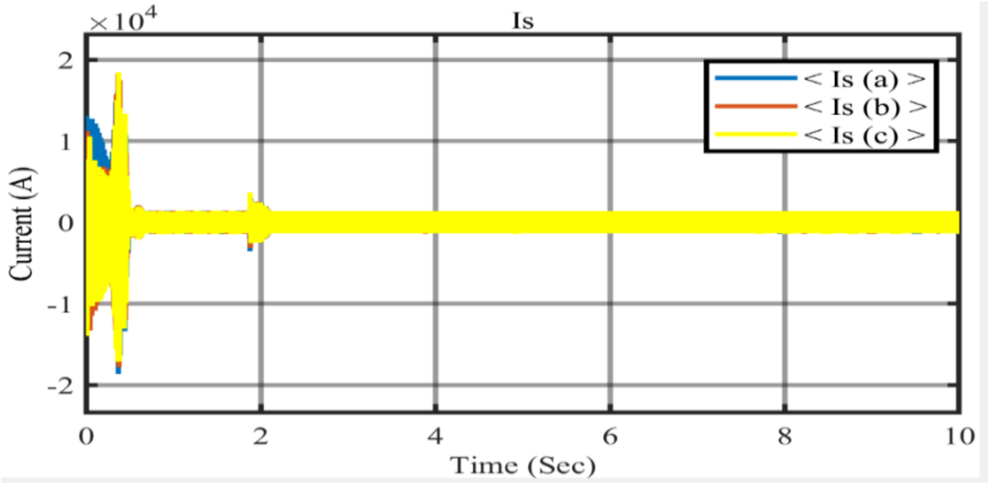

Figure 5.9 Response of three-phase stator currents in a DFIG

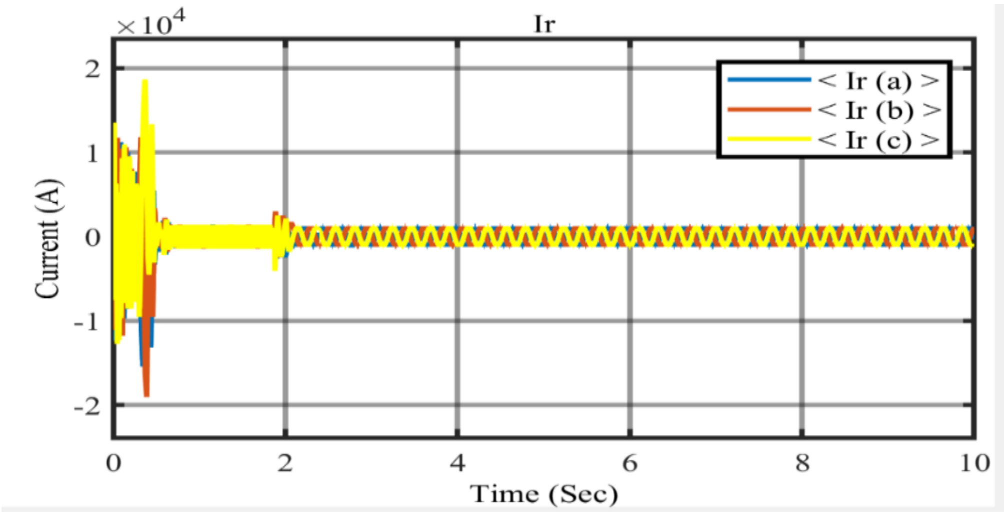

Figure 5.10 Response of three-Phase rotor currents in a DFIG

Figure 5.11 exhibits a significant overshoot, reaching a maximum of 695.3V at 0.007s, indicating a rapid response. There is a notable undershoot to -387.3V at 0.4475s before the signal begins to settle. The signal then gradually stabilizes and reaches a steady state near 0V by around 4.244s. This analysis shows that the system undergoes substantial initial oscillations before achieving stability.

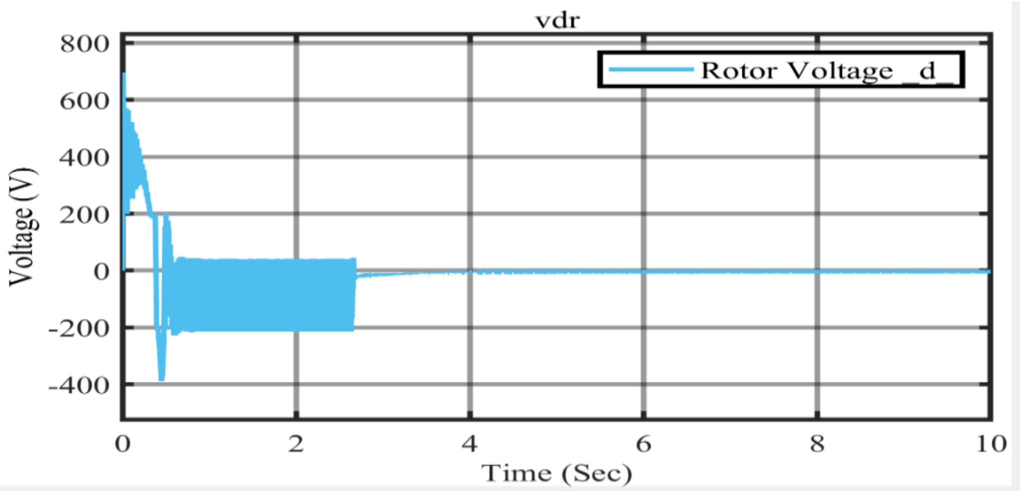

Figure 5.11 Response of rotor voltage (Vdr) in a DFIG

The rotor voltage Vqr signal exhibits a rapid rise to an overshoot peak of approximately 728.7V at 0.00025 seconds, indicating a very short rise time. This is followed by significant oscillations, with an undershoot reaching 226V at 0.4302 seconds. The signal stabilizes briefly around 441.1V at 0.4918 seconds before a sharp drop to 75.98V at 2.615 seconds. Finally, the signal settles near a steady-state value of 31.65V at approximately 5 seconds, demonstrating the system's dynamic response and eventual stabilization.

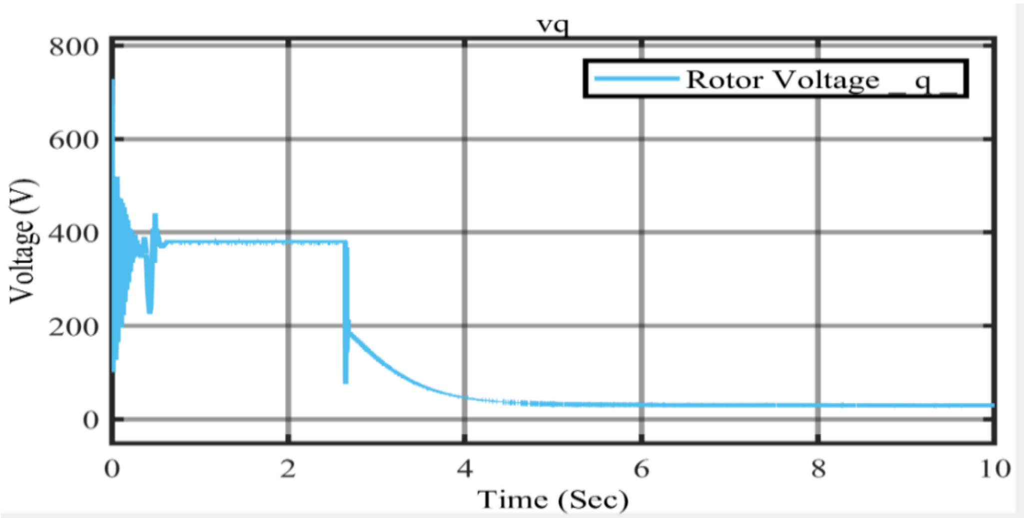

Figure 5.12 Response of rotor voltage (Vq) in a DFIG

5.6 Simulation of Control Systems.

This study develops an indirect speed control method to ensure that the aerodynamic torque follows the maximum power curve in response to varying wind conditions. Additionally, a vector controller is implemented to regulate the current loops of the rotor-side converter.

The system is based on a doubly fed induction generator (DFIG), featuring a wound rotor induction generator. The rotor is connected to a voltage source converter via slip rings, while the stator winding is directly connected to the grid, and the power converter is linked to the rotor winding

5.6.1 DFIG control under various wind speeds using a PI controller.

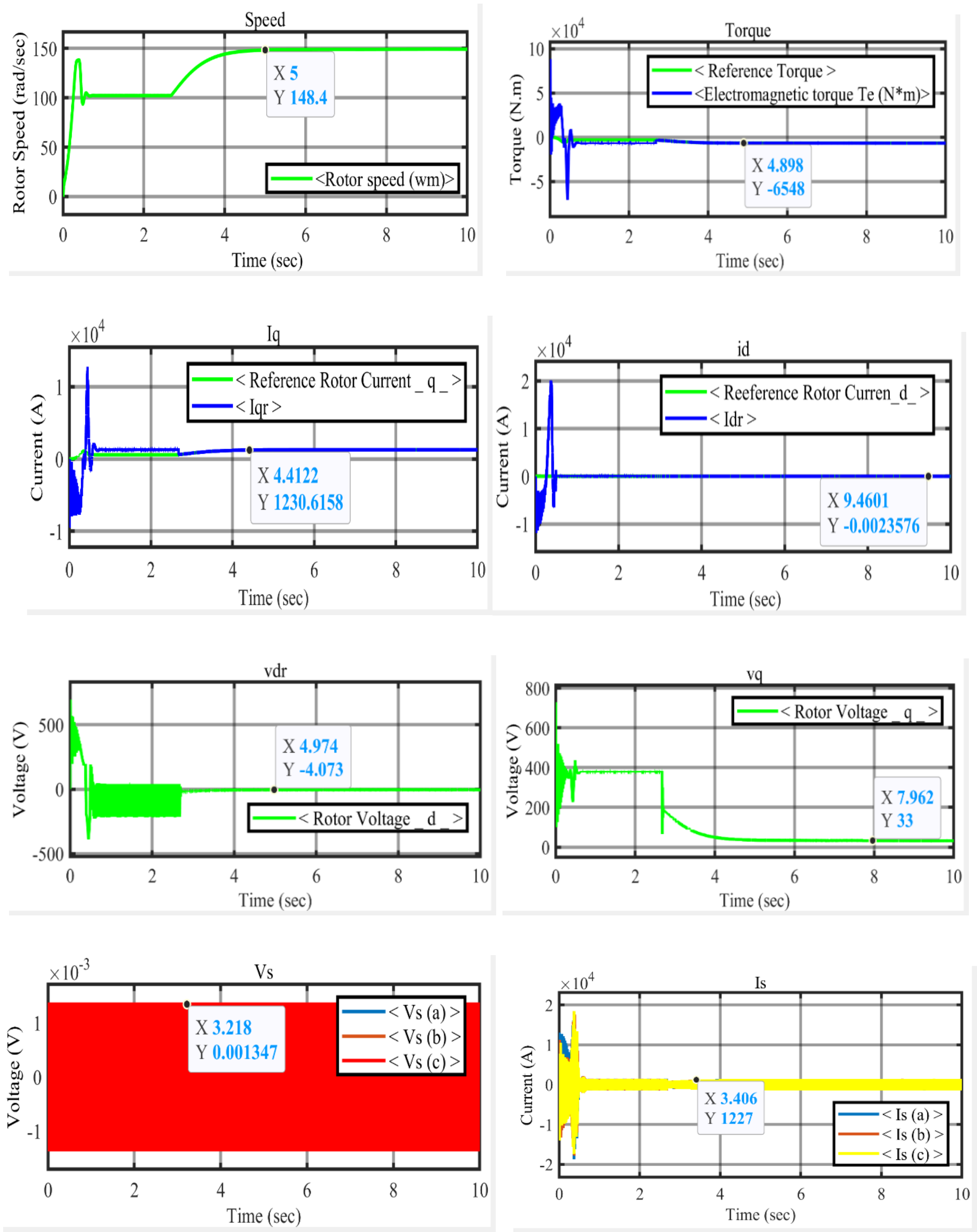

Figure 5.13 Simulation of DFIG with the PI controller

The PI controller demonstrates satisfactory performance in controlling the DFIG wind turbine. However, further tuning of the controller parameters might be necessary to optimize the transient response, and minimize overshoot and settling time. Additionally, for the system's robustness against external disturbances and fluctuations in operating conditions.

The peak overshoot, undershoot, steady-state error, and settling time of the rotor speed, electromagnetic torque, and rotor current components (i_q and i_d) are comprehensively analyzed and presented in Table 5-3.

Table 5-3 PI Controller performance metrics

	Rotor Speed (rad/sec)	Torque (N.m)	I_{qr} (A)	I_{dr} (A)
Peak overshoot	---	88040	12706	19697
Peak undershoot	94.26	-70560	-9538	-9969
Steady state error	---	---	0.0017	0.0135
Settling time (5%) (s)	4.952	4.107	3.979	3.721

5.6.2 Simulation outcomes for varying wind speeds utilizing Fuzzy Sliding mode controller (FSMC).

The Fig 5.13 shows the performance of the PI controller for various parameters, including rotor speed, torque, iqr, and idr. A notable limitation of the PI controller is the prolonged settling time for the idr component, which remains high and indicates sluggish system stabilization. Additionally, all parameters exhibit significant overshoot and undershoot, reflecting transient instability and suboptimal response characteristics. These deficiencies suggest that the PI controller is inadequate for meeting the desired system performance standards. To address these issues, an alternative control strategy with improved dynamic response, reduced overshoot, and faster settling times is required. This could involve advanced control strategy such as Fuzzy Sliding Mode Control (FSMC) to enhance system stability and efficiency.

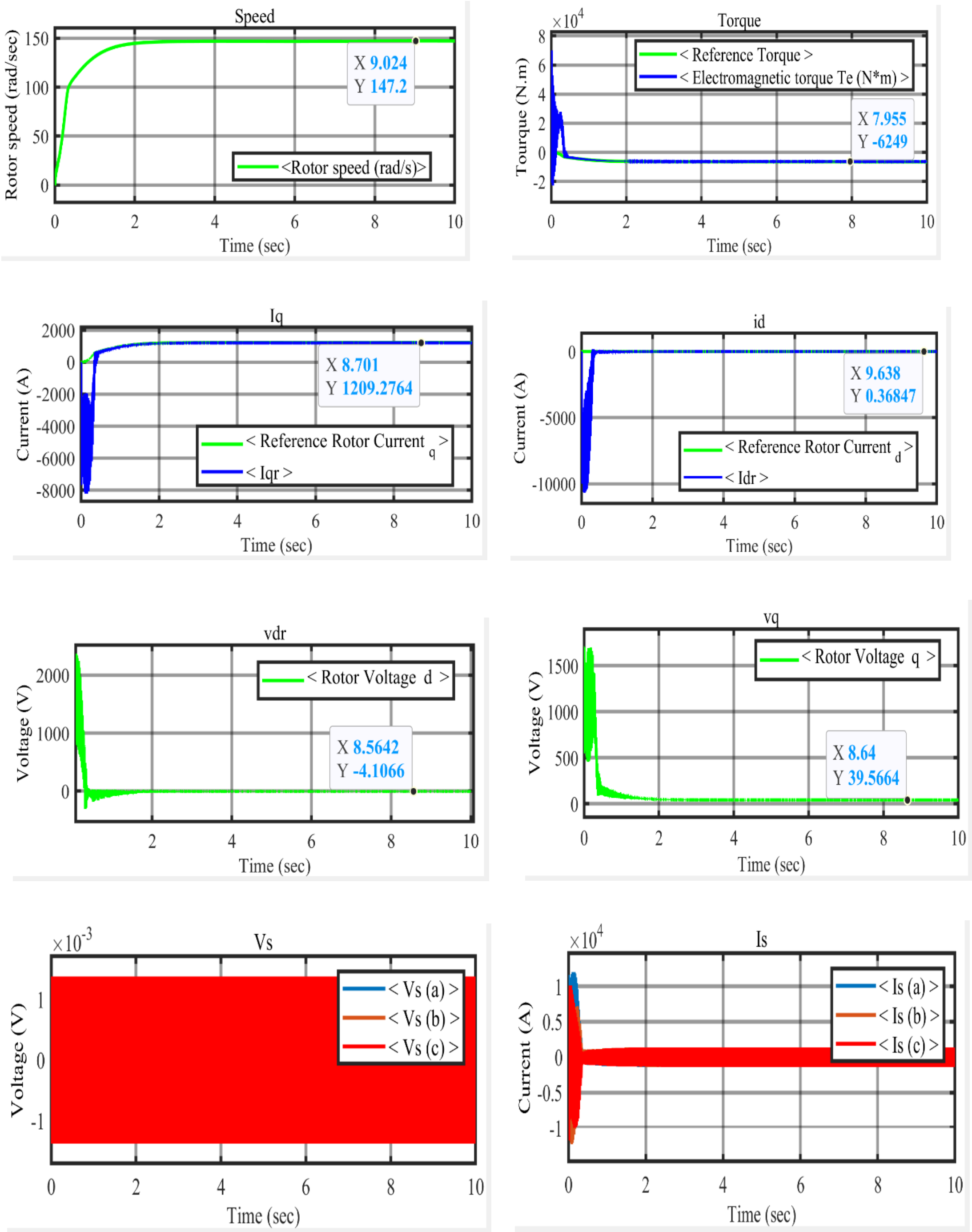

Figure 5.14 Dynamic Response of a DFIG with Fuzzy Sliding Mode Control

The system demonstrates accurate control dynamics and well-defined transient behavior. In about one second, the speed signal rises smoothly to about 147.2 rad/sec, with very little overshoot and complete stability by 3.625 seconds. The torque signal exhibits an early undershoot, peaking at around 0.5 seconds, and then settles with 4 seconds of minor oscillation at -6264 N·m. In a similar vein, there are brief transients in the voltages, rotor currents, and stator currents, but they soon stabilize, demonstrating the system's effective operation and good control.

5.6.3 Simulation outcomes for varying wind speeds utilizing Adaptive FuzzySliding mode controller (AFSMC).

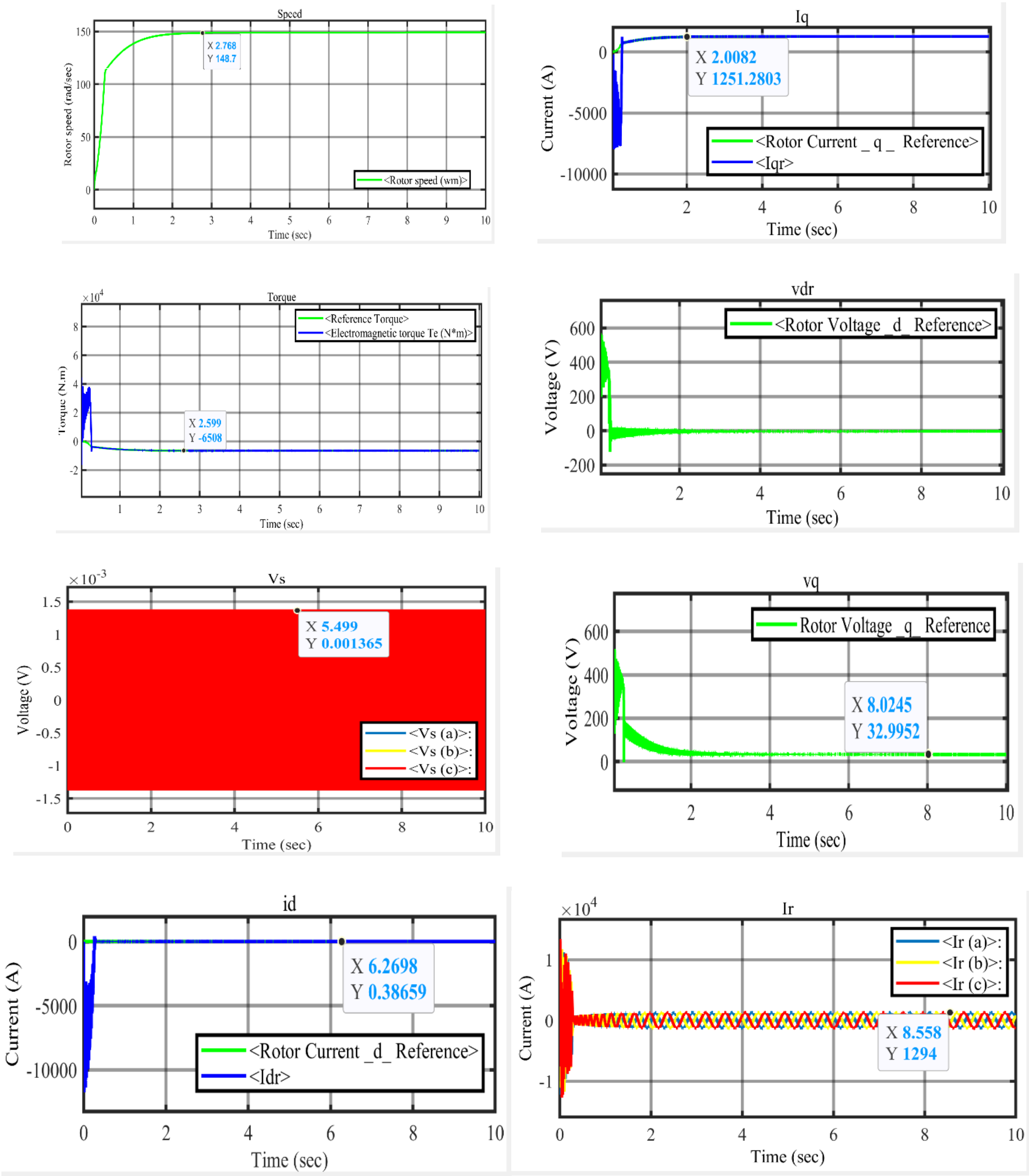

Figure 5.15 Dynamic Performance of a DFIG with Adaptive Fuzzy Sliding Mode Control

The AFSMC graph shows improved performance with reduced overshoot and quicker settling times across all parameters compared to the PI controller. For rotor speed, AFSMC stabilizes at 148.7 rad/sec in 2.768 seconds, whereas PI takes 4.952 seconds. The electromagnetic torque with AFSMC stabilizes at -6508 N·m in 2.6 seconds, compared to -

6548 N·m in 4.107 second with PI. The iqr current settles faster with AFSMC at 1251.2803 A in 2.0082 seconds versus 1230.6158 A in 3.979 seconds for PI. The idr current stabilizes in 0.2757 seconds at 0.33128 A with AFSMC, compared to 3.721 seconds and -0.0029895 A with PI. Rotor voltages vdr and vqr also show quicker stabilization and reduced oscillations with AFSMC. Overall, AFSMC provides enhanced stability and efficiency, making it superior for wind turbine systems.

5.6.4 Simulation Results of AFSMC-Based WT control: Steady-state Rotor speed and Electromagnetic Torque under varying wind speeds.

Figures from 5.16 to 5.18 shows the dynamic relationship between wind speed and energy output by showing how variations in wind speed direcly affects the rotor speed, which in turn changes the power generated. Increased rotor speed and torque at higher wind speeds greatly improves wind power extraction, but excessively high speeds can also results in inefficiencies.

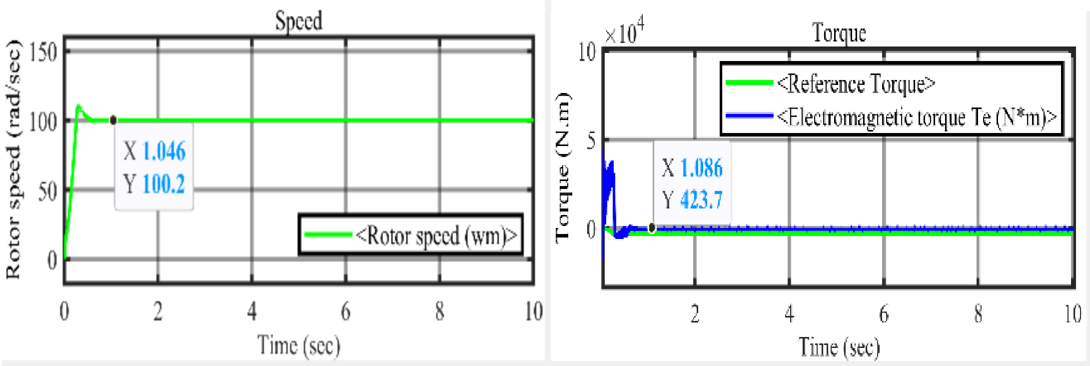

Figure 5.16 Simulation result of AFSMC at 3.75 m/s

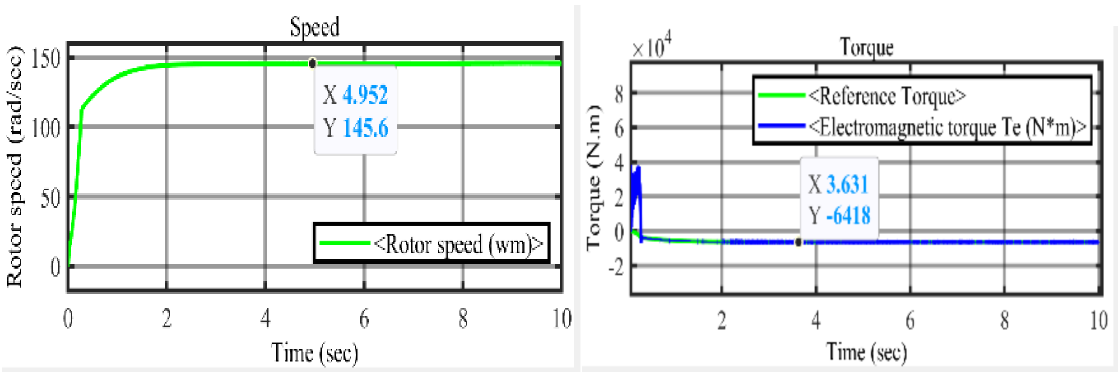

Figure 5.17 Simulation result of AFSMC at 7.2

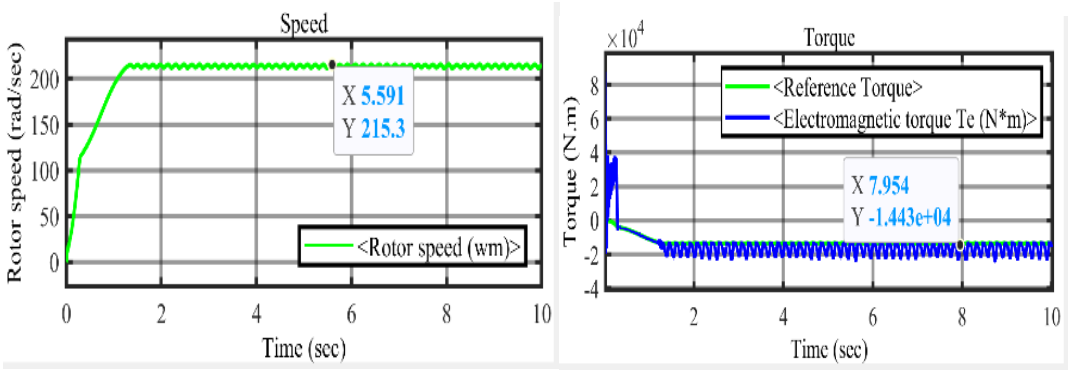

Figure 5.18 Simulation result of AFSMC at 13.5 m/s

Table 5-4 AFSM controller performance metrics.

	Rotor Speed (rad/sec)	Torque (N.m)	Idr (A)	Iqr (A)
Peak overshoot	---	38390	---	431.33
Peak undershoot	---	-7122	-7868.08	-10276.69
Steady state error	---	---	---	0.0410
Settling time (5%) (s)	2.768	2.6	2.0082	0.2752

5.6.5 Comparison between the PI, FSMC and AFSMC.

Figure 5.19 compares the performance of PI, FSMC, and AFSMC controllers for rotor speed of DFIG. The AFSMC controller demonstrates superior performance with a rise time of around 1.2 seconds, and a settling time of about 2.768 seconds. It shows negligible overshoot and undershoot, indicating high stability and accuracy. In contrast, the PI controller has a rise time of 1.5 seconds, and a settling time of around 4.952 seconds, with significant overshoot and oscillations. The FSMC controller performs better than PI with a rise time of 1.02 seconds, and a settling time of about 3.625 seconds, but still lags behind AFSMC in terms of stability and speed. Therefore, AFSMC offers the best control characteristics, ensuring rapid, stable, and accurate speed control.

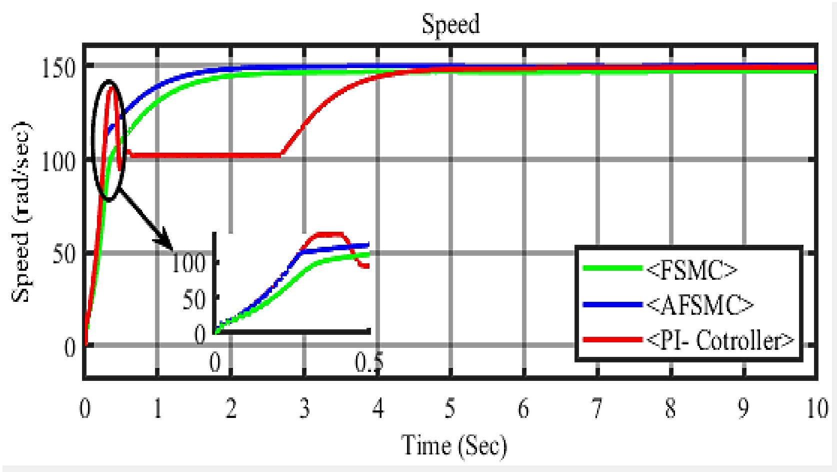

Figure 5.19 Performance Evaluation of PI, FSMC, and AFSMC for DFIG Speed Control

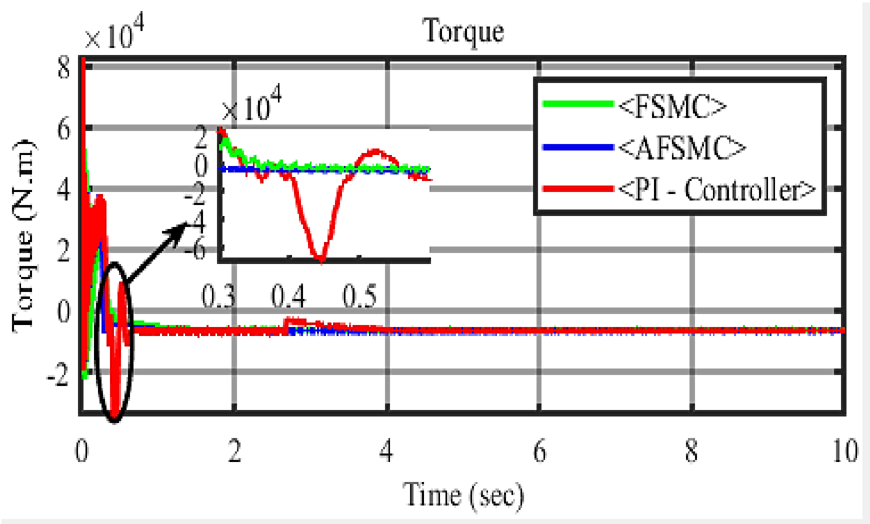

Figure 5.20 Performance Evaluation of PI, FSMC, and AFSMC for DFIG Torque Control.

Figure 5.20 shows a comparison of the torque reactions from PI, FSMC, and AFSMC controllers. The AFSMC controller shows top-notch performance, boasting a rise time of roughly 0.6 seconds, minimal overshoot and undershoot , and a settling time of approximately 2.6 seconds. However, the PI controller exhibits notable oscillations with a 0.9-second rise time, and approximately 4.107 second settling time. The FSMC controller outperforms PI but still falls short of AFSMC, with a rise time of 0.7 seconds, and settling time of approximately 4.0 seconds. Therefore, AFSMC offers excellent control features, guaranteeing quick, steady, and precise torque control.

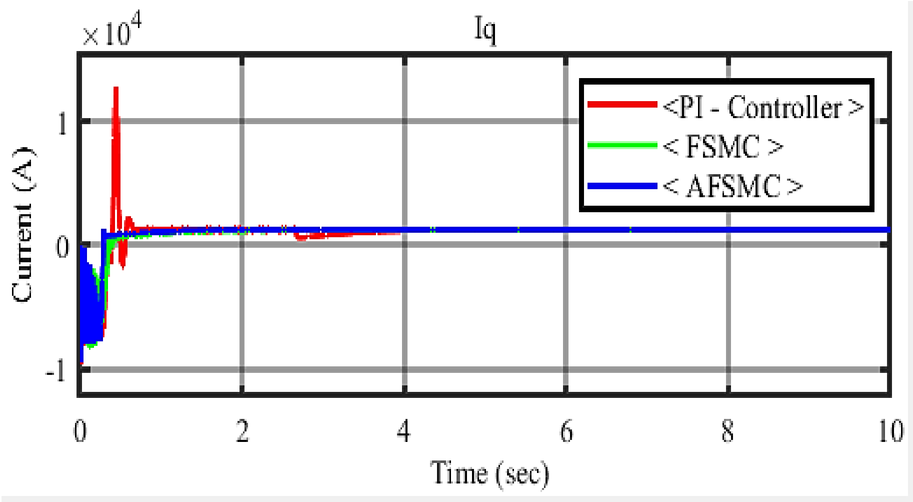

Figure 5.21 Performance Evaluation of PI, FSMC, and AFSMC in Controlling DFIG Iqr

The Figure 5.21 shows the comparison between the current response of PI, FSMC, and AFSMC controllers. The AFSMC controller shows the best performance with a rise time of around 0.02 seconds, a peak time of approximately 0.05 seconds, and minimal overshoot and undershoot, stabilizing quickly with a settling time of about 2.0082 seconds. In contrast, the PI controller exhibits significant oscillations with a rise time of 0.03 seconds, a peak time of 0.07 seconds, and a long settling time of around 3.979 seconds, showing considerable overshoot (reaching over 1×10^4A) and undershoot (dropping below -1×10^4A). The FSMC controller performs better than PI with a rise time of 0.03 seconds, a peak time of 0.06 seconds, and a settling time of about 3.5 seconds, but still has noticeable overshoot and undershoot. Thus, AFSMC provides superior control characteristics, ensuring rapid, stable, and accurate current control, making it better than the PI and FSMC controllers.

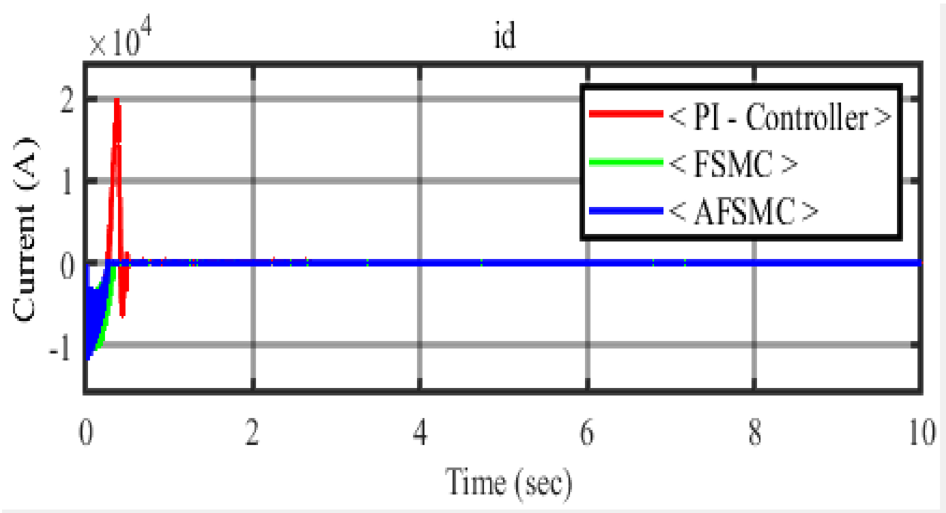

Figure 5.22 Current Profiles for PI, FSMC, and AFSMC Controllers

Figure 5.22 compares the effectiveness of three controllers: PI Controller, FSMC, and AFSMC by analyzing their impact on the current signal (id) over time. The horizontal axis represents time in seconds, spanning from 0 to 10 seconds, while the verical axis shows the current in amperes, ranging from approximately -1 to +2 ($\times 10^4$) amperes. The red curve, representing the PI controller, shows significant initial oscillations and an overshoot during the early phase (around 0.2 to 0.42 seconds). This overshoot is a key indicator of the PI controller's tendency to exceed the desired current level before gradually settling down. Although the signal eventually stabilizes around 0.6 seconds, the substantial overshoot and initial instability suggest that the PI controller struggles to quickly and accurately suppress disturbances. In contrast, the green curve, representing the FSMC, exhibits initial oscillations as well, but with a smaller overshoot compared to the PI controller. The FSMC signal stabilizes faster, between 0.2 to 0.3 seconds, showing an improved transient response. However, the presence of some oscillations before full stabilization indicates that FSMC still faces challenges in achieving perfect control. The blue curve, corresponding to the AFSMC, demonstrates the greatest performance among the three controllers. It shows minimal oscillations, a negligible overshoot, and a highly controlled and well-damped response. The signal quickly stabilizes to zero, more efficiently than both the PI controller and FSMC, highlighting AFSMC's superior ability to maintain stability and precision.

Overall, the graph illustrates that the AFSMC outperforms both the PI controller and FSMC in controlling the current. The AFSMC provides a faster, more stable response with minimal overshoot, making it the most effective of the three controllers. The PI controller, with its significant overshoot and slower stabilization, performs the worst, followed by the FSMC, which shows improvement but still struggles with some oscillations. This analysis suggests that AFSMC is particularly suitable for applications where precise, stable current control and minimal overshoot are essential.

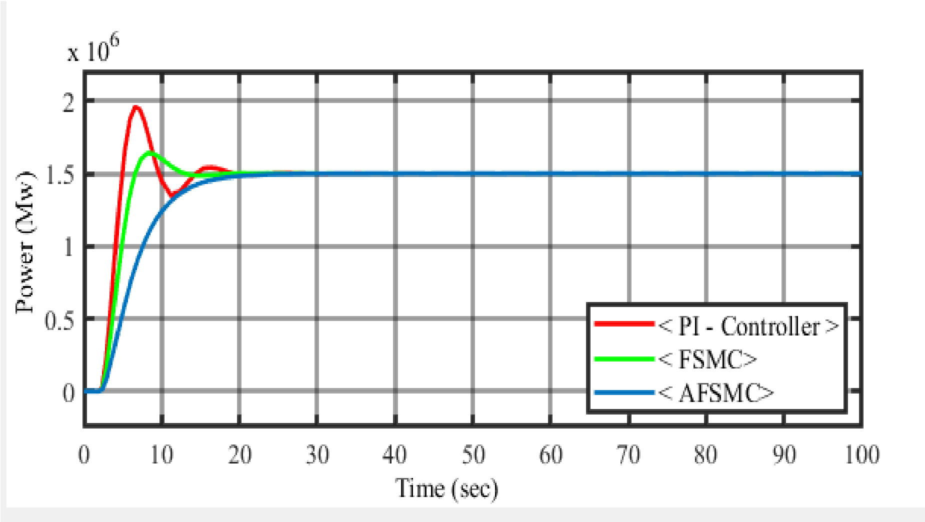

Figure 5.23 Comparative Power Response of AFSMC, FSMC, and PI Controllers.

Three control techniques (FSMC, AFSMC, and PI) aim to show the power output response of a DFIG-based wind turbine at a 1.5 MW outputs. When comparing the AFSMC controller to typical PI controller and FSMC, it is evident that the former performs better at stabilizing power output because it responds more quickly and has no overshoot.

CHAPTER SIX

CONCLUSION AND RECOMMENDATIONS

6.1 Conclusions

This thesis demonstrates the creation and assessment of Adaptive Fuzzy Sliding Mode Control (AFSMC) for DFIG wind turbines aimed at enhancing energy extraction and maintaining stability under various wind conditions. The proposed control approach effectively integrates the resilience of sliding mode control with the adaptability of fuzzy logic, addressing the challenges posed by nonlinearities and parameter uncertainties in DFIG systems.

Through MATLAB/SIMULINK simulations result, the AFSMC's performance was carefully evaluated. The results demonstrated significant improvements in key performance metrics compared to traditional control techniques such as Proportional-Integral (PI) and Fuzzy Sliding Mode Control (FSMC). Specifically, the AFSMC achieved a rise time of around 1.2 seconds for rotor speed control, indicating a rapid response to changes in wind conditions. The settling time was notably reduced to about 2.768 seconds, with minimal overshoot and undershoot, showcasing the controller's ability to maintain stability and precision in rotor speed tracking. Furthermore, the steady-state error was significantly minimized, ensuring that the rotor speed stabilized close to the desired reference value.

In terms of electromagnetic torque control, the AFSMC exhibited a rise time of roughly 0.21 seconds and a settling time of approximately 2.6 seconds. The torque response demonstrated minimal oscillations, reflecting the effectiveness of the AFSMC in regulating torque under varying operational conditions. The current responses (both direct and quadrature) also showed improved performance, with settling times of around 2.0082 and 0.2752 seconds respectively, further validating the controller's robustness.

The significance of this study lies in its contribution to improving the efficiency of wind energy conversion, providing a more robust solution to maximize power extraction. The AFSMC offers better adaptability to nonlinearities and uncertainties within wind energy systems, particularly in variable-speed scenarios. However, the controller's complexity is a notable limitation. Its computational demands may hinder real-time application, and the tuning process can be difficult without precise parameter adjustments. Additionally, the focus on simulations limits the validation of its practical applicability, as real-world factors like grid disturbances and extreme wind conditions were not thoroughly addressed.

6.2 Recommendations

It is advised for upcoming scholars to focus on:

1. Optimization techniques that can improve the Second-order Adaptive Fuzzy Sliding Mode Control. Wind turbine efficiency, resilience, and energy capture can all be increased by fine-tuning controller parameters using methods such as genetic algorithms or particle swarm optimization.
2. A deeper examination of the fluctuating patterns exhibited by wind turbines in varying operational scenarios.
3. The difficulties of implementing the control system in real-time, especially regarding the amount of computation needed and the hardware specifications.

Acknowledgements

The research for this paper was financially supported by Adama Science and Technology University, Adama, Ethiopia.

REFERENCES

A. A. Salem, N. A. (2021). *"Implementation and validation of an adaptive fuzzy logic controller for MPPT of PMSG-based wind turbines"* (Vol. 9).

Abate, A. (2019). "Optimal Controller Design for WTS Using USING DYNAMIC PROGRAMMING". *Addis Ababa Institute of Technology, Addis Ababa University*.

Ahmed G, A.-K. 1. (2019). "Dynamic Modeling of Wind Turbines Based on Estimated Wind Speed under Turbulent Conditions". *Energies*.

Aimin Pan, S. X. (2024). "Environmental impact of energy imports: Natural resources income and natural gas production profitability in the Asia-Pacific Economic Cooperation Countries". *Science Direct*.

Albadi, M. H. (2010). "On Techno-economic Evaluation ofWind-based DG". *Research Gate*.

Ayman Safwat1*, M. E.-G. (2020). "Controlling of a Wind Turbine Driving Doubly-Fed Induction Generator using Adaptive Fuzzy-Self Tuning Controller". *Paper Published in International Conference on Emerging and Renewable Energy Generation and Automation (ICEREGA'20).*

Ayyarao, T. S. (2019). "Modified vector controlled DFIG wind energy system based on barrier function adaptive sliding mode control". *Springer Open*.

Aziz Hadoune1, A. M. (2023). "Optimizing direct power controlof DFIG-based WECS usingsuper-twisting algorithm underreal wind profile". *Research Gate*.

Aziz Watil, A. E. (2020). "Multi-objective output feedback control strategy for a variable speed wind energy conversion system". *ELSEVIER*.

Belachew Desalegn, D. G. (2022). "Wind energy conversion technologies and engineering approaches to enhancing wind power generation: A review". *ScienceDirect*.

Betz, A. (2015). "WIND ENERGY CONVERSION THEORY, Betz Equation".

Bouchaib Rached, E. H. (2019). "Fuzzy Logic Control for Wind Energy Conversion System based on DFIG". *International Conference on Wireless Technologies, Embedded and Intelligent Systems (WITS).* Research Gate.

Bouchaib Rached, E. H. (April 2019). Fuzzy Logic Control for Wind Energy Conversion System based on DFIG. *Research Gate*.

Boumerid-Benshila Amine, A. A. (2020). "Modeling, Simulation and Control of a Doubly-Fed Induction Generator for Wind Energy Conversion Systems". *International Journal of Power Electronics and Drive Systems (IJPEDS)*.

Bri, Z. M. (2015). " Performance of an indirect field-oriented control for asynchronous machine". *International Journal of Engineering Technology*.

Cherngchai Sompracha, D. J. (2019). "Particle swarm optimisation technique to improve energy efficiency of doubly-fed induction generators for wind turbines". *The Journal of Engineering*.

ChristianT. (2010, August 14). *Wikipedia, the free encyclopedia*. Retrieved from Wikipedia, the free encyclopedia.

Elmostafa Chetouani, Y. E. (2023). " Self-adapting PI controller for grid-connected DFIG wind turbines based on recurrent neural network optimization control under unbalanced grid faults ". *ELSEVIER*.

Gonzalo Abad, J. L. (2018). " DOUBLY FED INDUCTION MODELING AND CONTROL FOR WIND ENERGY GENERATION ". *IEEE PRESS*, 209-210.

Group, B. o. (2019). "Wind Turbine Generators for Wind Power Plants".

Han, P. S. (2014). "Modeling, control and electromagnetic transient simulation of the doubly fed induction generator-based wind energy generation system". *journal in SAGE*.

Iliev, I. (2019). "Variable-speed operation of Francis turbines: A review of the perspectives and challenges". *ELSEVIER*, Pages 109-121.

Iulian Munteanu, A. I.-A. (2018). "Optimal Control of Wind Energy System". *London, Springer,*.

Jayshree Pande, P. N. (2021). "A Review of Maximum Power Point Tracking Algorithms for Wind Energy Conversion Systems". *Jornal of Marine Science and Engineering*.

Jesús Castro Martínez, J. L.-M. (2023). "Grid-forming control of doubly-fed induction generators based on the rotor flux orientation". *ScienceDirect*, Pages 162-176.

Jorge-Humberto, U.-Q. J. (2021). " PI/PID controller stabilizing sets of uncertain nonlinear systems: an efficient surrogate model-based approach ". *Spring Link,* pages 277–299.

K. Zeb, Z. A. (2017). *"Indirect field-oriented control of induction motor drive based on adaptive fuzzy logic controller"* (Vol. 99).

Kennedy J, E. R. (1995). particle swarm optimization. *Proc of the int IEEE conf on neural network*.

Kumsa, A. D. (2020). "Ethiopia renewable energy potentials and current state". *Research Gate*.

M. M. Gulzar, D. S. (2021). *"Adaptive fuzzy based optimized proportional-integral controller to mitigate the frequency oscillation of multi-area photovoltaic thermal system"* (Vol. 31).

Mahmoud Elgendi, M. A. (2023). "A review of wind turbines in complex terrain". *International Journal of Thermofluids*.

Mansoor Ahmad Soomro, Z. A. (2021). "Wind energy integration: Dynamic modeling and control of DFIG based on super twisting fractional order terminal sliding mode controller ". *ELSEVIER*, Pages 6031-6043.

Milton Ernesto, B. A. (2020). "Multi-objective PSO applied to PI control of DFIG wind turbine under electrical fault conditions".

Mohamed Horch, A. C. (2023). "A new fuzzy design for switching gain adaptation of sliding mode controller for a wind energy conversion system using a doubly fed induction generator". *HAL open science*.

Mostefa Amara, A. M. (2022). "Enhanced Control of Wind Energy Conversion System Based on DFIG Using Adaptive". *Journal Européen des Systèmes Automatisés*.

O. Apata, D. O. (2020). "An overview of control techniques for wind turbine systems". *ScienceDirect*.

Petras, I. (2018). "Fractional-Order Nonlinear Systems Modeling, Analysis and Simulation, Beijing, Beijing and Springer-Verlag Berlin Heidelberg,".

Power, i. 1. (2015). "Wind Farms during Grid Fault Occurrence,".

Ross Guttromson, J. W.-B. (2018). "Use of Wind Turbine Kinetic Energy to Supply Transmission Level Services". *SAND2018-3200*.

Shobole, M. T. (2015). "Fault Ride-through Capability of Wind Farm (Case Study of Adama Wind Farm Project, Dynamic Modeling and Simulation". *IEEE, Istanbul, Turkey*.

Tadesse, T. (2016). "Study of Doubly Fed Induction Generator Control Under Grid Fault". *Addis Ababa Institute Of Technology*.

Wind Farms during Grid Fault Occurrence. (2015). *in 17th International Middle East Power* .

REFERENCE LINKS

[L1] (n.d.). Retrieved from https://www.google.com/search?q=wind+energy+in+the+africa+and+sub+saharan.

[L2] (2012). *Mikrora.com/wind-turbine-parts-diagram/.* Retrieved from Mikrora.com/wind-turbine-parts-diagram/.

APPENDICES

A.1 Simulink block

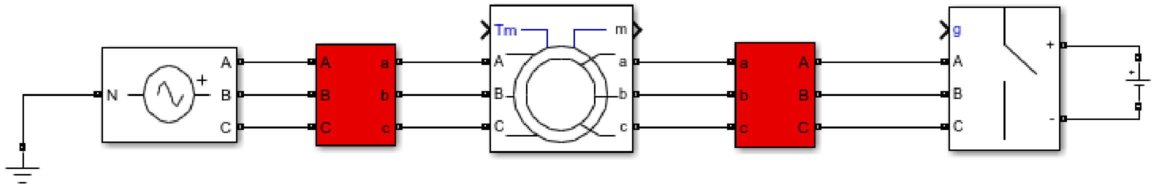

Figure A1.1 Simulation of the electrical system of a DFIG wind turbine

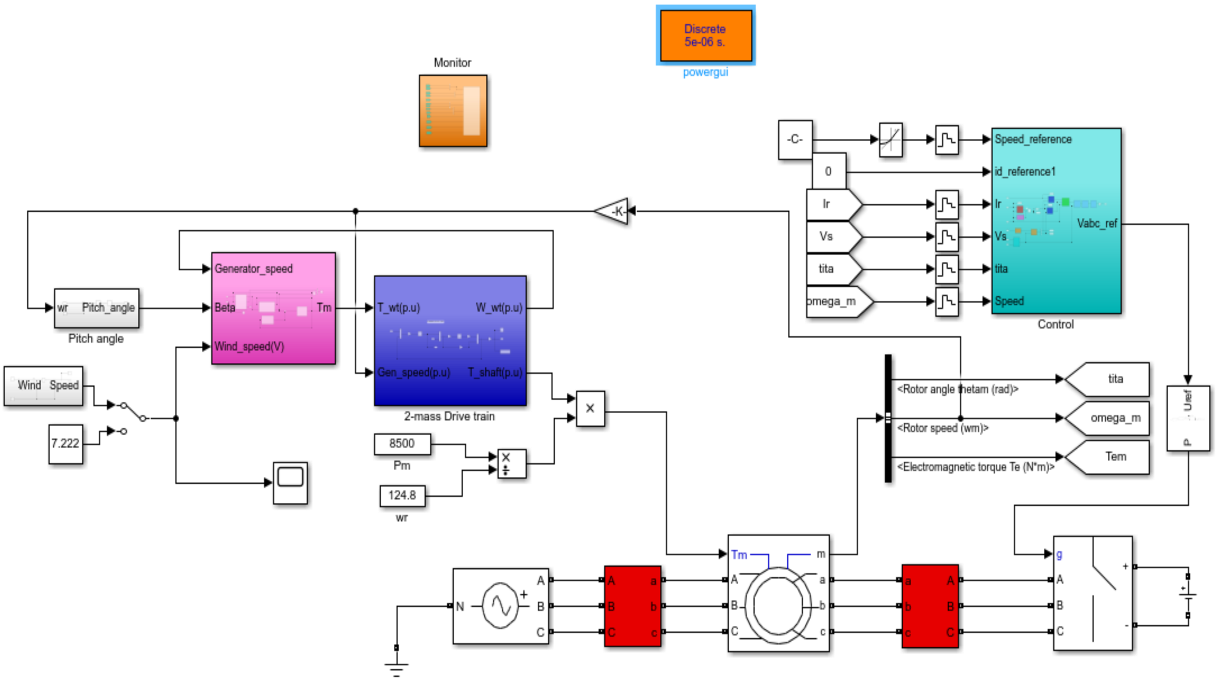

Figure A1.2 Overall Simulink design of the wind turbine dynamics model

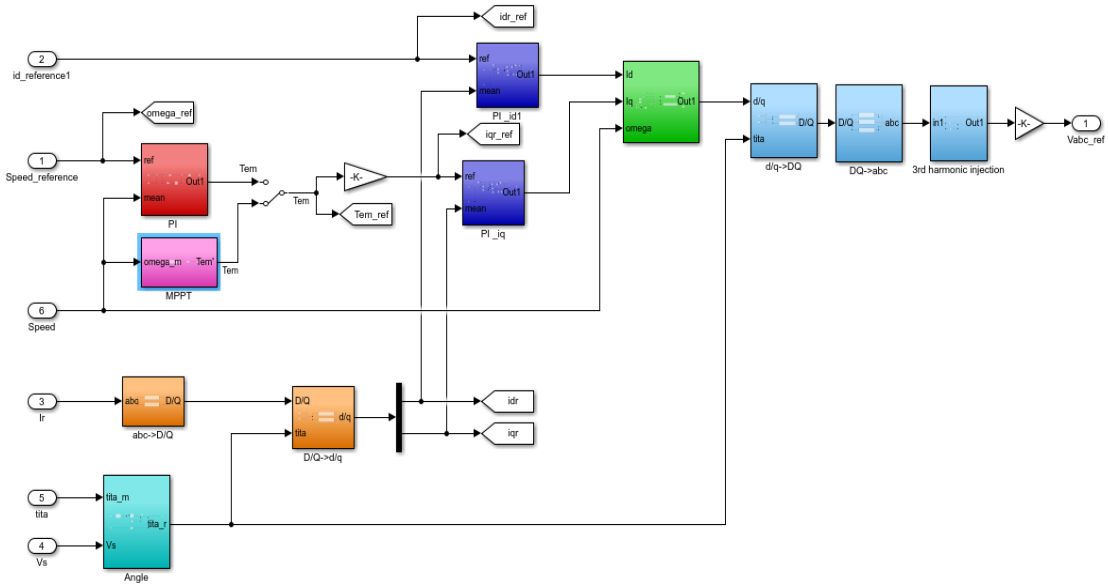

Figure A1.3 Simulation of a DFIG wind turbine control system

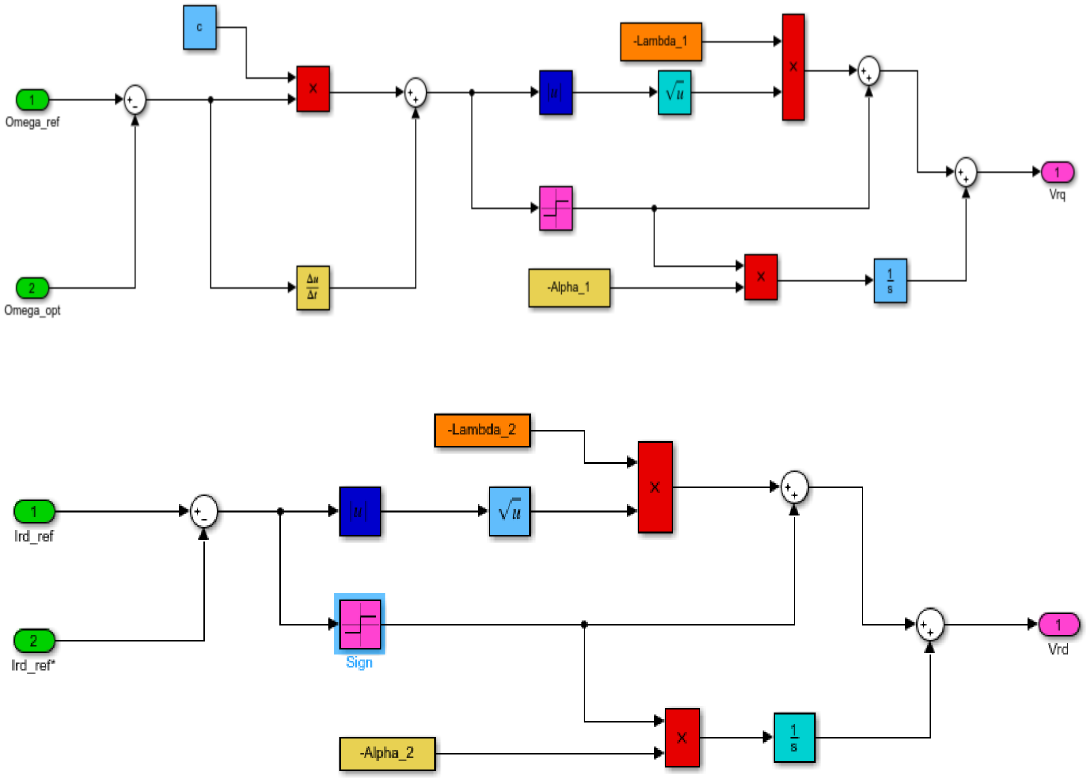

Figure A1.4 SMC controller’s Simulink design